
THE UNIVERSITY
*of* EDINBURGH

# Hillslope Morphology as an Indicator of Landscape Evolution in Tectonically Active Landscapes


THE UNIVERSITY *of* EDINBURGH

**Martin D. Hurst B.Sc.**

Ph.D. Geology – The University of Edinburgh – 2012

Thesis submitted for the degree of Doctor of Philosophy

University of Edinburgh

2012

# CONTENTS

# ABSTRACT

Hillslopes comprise the majority of unglaciated upland landscapes; they are the primary source for the production of sediment from bedrock, and the routing system by which sediment is delivered to the channel network. Yet the nature of hillslope response to changes in tectonic, climatic or base-level boundary conditions is poorly understood in terms of the spatial and temporal distribution of hillslope morphology. Here I exploit a previously published framework for exploring hillslope morphology in high relief landscapes (Roering et al., 2007), to address several critical questions: Does high resolution topography allow understanding of the processes and rates by which sediment is redistributed on hillslopes? If so, can hillslope morphology be used to map the spatial distribution of erosion rates and facilitate interpretation of the timing and magnitude of tectonic forcing, particularly in transient landscapes which are adjusting their erosion rates? And to what extent does variation in lithology influence hillslope evolution and morphology, and the ability to interpret process rates from hillslope form? In this thesis I sought to explain hillslope adjustment to changing boundary conditions through combining the predictions of analytical and numerical models with detailed analysis of real, high resolution topographic datasets (derived from LiDAR), focusing on two landscapes where the influence of tectonic forcing on base-level history is relatively well constrained, the Middle Fork Feather River in the northern Sierra Nevada, and the Dragon's Back Pressure Ridge, on the Carrizo Plain, both in California.

The Sierra Nevada of California is a west-tilted fault block composed primarily of granitoids formed during Mesozoic arc volcanism. The block underwent acceleration in uplift 5 - 3.5 Ma which is hypothesised to be caused be the drop-off of a dense root from the lower crust and replacement by hot asthenosphere, causing crustal buoyancy. A relict landscape has thus been uplifted and dissected by the major drainage routes crossing the range, which have eroded rapidly to form deep

canyons. The fluvial network is characterised by breaks in slope (knickpoints) which migrate into the landscape to transmit the signal of increased erosion, setting base-level conditions for adjacent hillslopes. Theoretical predictions for the morphology of hillslopes governed by a nonlinear sediment transport law, if the hillslopes have attained steady state (i.e. they are eroding in concert with base-level fall in adjacent valleys) reveal that the curvature of hilltops will be linearly proportional to erosion rates or rate of base-level fall. I present innovative techniques to extract hilltop networks and sample their adjacent hillslopes in order to test the utility of hilltop curvature for estimating erosion rates. This work is carried out in granitoid lithologies where the influence of bedrock heterogeneity is assumed no to be a first order control on hillslope morphology. Existing and new cosmogenic radionuclide analyses in the Feather River basin, California, suggest that erosion rates vary by over an order of magnitude from the remnant upland landscape to the incised river canyon. Hilltop curvature increases with erosion rates, allowing calibration of the hillslope sediment transport coefficient, which controls the relationship between hillslope gradient and sediment flux. This in turn allows the estimation of erosion rates throughout the landscape by mapping the spatial distribution of hilltop curvature. Additionally, despite the landscape containing gradient-limited hillslopes, hilltop curvature continues to increase with rising erosion rates, reflecting higher erosion rates than can be predicted by hillslope gradient. The distribution of hillslope morphology conforms well to predictions of a nonlinear sediment transport model, with measured values of hillslope relief varying with the product of hilltop curvature and hillslope length (proxy for erosion rate) in a manner similar to that predicted by Roering et al. (2007). Hilltop curvature can thus be used to estimate erosion rates in landscapes undergoing a transient adjustment to changing boundary conditions provided that the response timescale of hillslopes is short relative to channels.

Having focused on a landscape with roughly uniform bedrock geology to isolate drivers of geomorphic change, I sought to evaluate whether these techniques could be extended across lithologic contacts and throughout the landscape. Underlying geology influences the efficacy of soil production and transport on

hillslopes, and resistance to erosion by valley-forming processes. Here, quantitative analysis of LiDAR digital terrain models was performed to search for a topographic signature in two distinct lithologies in the Feather River catchment in northern California; granodiorite and deformed volcanics. The two sites, separated by <2 km and spanning similar elevations, are assumed to have similar climatic and denudation histories. Responding to increased erosion rates, transient hillslopes exhibit high gradient but low hilltop curvature in the metavolcanics relative to theoretical predictions for steady state hillslopes. However, hillslopes in the granodiorite have, for the most part, variation in hilltop curvature, hillslope length and hillslope relief similar to model predictions for steady state hillslopes. The curvature of hilltops adjacent to main stem channels implies that the coefficient of sediment transport is two times larger in the granodiorite (c. 8.8 $m^2$ $ka^{-1}$) than in the metavolcanics (c. 4.8 $m^2$ $ka^{-1}$). The data suggest that hillslopes get shorter as erosion rates increase due to the increased influence of debris flows in valley incision, suggesting that drainage density increases with erosion rate. The incision wave associated with more rapid erosion in the Feather River has propagated further into a basin developed on the metavolcanics and hence this substrate is less resistant to channel incision. I review an inventory of values for the transport coefficient for hillslope sediment transport but find that no clear patterns emerge with varying lithology. However in unconsolidated substrates, precipitation may play an important role in modulating sediment transport through variation in rain splash impact frequency and the frequency of wetting/drying, freeze/thaw, and expansion/contraction cycles.

Finally I apply the same techniques to study hillslope morphology to a landscape where the tectonic history has a documented influence on landscape development. The Dragon's Back pressure ridge, Carrizo Plain, CA, consists of a series of small catchments adjacent to the San Andreas fault, where previous detailed geologic mapping has allowed the spatial and temporal distribution of uplift to be constrained. This landscape offers a hitherto unique opportunity to study the temporal evolution of hillslope morphology via ergodic substitution. I show that the time evolution of a sensitive indicator of erosion rate, hilltop curvature, can be

predicted using a nonlinear sediment flux law. Further to this, the temporal evolution of relief and hilltop curvature experiences hysteresis as the landscape grows and decays. Relative to steady-state predictions, hillslope morphologies exhibit higher than expected values for relief during active uplift or landscape growth, and lower than expected relief during landscape decay. Therefore landscapes growing due to fault activity can be distinguished from those with quiescent faults undergoing topographic decay.

# DECLARATION

This thesis has been composed by myself and represents my own work. I acknowledge my co-authors in chapters two to four, which are written in paper format. I am first author on all papers included here and as such wrote the text, prepared all the diagrams and developed the intellectual arguments with a couple of exceptions stated herein. Dr. Rachel Walcott assisted in the development of techniques to extract hilltop networks. Dr. Mikael Attal contributed to discussions regarding all aspects of the work presented, produced Figure 2.15 and 4.3 to beautifully illustrate discussion of hillslope response to changes in rate of base-level fall. Dr. Kyungsoo Yoo contributed to early stages of research design and the interpretation of results for chapters 2 and 3. Dr. Simon M. Mudd contributed to all aspects of research design, execution and interpretation. Whilst I prepared all manuscripts, all authors contributed to manuscript refinement and editing prior to submission and following each review process. I am also solely responsible for writing the computer code employed in these works, though some functions were modified from code published by Pelletier (2008). I received assistance from Lyndsey MacKay in streamlining some aspects of the GIS analysis for extracting hilltops. This work has not been submitted for any other degree or professional qualification.

Martin David Hurst

# ACKNOWLEDGEMENTS

Most of all I would like to thank Simon for his seemingly relentless enthusiasm, understanding and patience. I cannot overstate how valuable it has been to have such an approachable character to mentor me through the last four years. I am also extremely grateful to Mikael for his positive attitude to absolutely everything and his willingness to have what was often the same discussion with me over and over again! Fieldwork with such knowledgeable and entertaining peers was hugely rewarding both intellectually and personally. Also thank you for agreeing that sometimes football is almost as important as data! There are a whole host of people I need to thank that helped make trips to the Feather River special: Kyungsoo "The Korean Mastermind" Yoo, Beth "Soda" Weinmann, Kate "FedEx" Maher, Kristin "Steak" Mayer, Sherman "POMD", Leigh "Mumford & Sons" Hammell, Tony "The French Commando" Dosseto, Manny "Mighty Probe" Gabet, Csaba "The Hungarian Augermeister" Toth. Kyungsoo and Beth also provided valuable input to this research and have been a pleasure to collaborate with. Sorry to Beth for the 911 incident, and the great soda shortage of 2009.

I am indebted to Rachel Walcott for help me getting started with the true powers of ARC and Python and Lindsay Mackay for help streamlining some GIS methods. My work benefited greatly from discussion with a number of valued colleagues, past and present members of LSD, particularly Daniel Hobley, Dave Milodowski, Matt Booth and Hugh Sinclair. Thanks to Tibor Dunai and Steve Binnie for help getting to grips with CRNs, and Elaine Macdougall for her tireless efforts in the lab. Discussion of techniques to extract quantitative information about above ground biomass from LiDAR with Edward Mitchard were extremely helpful. I would like to thank George Hilley for his insights with respect to the Dragons Back site (chapter 4). I am grateful to Josh Roering for many valuable discussions, and for welcoming me to visit Oregon in 2010. Discussion and collaboration with Jill Marshall was stimulating, and I thank her for allowing me to play sheep and take advantage of her unparalleled networking abilities! Thanks to Al "The Woog" Handwerger, the hostess with the most-est, and unparalleled knowledge of places to

get good chicken wings and burgers in Oregon, and his co-conspirator Mike D too. I also extend my gratitude to Mariela, Andy, Christina and Mia for a thoroughly enjoyable visit to Boulder.

I probably wouldn't have finished this thing without James "Jimbo the Alarm Clock" Horton, contributing many hours of pranity seservation techniques, large flates of pilth, large gates of ploodness, large cots of poffee, Wears of Gaw etc.! My Mum, Dad and sister have been supportive throughout, probably more than they even realise, particularly Switzerland 2009. And finally of course Mhairi, mah hairy, for constant love and support in so many ways, despite me constantly running away for fieldwork.

Apologies to anyone I have forgotten.

# ACRONYMS

| | | |
|---|---|---|
| CRN | - | Cosmogenic Radionuclides |
| DBPR | - | Dragon's Back Pressure Ridge |
| DEM | - | Digital Elevation Model |
| GSD | - | Grain Size Distribution |
| LiDAR | - | Light Detection and Ranging |
| MAP | - | Mean Annual Precipitation |
| MAT | - | Mean Annual Temperature |
| OSL | - | Optically Stimulated Luminescence |
| RSM | - | Relief Shadow Modelling |
| SAF | - | San Andreas Fault |

# NOTATION

| Symbol | Units ([L]ength, [M]ass, [T]ime) | Description |
|---|---|---|
| $D$ | $L^2\ T^{-1}$ | Sediment transport coefficient |
| $E$ | $L\ T^{-1}$ | Erosion rate |
| $E_R$ | $L\ T^{-1}$ | Reference erosion rate (see Equation 1.7) |
| $E^*$ | | Dimensionless erosion rate |
| $K$ | $L^{1-2m}\ T^{-1}$ | Proportionality coefficient for stream power model |
| $K_{sn}$ | $L^{2m/n}$ | Channel steepness normalised for drainage area |
| $L_C$ | L | Characteristic length scale related to hillslope length |
| $L_H$ | L | Horizontal hillslope length |
| $\rho_r$ | $M\ L^{-3}$ | Bulk density of rock |
| $\rho_s$ | $M\ L^{-3}$ | Bulk density of dry soil |
| $q_s$ | $L^2\ T^{-1}$ | Volumetric sediment flux |
| $R$ | L | Hillslope relief |
| $R^*$ | | Dimensionless relief |
| $\overline{S}$ | L/L | Mean hillslope gradient |
| $S_C$ | L/L | Critical hillslope gradient |
| $S_{Ch}$ | L/L | Channel slope |
| $S_{Th}$ | L/L | Threshold hillslope gradient |
| $t$ | T | Time |
| $U$ | $L\ T^{-1}$ | Vertical component surface uplift |
| $x$ | L | Spatial coordinate along hillslope length |
| $x^*$ | | Dimensionless spatial coordinate along hillslope length |
| $\zeta$ | L | Elevation of the surface |
| $\zeta_0$ | L | Elevation of a moving reference frame e.g. base-level |

# 1 GENERAL INTRODUCTION

## *1.1 Overview*

In landscapes which are actively eroding, surface processes tend to evacuate all weathering products, leaving little or no evidence of a past state. Yet landscape morphology reflects the processes acting upon it and leaves clues as to how rapidly the landscape is evolving. This thesis is concerned with understanding rates and patterns of landscape evolution by interpreting hillslopes as records of the history of erosion. The work is focused on tectonically active landscapes where geomorphologists are particularly interested in understanding surface processes with a view to inverting for rates of tectonic uplift (Whittaker, 2012; and references therein). The increased availability of airborne Light Detection and Ranging (LiDAR) derived DEMs allow morphological properties of hillslopes to be quantified in detail and at fine scales. The research presented herein has focused on extracting geometric properties of hillslopes from such high resolution topographic data to test the predictions of existing sediment transport models (Roering, 2008; Roering et al., 2007). I also utilise hillslope morphology as an indicator of erosion rates over geomorphically significant timescales (millennia to millions of years). The techniques were developed to aid a larger research effort into understanding the geochemical evolution of hillslope soils in response to changing rates of geomorphic driving conditions in the Feather River watershed of northern California (Yoo et al., 2011).

In this thesis, chapters two to four are in the form of research papers either accepted or in review with scientific journals, as documented at the start of these chapters. Each can be read as a single, autonomous body of work. Chapter two

presents the methodology also implemented in those remaining chapters, including cosmogenic radionuclide (CRN) methods and topographic analyses. Chapter two also tests the utilisation of hilltop curvature to predict the spatial distribution of erosion rates in the northern Sierra Nevada of California. Chapter three investigates similarities and differences in hillslope morphology underlain by two distinct lithologies in the Sierra Nevada to investigate the influence that changing lithology might play in dictating landscape evolution. Chapter four focuses on a landscape with a well constrained spatially distributed uplift field on the San Andreas Fault, where a space for time substitution can be made to reveal the temporal evolution of hillslope morphology (Hilley and Arrowsmith, 2008). Finally, chapter five presents a synthesis of the research presented herein and discussion of the implications for understanding hillslope sediment transport and morphology and the rates and patterns of landscape evolution.

The remainder of this chapter is devoted to providing a broad rationale for this study, followed by a more detailed discussion of the motivation and context regarding important research questions addressed by this work. This section concludes by presenting the analytical framework for hillslope evolution which is integral to the work presented, before concluding with a detailed outline of the structure of this thesis.

## *1.2 Rationale and Motivation*

The Earth's Surface is the frontier at which geology and tectonics interact with climate-driven weathering and erosion processes (Molnar and England, 1990). Tectonic processes in the Earth's crust set up topography, and surface processes redistribute mass from elevated topography to sedimentary basins. Landscape morphology may therefore contain information about the types of surface processes

operating, the rate at which sediment is being generated or redistributed, or the rates at which topography is growing due to tectonic processes.

### 1.2.1 Quantifying Erosion Rates

Techniques to quantify landscape change are vital to a variety of disciplines. Erosion rates in channels dictate hillslope morphology and evolution and therefore influence the likelihood of hazards associated with landslides and debris flows. Erosion rates on hillslopes influence the grain size distribution (GSD), maturity and supply rate of sediment fed river channels, all of which can subsequently influence erosion (Attal et al., 2011; Cowie et al., 2008; DiBiase and Whipple, 2011) and dictate the textural properties of the resulting deposits in sedimentary basins (Armitage et al., 2011; Duller et al., 2010). Moreover erosion rates may tend towards a balance with tectonic uplift and hence in ideal settings measured erosion rates could provide an estimate of rates of tectonic uplift (US Army Corps of Engineers, 1984; Willett and Brandon, 2002).

Hillslopes are the most spatially extensive component of the terrestrial Earth surface. In unglaciated landscapes the vast majority of sediment transported by rivers to depositional basins originates on hillslopes. Valley forming processes set the boundary conditions for hillslopes, controlling their evolution and morphology. Hence there is the potential for hillslopes to provide a record of erosion processes and rates in the fluvial network (Mudd and Furbish, 2007). The ability to interpret erosion rates based on topography alone raises the tantalising prospect of being able to interpret tectonic and/or climatic conditions based on landscape morphology (Kirby and Ouimet, 2011; Komar and Inman, 1970; Riihimaki and Reiners, 2012; Whittaker, 2012).

Erosion rates can be quantified by measuring the concentration of cosmogenic radionuclides (CRNs) in rock or sediment samples. CRNs are elemental isotopes

(usually radioactive) which are produced in the atmosphere and the upper few metres of the Earth's surface due to the interaction of cosmic radiation and matter (e.g. Gosse and Phillips, 2001). The rate at which certain isotopes accumulate is known to be a function of latitude and altitude (Dunai, 2000; Lal, 1991; Nishiizumi et al., 1986a; Stone, 2000). By measuring how much of a particular isotope is in a rock or sediment sample, I can understand how long the sample has been located in the upper few metres of the Earth's surface. Hence when erosion rates are rapid, a sample will contain fewer CRNs. For example, one can sample the sand-sized sediment in a stream bed, and assuming there has been no long-term storage of sediment upstream, and that the sample is a fully mixed sample from sources distributed throughout the catchment, the amount of the CRN $^{10}$Be can be used to calculate a catchment-averaged erosion rate (Bierman and Steig, 1996; Brown et al., 1995; Granger et al., 1996). However to measure the number of atoms of a particular radionuclide requires extensive and expensive laboratory preparation and analysis in an accelerator mass spectrometer (AMS) which typically is also expensive. A strong motivation for this study was to reduce the cost required to generate information on the distribution of erosion rates across entire landscapes by using topography as an indicator of erosion rates. The techniques presented should not be considered a replacement for CRN analysis, but by calibrating topographic parameters to a small set of CRN-derived erosion rates one should then be able to predict erosion rates across entire landscapes.

On visiting landscapes with high relief, steep hillslopes and exposed bedrock, one would generally conclude they have been eroding rapidly relative to a landscape with gentle hillslopes covered in soil. Further to this, a geologist might interpret that some form of surface uplift must drive that erosion, since steep slopes facilitate high erosion rates, which usually has some surface gradient dependency. The concept of using the form of the landscape to infer how rapidly it is eroding was first considered by Davis (1892) and later by Gilbert (1909). Culling (1960) presented a framework for understanding this analytically for hillslopes, deriving partial differential

Equations to describe the evolution of a hillslope through time, driven by diffusion-like creep processes (see section 1.5). Testing of relationships between erosion rate and topography was previously limited by my inability to quantify the former. The seminal work of Ahnert (1970) provided the first empirical support that topography relief scaled with basin averaged erosion rates (Figure 1.1a). Ahnert (1970) quantified erosion rates by measuring the concentration of dissolved sediment in some of the world's major rivers and showed that the results scaled linearly with basin relief (maximum elevation minus minimum elevation in a basin).

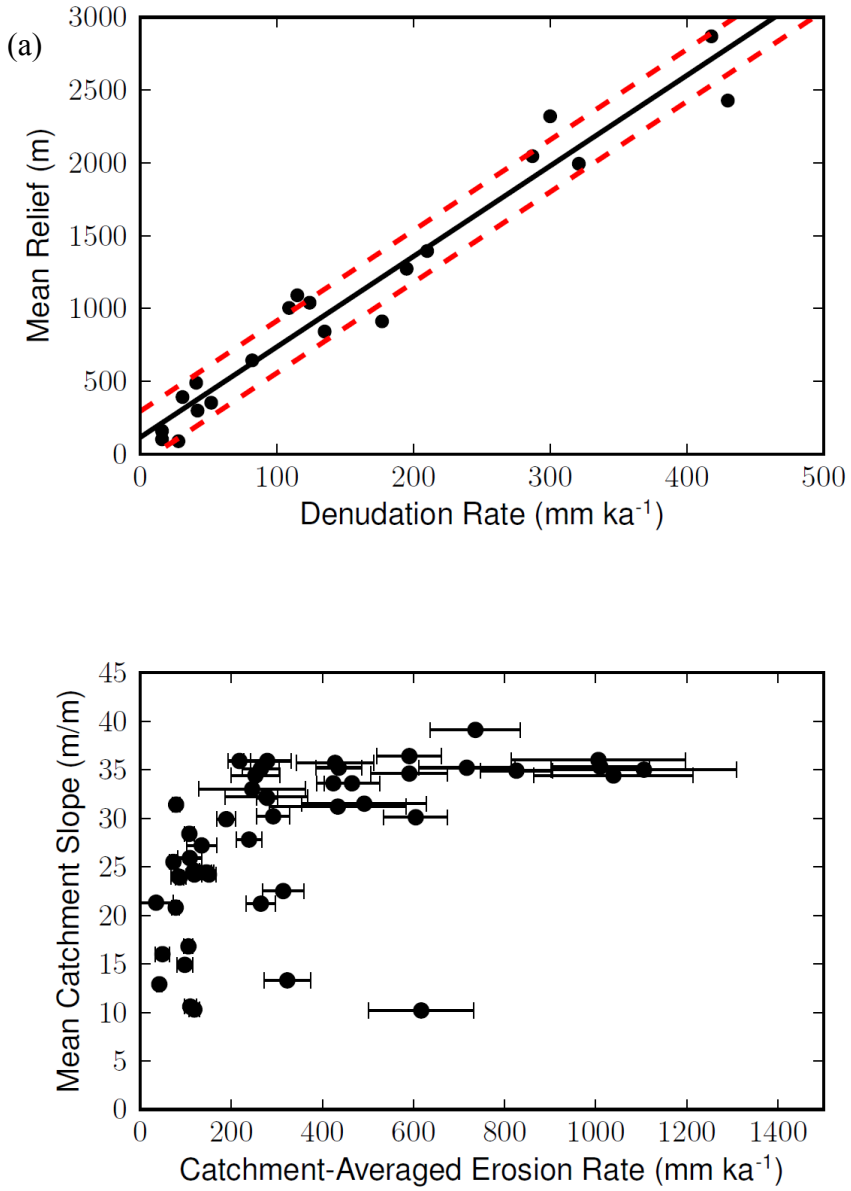


Figure 1.1(a) Relationship between denudation rate and basin relief for some of the world's major drainage pathways (recreated from Ahnert (1970). Relief increases linearly with denudation up to 400 mm $ka^{-1}$. Solid line is a least-squares regression fit ($R^2$ = 0.86) and the dashed red lines represent one standard deviation about this. (b) Results from (Binnie et al., 2007) and (DiBiase et al., 2010) showing a nonlinear relationship between mean catchment erosion rates measured using CRNs, and mean catchment hillslope gradients in the San Gabriel and San Bernardino Mountains.. Hence hillslope gradients are a poor indicator of erosion rates in rapidly eroding terrain.

Physically-based models for sediment transport on hillslopes predict that hillslope morphology adjusts to denudation (Roering et al., 2007) and it may be possible to use hillslope morphology to distinguish the most appropriate sediment transport model (Roering, 2008) or infer denudation rate. When a change in base-level occurs due to, say, an acceleration in river incision rate, hillslopes respond nearest to the channel initially, by steepening, and subsequently a wave of adjustment is transmitted upslope towards the divide (Ahnert, 1987; Fernandes and Dietrich, 1997; Furbish and Fagherazzi, 2001; Mudd and Furbish, 2005; Roering et al., 2001a). Hence hillslope morphology may also reflect the history of denudation provided that a hillslope is still adjusting to a particular change in boundary conditions (Mudd and Furbish, 2007). To date, relatively few studies have explored and quantified hillslope morphology in landscapes that are adjusting to a change in boundary conditions (i.e. change in uplift rate or rate of base-level fall) (DiBiase et al., 2012).

Rapidly eroding landscapes are dominated by steep hillslopes, since sediment transport on hillslopes is generally slope dependent. For hillslopes to keep pace with rapidly eroding channels, they must steepen to allow sediment to be transported more effectively. However, in contrast to the results of Ahnert (1970), many studies have now demonstrated that at high erosion rates hillslope relief or mean hillslope gradient is limited due to a process transition to landslide dominated sediment transport (Binnie et al., 2007; Burbank et al., 1996; DiBiase et al., 2010; Montgomery, 2001; Montgomery and Brandon, 2002; Ouimet et al., 2009; Schmidt and Montgomery, 1995). Whilst nonlinear (Andrews and Bucknam, 1987; Roering et al., 1999) or threshold (Howard, 1994) sediment transport models can account for such a relationship, hillslope gradients calculated from DEMs cannot be used as a meaningful indicator of erosion rates in tectonically active landscapes. Much research has subsequently been devoted to the channel network since channel gradients (normalised for drainage area to give a metric called channel steepness index) also increase nonlinearly with erosion rate, but tend to continue to increase at

erosion rates beyond those at which threshold hillslopes emerge (DiBiase et al., 2010; Ouimet et al., 2009). This channel steepness index metric has been demonstrated to be a useful topographic metric for erosion rate at a variety of field settings using widely available coarse resolution topographic data (10-90 m) (Cyr et al., 2010; DiBiase et al., 2010; Kirby et al., 2003; Matsushi and Matsuzaki, 2010; Ouimet et al., 2009; Palumbo et al., 2010; Snyder et al., 2000).

The onset of the 'digital era' in the last three decades has lead to significant advances in my ability to examine the Earth's surface, progressing from digitised topographic maps to remotely sensed digital elevation models (DEMs) of increasing accuracy and resolution. The acquisition and availability of DEMs has enhanced my ability to extract quantitative information about landscape form (Evans, 1980; Moore et al., 1991; O'Callaghan and Mark, 1984; Zevenbergen and Thorne, 1987). Airborne LiDAR surveys are providing a wealth of high resolution topographic data and there is significant effort being made to make it widely available (e.g. the OpenTopography Facility with support from the National Science Foundation). The increased availability of LiDAR is changing the way geomorphologists extract information about the Earth surface, with a shift occurring towards quantitative interrogation of the land surface (Slatton et al., 2007). Satellite remote sensing techniques are advancing towards a similar level of precision. Recently there has been a focus on software development in order that the geomorphic community might equip itself with toolsets that can be applied repeatedly in an automotive fashion, allowing large datasets to be generated rapidly from topographic data (e.g. DiBiase et al., 2012; Hurst et al., 2012; Passalacqua et al., 2010a; Passalacqua et al., 2010b).

### 1.2.2 Testing Geomorphic Transport Models

Geomorphic transport models (GTMs) are physically-based mathematical expressions which describe sediment transport and/or erosion as a function of topography and parameters which can be readily quantified/calibrated/estimated from field measurements (Dietrich et al., 2003). They are combined with Equations for the conservation of mass to forward model the evolution of components of landscapes or landscapes as a whole, be they real or synthetic. Erosion rates measurements from real landscapes are vital to testing the validity of GTMs for providing a good approximation of sediment flux/erosion in that landscape. Whilst GTMs might be able to reproduce attributes of real topography, the critical test of their applicability is whether they imitate the time evolution in sediment flux/erosion rate and landscape morphology, particularly when the landscape is responding to a change in boundary conditions (e.g. Whipple, 2004).

GTMs for hillslope evolution have been tested in landscapes where the assumption of steady state (i.e. hillslope is lowering at the same rates as adjacent channels) seems valid (e.g. Roering et al., 2007). In this thesis I focused on landscapes known to be adjusting to some change in boundary conditions in order to i) test whether GTMs for hillslopes were valid in such settings and ii) test whether hillslope morphology could still indicate erosion rates and/or provide evidence for the style and rate of landscape adjustment. Transient landscapes are anticipated to be experiencing a range of erosion rates and so I sought to test whether the distribution of hillslope morphology could offer a new approach to mapping, quantifying and interpreting the distribution of erosion and topography during landscape adjustment. For such a relationship to hold will require that hillslopes can adjust rapidly to changing rates of channel lowering, so that a new erosion rate signal is able to propagate quickly to the divide in order that the hillslope can adjust its form. Whilst the predictions of model solutions for steady-state morphologies are predicted to vary systematically with erosion rates, no analytical solutions currently exist to relate

hillslope morphology to the nature of changing boundary conditions they are experiencing. Thus there is scope for an in-depth exploration of variation in hillslope morphology in transient landscape settings. Hillslope form alone may be able to inform us as to the style of transience a landscape is experiencing.

## *1.3 Objectives*

Previously, the coarse resolution of DEMs (typically $10^1$-$10^2$ m horizontal grid spacing) meant that exploration of hillslope morphology and the derivation of hillslope-based erosion rate metrics were scale-limited, such as measurements of relief (typically over scales of $10^2$ – $10^4$ m) or hillslope gradient ($10^1$-$10^2$ m) (e.g. see Figure 1.1). The advent of high-resolution (c. $10^0$ m) DEMs has meant that the scale of observation is similar to the scale at which hillslope processes are operating. Hence measuring hillslope morphology at the process-scale better facilitates linkages between sediment transport models and the landforms they produce. High resolution DEMs provided the potential to extract metrics such as curvature (e.g. Laplacian, profile, planform), topographic roughness (related to local slope gradients) and hillslope length. A recent study by DiBiase et al. (2012) has highlighted the wealth of potential information stored on hillslopes which can be examined using high resolution datasets. This thesis focuses on the development of new techniques to explore the spatial distribution of hillslope morphology, and their application to investigate sediment transport and landscape evolution in tectonically active landscapes. Hence I aimed to fulfil the following principal objectives:

a) Develop techniques for extracting metrics of hillslope morphology which can be related directly to the predictions of GTMs applicable to hillslopes (e.g. Culling, 1960; Howard, 1994; Roering et al., 2007). The techniques should be automated in a manner that facilitates the quantification of hillslope metrics over large spatial extents and allows

them to be related to any morphological properties derived in adjacent valley networks (e.g. channel steepness indices, channel concavity, valley slope). These novel techniques will be used to explore the spatial distribution of hillslope morphology in actively eroding landscapes.

b) Test the extent to which mapping hilltop curvature can provide a reliable predictor of the spatial distribution of erosion rates in a landscape with known highly variable erosion rates (Riebe et al., 2000).

c) Compare morphological predictions of various hillslope sediment transport models to real topography to demonstrate which particular model is most appropriate to predict hillslope sediment flux in a given landscape.

d) Explore the role the variable underlying bedrock type plays in modifying hillslope form and sediment transport to test whether the common assumption that bedrock type is not a first-order control on many surface process is valid or whether lithology needs to be accounted for more explicitly when trying to understand the evolution of the earth surface.

e) Investigate through modelling and topographic analysis how hillslope morphology reflects landscape response to transient boundary conditions such as base-level fall or a change in the rate of tectonic uplift. For known cases of transient landscape adjustment, test whether hillslope morphology can be inverted to derive the temporal history of such forcing.

Objectives a, b c and e are all addressed in chapter two which focuses on using hillslope metrics as predictors of erosion rates in the Feather River in the northern Sierra Nevada, California. Objectives b, c and d are focused on exploring the important role that lithology plays in modifying hillslope sediment transport and morphology in that same landscape in chapter three. Finally in chapter four links between transient surface uplift and hillslope morphology are presented for the Dragon's Back pressure ridge study-site on the San Andreas Fault (objectives b, c and e).

## *1.4 Framework and Terminology*

The morphology and evolution of hillslopes is considered from the perspective of conservation of mass, which facilitates both analytical predictions of hillslope behaviour for different sediment transport models, and the numerical simulation of hillslope evolution over geomorphically significant timescales (thousands to millions of years). Here I present an overview of mass balance principles applied to hillslopes, and some predictions of expected hillslope morphologies under certain conditions. Fundamental to this analysis is the concept of steady state, which can take on a variety of definitions in geomorphology. Here steady state is considered a condition where a hillslope is down-wasting at the same rate everywhere, in concert with adjacent channels.

### 1.4.1 Conservation of Mass Applied to Hillslopes

Hillslope morphology and evolution can be considered through principles of mass conservation. I use the notation [L]ength, [M]ass and [T]ime to describe parameter units. The elevation of the surface $\zeta$ [L] at any point along a 1D hillslope (with spatial dimension $x$ [L]) is controlled by the divergence of volumetric sediment

transport $q_s$ [$L^2$ $T^{-1}$]. If more sediment is transported in than is removed, then there is net deposition and $\zeta$ increases, while if there is more sediment removed than is supplied then $\zeta$ decreases (Culling, 1960):

$$\frac{\partial \zeta}{\partial t} = \frac{\rho_r}{\rho_s} U - \frac{\partial q_s}{\partial x} \qquad [1.1]$$

where $U$ is surface uplift [L $T^{-1}$], $\rho_r$ and $\rho_s$ [M $L^{-3}$] are the densities of rock and dry soil respectively, and $t$ [T] is time. This approach assumes that a hillslope is transport limited; the maximum sediment supply rate (e.g. via conversion from bedrock below) exceeds volumetric sediment flux everywhere on the hillslope such that its evolution and morphology are dictated by how efficiently sediment can be transported. Throughout this thesis I use the terms soil/regolith interchangeably to mean sediment at/near the Earth's surface that is readily transportable. Imagine a 1 $m^3$ box of soil on a hillslope (Figure 1.2); Equation 1.1 simply states that the elevation of the upper surface of the box is set by how much uplift there is plus how much sediment is transported into the box from upslope, minus how much material is transported away downslope. The hillslope sediment flux term $q_s$ allows any spatially discrete model of hillslope sediment transport to be inserted into the mass balance.

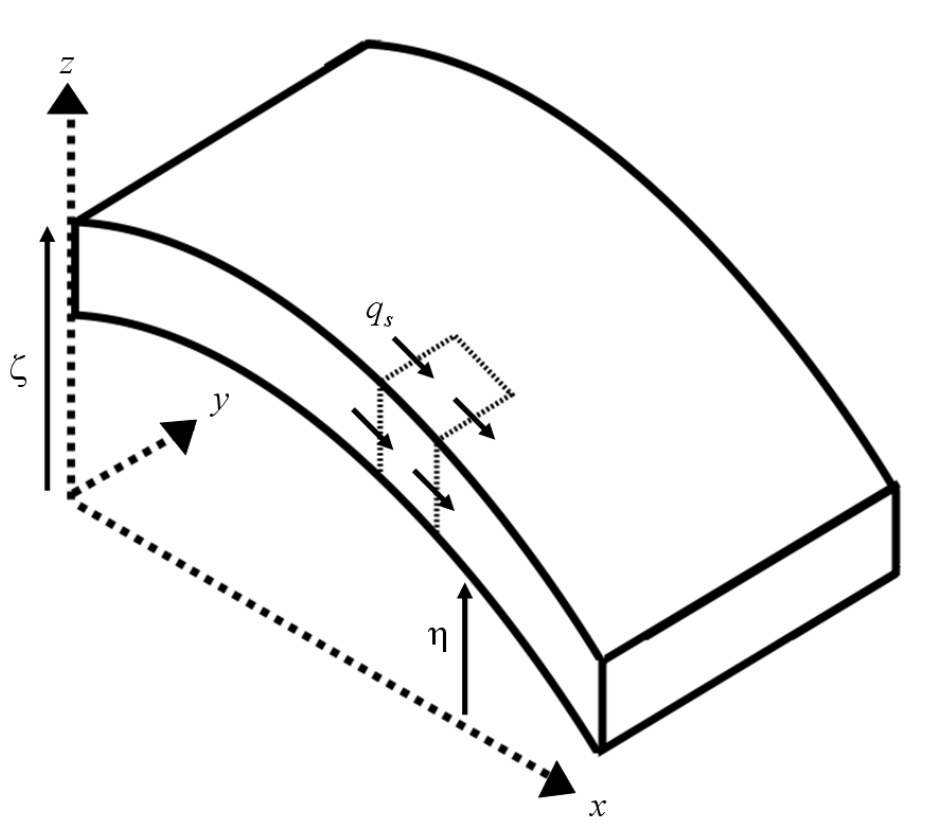


Figure 1.2: Diagramatic representation of conservation of mass principle. The elevation of the surface $\zeta$ in the box is set by how much sediment is transported into the box from upslope, minus how much is evacuated downslope ($\partial q_s$), plus the amount of surface uplift $U$ that occurs. N.B. Equation 1.1 is one-dimensional so only considers transport in the $x$-direction.

### 1.4.2 Hillslope Sediment Flux Models

The soil produced on a hillslope is transported downslope primarily by disturbance-driven soil creep, overland flow and landsliding. Gilbert (1909) attributed soil creep to three mechanisms: freeze-thaw, heating-cooling and wetting-drying cycles. The expansion stage of these cycles acts normal to the slope, whilst the contraction phase acts vertically due to gravity. This facilitates progressive downslope movement. Steeper slopes increase the horizontal component of expansion and therefore the rate of soil creep, hence steeper slopes transport more sediment. Root growth causes expansion of the soil normal to the hillslope, whilst root decay allows soil to settle vertically (Gabet et al., 2003). Tree throw can aid soil transport, uprooting large amounts of sediment, creating accommodation space and removing support for soil upslope (Gabet et al., 2003; Roering, 2004). Bioturbation by burrowing organisms moves soil and disturbs the soil layer, aiding the transport of sediment down slope (Black and Montgomery, 1991; Gabet, 2000; Yoo et al., 2005).

The convex profile of hillslopes was first attributed to slope-dependant soil creep by Davis (1892) and later Gilbert (1909). Hillslope sediment flux was first described numerically as a linear function of slope by Culling (1960):

$$q_s = -D\frac{\partial \zeta}{\partial x} \qquad [1.2]$$

where $D$ [$L^2T^{-1}$] is a coefficient of sediment transport with units of diffusivity. This flux function was assumed adequate for modelling purposes and applied to problems such as the evolution of fault scarps (e.g. Hanks et al., 1984; Nash, 1980b) or wave cut terraces (Nash, 1980a; Rosenbloom and Anderson, 1994) and is supported by field evidence of transport rates determined by CRN analysis (McKean et al., 1993). Recent physically-based models of sediment transport by rainsplash can be

approximated by such a linear sediment flux law (Dunne et al., 2010; Furbish et al., 2007).

Assuming the hillslope has attained steady state and hence uplift rate ($U$ [L $T^{-1}$]) is balanced by erosion rate ($E$ [L $T^{-1}$]) ($\partial\zeta/\partial t = 0$, $U=E$) and substituting Equation 1.2 into Equation 1.1 gives:

$$E = -D\frac{\rho_s}{\rho_r}\frac{\partial^2\zeta}{\partial x^2} \qquad [1.3]$$

i.e. topography curvature ($C = \partial^2\zeta/\partial x^2$), which can be readily calculated from DEMs, is predicted to be proportional to erosion rate.

Not all steady state landscapes contain hillslopes exhibiting constant curvature as predicted by Equation 1.3, but instead hillslopes become increasingly planar downslope (Anderson, 1994; Andrews and Bucknam, 1987; Roering et al., 1999). Having observed that linear flux only holds for low angle hillslopes, Roering et al. (1999) derived a physically-based expression for sediment transport, in which flux is a non-linear function of slope, incorporating a critical slope term ($S_c$) at which sediment flux becomes infinite, limiting the maximum angle hillslopes can obtain:

$$q_s = -D\frac{\partial\zeta}{\partial x}\left[1-\left(\frac{1}{S_c}\frac{\partial\zeta}{\partial x}\right)^2\right]^{-1} \qquad [1.4]$$

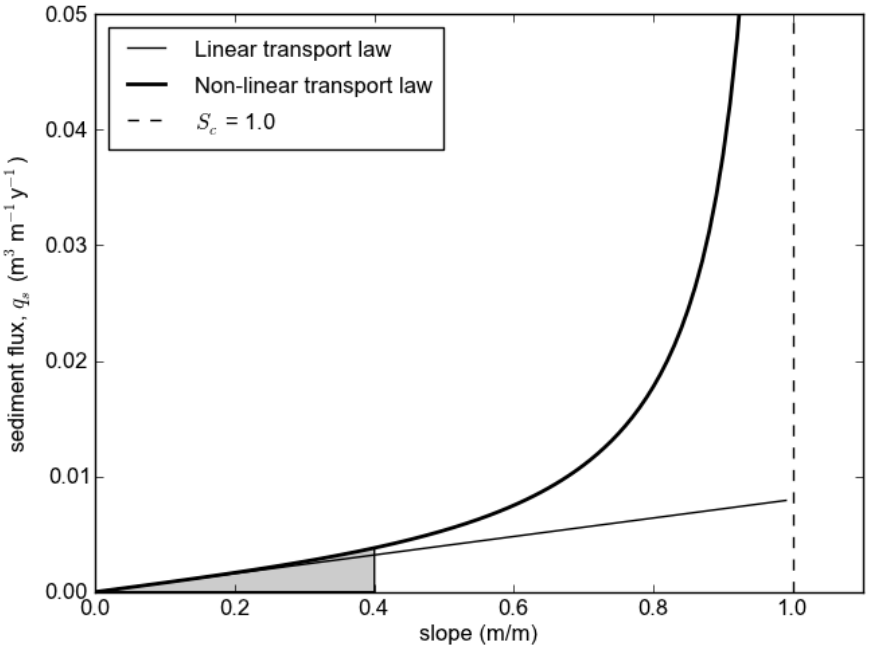


Figure 1.3: Theoretical relationship between hillslope gradient and sediment flux for a linear transport law (Equation 1.2) and nonlinear flux model (Equation 1.4). For the nonlinear model (bold line) sediment flux tends to infinity as slope approaches $S_C$. The grey shaded region represents slope gradients for which there is a > 90% linear component to sediment transport (i.e. $q_s$ is <10% greater than a linear model would predict) and hence a relationship between erosion rate and topographic curvature should hold (Equation 1.3).

A hillslope responding to increased erosion steepens to a limited gradient at which sediment flux increases to accommodate further increases in erosion rate, resulting in planar hillslopes. This model mimics the behaviour of the linear flux law at low gradients (Figure 1.3), validating the latter's use in previous studies and verifying that the coefficient $D$ can be considered the same for both models (Roering et al., 2001a). Estimates of $D$ when wrongly assuming the linear transport law is appropriate will be too high in settings where non-linear transport is occurring, since the nonlinearity means sediment transport will be more efficient (Roering, 2008).

Equation 1.4 has been validated through application to real landscapes. In the Oregon Coastal Range, $C$ tends to zero with increasing hillslope gradient away from drainage divides (Roering et al., 1999). Here the critical gradient has been estimated at $S_c$ = 1.25 (51°), higher than the internal friction angle common for soils, but in other landscapes $S_c$ has been found to be lower (e.g. DiBiase et al., 2010). This flux law has been supported experimentally through analogue and numerical modelling (Roering, 2004; Roering et al., 2001b), as well as by comparing to the morphology of real landscapes (Roering et al., 1999; Roering et al., 2007; DiBiase et al., 2010). Critical to the applicability of this model is the assumption of transport limited conditions on hillslopes. By this is meant a soil mantled landscape is required in which there is sufficient soil depth developed that material at the near-surface is readily transportable.

### 1.4.3 Non-dimensional Framework for Hillslope Morphology

The use of topographic curvature as an indicator of erosion rate still holds when applying a nonlinear sediment flux model provided that the surface slope ($\partial\zeta/\partial x$) is small so that the bracketed term in Equation 1.4 tends towards 1. The shaded region in Figure 1.3 shows the values of slope for which $C$ may still reflect $E$,

though these values will be dependent on $D$ and $S_C$. Given this, Equation 1.3 can be written as:

$$E = -D\frac{\rho_s}{\rho_r}C_{HT} \qquad [1.5]$$

where $C_{HT}$ is the topographic curvature *only* at hilltops where the topographic gradient is low. This inherently assumes that at hilltops, sediment transport is still driven by creep-type processes, whilst downslope a process transition may occur to landslide-dominated flux. Non-dimensionalization of erosion rate and relief allows comparisons between landscapes with distinct process rates and morphology. Roering et al. (2007) cast erosion rate and relief in non-dimensional form, as functions of readily quantifiable topographic parameters. Substituting Equation 1.4 into Equation 1.1 and integrating, Roering et al. (2007) derived the steady state profile of a hillslope:

$$\zeta(x) = \frac{DS_C^{\,2}}{2(\rho_r/\rho_s)E}\times \left[\ln\left(\frac{1}{2}\left(\sqrt{1+\left(\frac{2(\rho_r/\rho_s)Ex}{DS_C}\right)^2}+1\right)\right)-\sqrt{1+\left(\frac{2(\rho_r/\rho_s)Ex}{DS_C}\right)^2}+1\right] \qquad [1.6]$$

Hillslope relief is the difference between the elevations at the hilltop and the divide:

$$R = \zeta(x=0) - \zeta(x=L_H) \qquad [1.7]$$

Roering et al., (2007) described the hillslope by defining a dimensionless relief $R^* = R/(S_c L_H)$, a dimensionless spatial coordinate $x^* = x/L_H$, and a dimensionless erosion rate $E^* = E/E_R$, where $E_R$ [L $T^{-1}$] is a reference erosion rate which they defined as:

$$E_R = \frac{D S_C}{2 L_H (\rho_r / \rho_s)}. \qquad [1.8]$$

Substituting dimensionless parameters and Equations 1.5, 1.6 and 1.8 into Equation 1.7, it is possible to express dimensionless relief $R^*$ as a function of dimensionless erosion rate $E^*$:

$$R = \frac{1}{E}\left\{\sqrt{1+(E)^2} - \ln\left[\frac{1}{2}\left(1+\sqrt{1+(E)^2}\right)\right] - 1\right\}. \qquad [1.9]$$

Further both $E^*$ and $R^*$ can be expressed as functions of the measurable hillslope properties $C_{HT}$, $L_H$ and mean hillslope gradient $\bar{S}$ :

$$E^* = \frac{E}{E_R} = \frac{\rho_r}{\rho_s} \cdot \frac{2 E L_H}{D S_C} = \frac{2 C_{HT} L_H}{S_C} \quad \text{and} \qquad [1.10]$$

$$R^* = \frac{\bar{S}}{S_C} \qquad [1.11]$$

Equation 1.9 predicts a non-linear relationship between $E^*$ and $R^*$, which all hillslopes with a morphology that is adjusted to the boundary conditions should obey

(providing Equation 1.4 gives a reasonable approximation of sediment transport processes on the hillslope). This relationship between dimensionless erosion rate and relief is shown in Figure 1.4. When $E^*$ is < 1 $R^*$ increases proportionally to $E^*$, but as erosion rate becomes large, $R^*$ is limited and ceases to increase significantly with increasing $E^*$. This framework allows us to compare the morphology of landscapes in contrasting bedrock lithologies and climates (e.g. Gabilan Mesa verses Oregon Coastal Range as shown in Figure 1.4), where constraints can be placed on $C_{HT}$, $L_H$ and $S_C$, all of which can be readily quantified from LiDAR data.

The objectives of this thesis (see section 1.3) were principally tackled keeping in mind the framework described by Roering et al. (2007) and presented above. The framework is an appealing context in which to explore hillslope morphology because it facilitates comparison of real topography to model predictions. Large datasets of hillslope morphology can also be collapsed into two parameters, $E^*$ and $R^*$, to facilitate easy quantitative and visual comparison (e.g. Figure 1.4). I recognised the resulting potential to generate large datasets on the spatial distribution of hillslope morphology which would allow me to validate (or otherwise) the analytical relationships presented by Roering et al. (2007), particularly whether a linear relationship between $E$ and $C_{HT}$ exists, and whether distributions of $E^*$ vs $R^*$ match those predicted by the model, assuming steady-state. Subsequently I could also address previously unexplored questions regarding the spatial distribution of erosion rate and its variation based on hilltop curvature, and to look at how hillslope morphology varies in transient landscapes through comparison to steady-state predictions made by Equation 1.9.

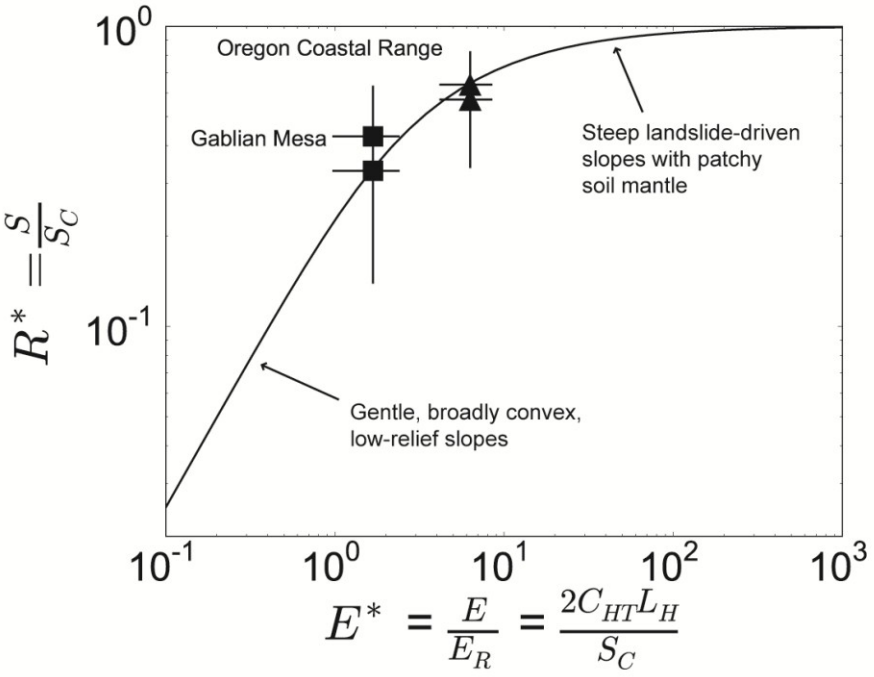


Figure 1.4: Relationship between dimesionless erosion rate and dimensionless relief predicted for steady state hillslopes using Equation 1.9 (solid line) and the results for two mature landscapes assumed to be in steady-state in the western USA. There are two symbols per site due to using two different approaches to calculating $R^*$, $R^* = S/S_C$ and $R^* = R/(L_H S_C)$. Recreated from Roering et al. (2007).

## *1.5 Thesis Outline*

This thesis consists of three main chapters, each of which is presented in paper format and as such can be treated as a standalone body of work. However taken sequentially this work builds an understanding of the controls on hillslope morphology and how I can interpret morphology to infer boundary conditions driving hillslope evolution.

The focus of chapter two is to constrain erosion rates at the scale of individual hillslopes.. The chapter tests the utility of hilltop curvature for estimating erosion rates using a LiDAR derived DEM. Erosion rates are constrained from published and new cosmogenic radionuclide (CRN) analysis in the Feather River basin, California, where erosion rates vary by over an order of magnitude (10 to 200 mm $ka^{-1}$). I demonstrate that erosion rates scales non-linearly with slope/relief but linearly with hilltop curvature, allowing calibration of $D$, which controls the relationship between gradient and sediment flux. I then go on to estimate erosion rates throughout the landscape by mapping the spatial distribution of hilltop curvature. Hilltop curvature continues to increase with increasing erosion rates after gradient-limited hillslopes have emerged and therefore hilltop curvature can potentially reflect higher erosion rates than can be predicted by hillslope gradient. Hilltop curvature can be used to estimate erosion rates in landscapes undergoing a transient adjustment to changing boundary conditions if the response timescale of hillslopes is short compared to channels. Finally I make predictions about the likely path hillslope morphology follows in dimensionless parameter space (Figure 1.4) when undergoing adjustment, predictions that are treated in more detail in chapter five. This paper has been published in the *Journal of Geophysical Research: Earth Surface* (Hurst et al., 2012).

Chapter three builds on the results presented in chapter two to investigate the influence of varying substrate lithology on hillslope morphology in the Feather River. Many geomorphic studies focus on landscapes with roughly uniform bedrock geology to isolate drivers of geomorphic change such as climatic or tectonic processes. Underlying geology influences the efficacy of soil production and transport on hillslopes, and resistance to erosion by valley-forming processes. I perform similar analyses to those presented in chapter two to search for a topographic signature of hillslopes in two distinct lithologies: granodiorite and metavolcanics. The two sites are separated by less than 2 km and span similar elevations so are assumed to have similar climatic and denudation histories. Responding to increased erosion rates, transient hillslopes exhibit high gradient but low hilltop curvature in the metavolcanics, similar to expected style of transience predicted at the end of chapter two. However hillslopes in the granodiorite have, for the most part, morphology similar to model predictions for steady state hillslopes. I use the curvature of hilltops adjacent to main stem channels to infer that $D$ is two times larger in the granodiorite. Hillslopes get shorter as erosion rates increase due to the increased influence of debris flows in valley incision, so that that drainage density increases with erosion rate. I find that an incision wave associated with increased erosion in the Feather River has propagated further into a basin developed on the metavolcanics and infer this substrate is less resistant to channel incision. Finally I present an inventory of values for the transport coefficient for hillslope sediment transport to highlight that no clear patterns emerge with varying lithology. This paper has been published in the *Journal of Geophysical Research: Earth Surface* (Hurst et al., 2013).

Chapter four focuses on developing an understanding of the style of morphological adjustment a hillslope undergoes when forced to increase or decrease its erosion rate. This is achieved through analysis of a landscape with a well constrained uplift field adjacent to the San Andreas Fault (SAF), California. The Dragon's Back pressure ridge offers a unique opportunity to substitute space for time

in a real landscape in order to understand the morphological response of hillslopes to both the onset and cessation of uplift and the resulting erosion (Hilley and Arrowsmith, 2008). Understanding the nature of hillslope morphological adjustment to various transient boundary conditions may allow interpretation of the style of transience and magnitude of change in boundary conditions based on hillslope morphology alone. Hillslope morphology was found to be sensitive to not only to erosion rate indicators but also the style of transience the hillslope is experiencing. Thus hillslope morphology differs for hillslopes adjusting to increased erosion compared to those responding to cessation of uplift, which can aid subsequent interpretation of tectonic boundary conditions. The results presented also highlight that the techniques developed for this thesis may be applicable to the study of active tectonics with a view to earthquake hazard prediction in settings where there is little historical evidence of seismicity. Instead hillslope morphology may be indicative of active faulting. This paper has been submitted to *Nature Geoscience*.

Finally in chapter five the findings of this thesis are placed in the broader context of current theory on hillslope geomorphology and the use of topographic indicators of surface process rates. The significance and implications of these findings are discussed and future research needs highlighted, as well as suggestions for the applicability of the techniques developed for this thesis to outstanding problems.

# 2 HILLTOP CURVATURE PREDICTS THE SPATIAL DISTRIBUTION OF EROSION RATES

A version of this chapter has been published:

Hurst, M. D., S. M. Mudd, R. Walcott, K. Yoo, and M. Attal, (2012) Hilltop Curvature Predicts the Spatial Distribution of Erosion Rates, *Journal of Geophysical Research – Earth Surface*, 117, F02017, doi:10.1029/2011JF002057.

## *Chapter Abstract*

Erosion rates dictate the morphology of landscapes and therefore quantifying them is a critical part of many geomorphic studies. Methods to directly measure erosion rates are expensive and time consuming, whereas topographic analysis facilitates prediction of erosion rates rapidly and over large spatial extents. If hillslope sediment flux is nonlinearly dependent on slope then the curvature of hilltops will be linearly proportional to erosion rates. In this contribution I develop new techniques to extract hilltop networks and sample their adjacent hillslopes in order to test the utility of hilltop curvature for estimating erosion rates using high-resolution (1 m) digital elevation data. Published and new cosmogenic radionuclide analyses in the Feather River basin, California, suggest that erosion rates vary by over an order of magnitude (10 to 250 mm $ka^{-1}$). Hilltop curvature increases with erosion rates, allowing calibration of the hillslope sediment transport coefficient, which controls the relationship between gradient and sediment flux. Having constraints on sediment transport efficiency allows estimation of erosion rates throughout the landscape by mapping the spatial distribution of hilltop curvature. Additionally, I show that hilltop curvature continues to increase with rising erosion rates after gradient-limited hillslopes have emerged. Hence hilltop curvature can potentially reflect higher erosion rates than can be predicted by hillslope gradient, providing soil production on hilltops can keep pace with erosion. Finally, hilltop curvature can be used to estimate erosion rates in landscapes undergoing a transient adjustment to changing boundary conditions if the response timescale of hillslopes is short relative to channels.

## 2.1 Introduction

The topographic form of landscapes reflects interplay between tectonics and climate-driven surface processes. These interactions dictate erosion rates and control topography since tectonic processes generally act to increase slope, whilst climate modifies the efficiency of erosional processes. Quantitative understanding of relationships between erosion rates and landscape morphology is essential to geomorphic and geochemical modelling efforts, which aid my ability to interpret landscape form (e.g. Tucker and Hancock, 2010; Yoo and Mudd, 2008b). Moreover, if critical relationships between topographic form and erosion rates can be identified there is potential to interpret tectonic or climatic conditions based on topography alone (e.g. Ahnert, 1970; Burbank et al., 1996; Wobus et al., 2006a). Knowledge of erosion rates at the scale of individual hillslopes is important to understanding sediment production and nutrient cycling (e.g. Heimsath et al., 1997; Porder et al., 2007; Yoo and Mudd, 2008a), and the processes that supply sediment to channels (e.g. Roering et al., 2010; Roering et al., 2007).

The interdependency of topography and erosion rate has been established through the demonstration that hillslope gradient and topographic relief increase with erosion rates (e.g. Ahnert, 1970; Gilbert, 1877; Montgomery and Brandon, 2002; Palumbo et al., 2010). However, several studies have identified that any such relationship breaks down at high erosion rates as hillslope angles reach a limiting gradient (e.g. Binnie et al., 2007; Burbank et al., 1996; DiBiase et al., 2010; Matsushi and Matsuzaki, 2010; Montgomery, 2001; Ouimet et al., 2009; Schmidt and Montgomery, 1995). DiBiase et al. (2010) have recently shown that mean slope derived from high resolution topography (1m) whilst non-linearly related to erosion rates, continues to increase with erosion rates beyond those at which limited slope angles have been observed in coarser (>10 m) topographic datasets.

Characteristics of the longitudinal profiles of rivers have also been used successfully to infer the distribution of erosion rates in a landscape. Assuming that channel form and evolution can be approximated by a model for bedrock channel evolution in which erosion rate is proportional to bed shear stress or stream power (Whipple and Tucker, 1999), the channel steepness index (a measure of channel slope normalised for drainage area) should increase with erosion rate (e.g. Cyr et al., 2010; DiBiase et al., 2010; Kirby et al., 2007; Kirby et al., 2003; Ouimet et al., 2009; Snyder et al., 2000; Wobus et al., 2006a). Both Ouimet et al. (2009) and DiBiase et al. (2010) demonstrated a non-linear relationship between basin-averaged channel steepness indices and basin-averaged erosion rates in a landscape where hillslopes are invariantly steep. Cyr et al. (2010) demonstrated that channel steepness may reflect erosion rates where hillslopes have become decoupled or lithologic contrasts prevent hillslope gradient from being an appropriate topographic metric. Channel steepness indices have been particularly successful as an erosion rate metric in studies focusing at the scale of entire mountain belts, in landscapes with rapid erosion and steep hillslope gradients (e.g. DiBiase et al., 2010; Kirby and Ouimet, 2011; Ouimet et al., 2009).

The relationship between fluvial incision rates and channel steepness indices is complicated by the existence of thresholds for fluvial erosion (Attal et al., 2011; Snyder et al., 2003b) which have been demonstrated to cause nonlinearity in the relationship between channel steepness indices and erosion rate (DiBiase and Whipple, 2011). Channel width adjustments in response to changes in boundary conditions (Finnegan et al., 2005; Whittaker et al., 2007b) may also influence the distribution of erosion and therefore steepness indices (Attal et al., 2011), so quantifying variation in channel widths is important if one is to apply this erosion metric (DiBiase and Whipple, 2011; Kirby and Ouimet, 2011). The presence or absence of fluvial sediment can also significantly modulate erosion rates by providing the tools which drive erosion or acting as a protective cover to underlying bedrock (Cowie et al., 2008; Sklar and Dietrich, 1998).

Channel steepness is an appropriate metric for erosion rate where valley forming processes become dominantly fluvial (typically at drainage areas >1 $km^2$ (e.g. Montgomery and Dietrich, 1988; Montgomery and Foufoula-Georgiou, 1993; Stock et al., 2005b)). Hence, channel steepness is an inappropriate metric at the hillslope scale. The geomorphic characteristics of hillslopes have the potential to overcome this scale problem (Mudd and Furbish, 2007) and would not be subject to the same limitations as channel-based erosion rate metrics. The ability of hillslopes to reflect their boundary conditions is primarily dictated by the rate at which they respond to changes in erosion rates, with rapid response favouring the use of hillslope properties as erosion rate metrics.

My principal objective was to develop a method for using topographic metrics to infer erosion rates that i) can be applied where erosion rates are rapid enough that hillslope gradients become invariably steep, ii) can be applied at hillslope or zero-order basin scale, and iii) can be applied in landscapes experiencing a range of erosion rates due to transient adjustment in the channel network. My strategy used a novel technique which exploits the topography of hilltops throughout a landscape. It has previously been established that where hillslope sediment transport can be approximated as a non-linear function of slope, the curvature of hilltops is linearly related to erosion rates (Andrews and Bucknam, 1987; Roering et al., 1999). My approach relied on hilltops being soil-mantled and assumptions that sediment transport on hilltops is dominated by creep-like processes, the efficacy of which is assumed spatially and temporally constant. Hilltop curvature has previously been used to predict erosion rates for individual hillslopes in landscapes where hilltops are soil-mantled and assumed to be in steady state (Roering et al., 2010; Roering et al., 2007). Here, for the first time, I develop algorithms to extract and analyse individual hillslopes across entire landscapes in order to assess the utility of hilltop curvature as an erosion rate metric and indicator of the spatial distribution of erosion rates across entire landscapes, and under conditions of landscape transience.

In this contribution, I used a high-resolution (1 m) digital elevation model (DEM) derived by airborne light detection and ranging (LiDAR) by the National Center for Airborne Laser Mapping (NCALM). I used the DEM to compare hilltop curvature with erosion rates derived from cosmogenic radionuclides (CRN) in the Feather River basin in the northern Sierra Nevada of California. From the resulting relationship between erosion rate and hilltop curvature I estimated the efficiency of sediment transport, allowing us to predict erosion rates across the entire landscape. To do this, I developed new techniques to define hilltops and their adjacent dispersing hillslopes, and then extracted the important geomorphic parameters of hilltop curvature, mean slope, hillslope relief and hillslope length.

## 2.2 Theoretical Background

The form and evolution of hillslopes in soil-mantled landscapes has been predominantly investigated through principles of conservation of mass (Dietrich et al., 2003). Such an approach was first described qualitatively by Gilbert (1909) and expressed mathematically by Culling (1960). Here I consider a hillslope in a moving reference frame where the surface elevation $\zeta$ [L], (dimensions of [M]ass, [L]ength and [T]ime denoted in square brackets) is measured relative to the elevation of a moving reference elevation $\zeta_0$ [L] (e.g. Mudd and Furbish, 2005). The surface elevation is then:

$$\frac{\partial \zeta}{\partial t} = -\frac{\partial \zeta_0}{\partial t} - \nabla \cdot q_s \qquad [2.1]$$

where $q_s$ [$L^2$ $T^{-1}$] is volumetric sediment flux per unit width and $t$ is time. I assume that mass gain/loss due to aeolian processes is negligible. My mass balance does not account for volume changes in soils due to chemical denudation. Riebe et al. (2001b)

demonstrated that chemical denudation scales with total denudation in my study area, but that chemical denudation rates are small compared to physical denudation rates and should have minimal impact on hillslope morphology (e.g. Mudd and Furbish, 2004).

The choice of reference elevation is arbitrary but it is convenient to equate the lowering rate of the reference elevation to the rate of local base-level lowering at the base of the hillslope ($E$, [L $T^{-1}$] i.e., the bedrock stream incision) such that:

$$\frac{d\zeta_0}{dt} = -\frac{\rho_r}{\rho_s} E \qquad [2.2]$$

where $\rho_r$ and $\rho_s$ [M $L^{-3}$] are the densities of bedrock and dry soil, respectively. If the entire hillslope lowers at the same rate as the channel then Equation (2.1) reduces to:

$$\frac{\rho_r}{\rho_s} E = \nabla q_s \qquad [2.3]$$

On gently inclined hillslopes where gravity driven sediment flux occurs due to creep-like processes, $q_s$ can be approximated as a linear function of slope. The convex profile of hillslopes was first attributed to slope dependent soil creep by Davis (1892) and Gilbert (1909), who observed that hillslope gradients tended to increase steadily with distance from topographic divides (hilltops). Hillslopes often become planar away from topographic divides in high relief landscapes, hypothesised to be driven both by a process transition to landslide-dominated sediment flux (e.g. Binnie et al., 2007; Roering et al., 2007) and the associated increase in particle displacement distances during transport (e.g. Foufoula-Georgiou et al., 2010; Tucker and Bradley, 2010). This transition can be approximated by

coupling a linear, slope dependent model for sediment flux driven by soil creep (Culling, 1960) with a threshold hillslope angle ($S_{Th}$) beyond which sediment flux is infinite so that steeper slopes cannot be maintained (e.g. Densmore et al., 1998; Howard, 1994):

$$q_s = -D\nabla\zeta; \qquad \nabla\zeta < S_{Th} \qquad [2.4a]$$

$$q_s = \infty; \qquad \nabla\zeta \geq S_{Th} \qquad [2.4b]$$

where $D$ [$L^2T^{-1}$] is a transport coefficient and $\zeta$ [L] is the elevation of the surface. A similar flux law has been formulated by allowing sediment flux to increase in a non-linear fashion with hillslope gradient so that as slope approaches a critical angle ($S_C$), sediment flux asymptotically approaches infinity (Andrews and Bucknam, 1987; Roering et al., 1999):

$$q_s = -D\nabla\zeta\left[1-\left(\frac{|\nabla\zeta|}{S_C}\right)^2\right]^{-1} \qquad [2.5]$$

The applicability of this nonlinear, diffusion-like transport equation is limited by the need for transport limited conditions, that is to say that the availability of soil/regolith for transport is plentiful such that landscape morphology is dictated by the efficacy of transport sediment rather than limited by the need to weather bedrock. When hillslope gradient $\nabla\zeta$ is small enough for the bracketed term in Equation 2.5 to be negligible, I can substitute Equation 2.5 into Equation 2.3 and solve for erosion rates where slope angles are low (i.e. on hilltops):

$$E = -\frac{\rho_s}{\rho_r} D\, C_{HT} \qquad [2.6]$$

where $C_{HT}$ is the hillslope curvature, i.e.$\nabla^2 \zeta$ at the hilltop, since this is where I expect slope to be lowest. Equation 2.6 states that the erosion rate on a steadily denuding hillslope is a linear function of the Laplacian of elevation at the hilltop $C_{HT}$ and the transport coefficient $D$.

Roering et al. (2007) provided a comprehensive framework for analysing relationships between denudation and topography by deriving analytical solutions for the form of steady state hillslopes governed by Equation 2.5. Moreover they non-dimensionalised erosion rate and relief to allow comparisons between landscapes with distinct process rates and morphology. They also cast dimensionless erosion rate and relief as functions of readily quantifiable topographic parameters. Dimensionless relief was defined according to $R^* = R / (S_c L_H)$ (hillslope relief $R$ is the elevation difference between hilltop and channel $\zeta(x=0)-\zeta(x=L_H)$) and dimensionless erosion rate was defined as $E^* = E / E_R$ where $E_R$ [$LT^{-1}$] is a reference erosion rate defined by:

$$E_R = \frac{D S_C}{2 L_H (\rho_r / \rho_s)} \qquad [2.7]$$

By combining Equation 2.7 and Equation 2.6 they defined dimensionless erosion rate as a function of topographic attributes $C_{HT}$ and $L_H$, so that for steady state hillslopes $E^*$ is proportional to $E$:

$$E^* = \frac{E}{E_R} = \frac{2 C_{HT} L_H}{S_C} \qquad [2.8a]$$

Furthermore, by deriving the elevation profile of a one dimensional hillslope analytically and nondimensionalising, Roering et al. (2007) solved for a nonlinear relationship in dimensionless relief as a function of dimensionless erosion rate, with $R^*$ tending to a value of 1 at high $E^*$ (see section 1.4.3 for full derivation):

$$R^* = \frac{\overline{S}}{S_C} = \frac{1}{E^*}\left\{ \sqrt{1+(E^*)^2} - \ln\left[\frac{1}{2}\left( 1+\sqrt{1+(E^*)^2} \right)\right] - 1 \right\} \qquad [2.8b]$$

where $\overline{S}$ is the mean gradient of the along the entire hillslope length.

Similarly, predictions of a relationship between dimensionless erosion rate and relief were derived for the threshold sediment transport model (Equation 2.4) by DiBiase et al. (2010) following the same nondimensional scheme:

$$R^* = 1 - \frac{1}{E^*}; \qquad E^* \geq 2 \qquad [2.9a]$$

$$R^* = \frac{E^*}{4}; \qquad E^* < 2 \qquad [2.9b]$$

Since topographic parameters $C_{HT}$, $L_H$ and $\overline{S}$ can be extracted from high resolution topography, relationships between erosion rate (following Equation 2.8a) and topographic form ($R^* = \overline{S} / S_C$) can be investigated in a non-dimensional framework. For hillslopes governed by either Equation 2.4 or Equation 2.5, as erosion rates increase, relief initially increases, but since relief is limited (through $S_{Th}$ or $S_C$), it becomes insensitive to changes at high erosion rates (Andrews and Bucknam, 1987; Binnie et al., 2007; Burbank et al., 1996; Howard, 1994; Roering et al., 1999). The non-linear and threshold models (Equations 2.8 and 2.9 respectively) are distinct at intermediate erosion rates ($E^*$ in range 1 to 10) where Equation 2.8b predicts lower

$R^*$ than Equation 2.9 for a given value of E*. Therefore quantifying $E^*$ and $R^*$ may allow for distinguishing the applicability of flux models based on topography alone (DiBiase et al., 2010).

Both the threshold (Equation 2.4) and non-linear (Equation 2.5) flux models have empirical and experiment support (e.g. Gabet, 2000; Pelletier and Cline, 2007; Roering et al., 2001b). Equation 2.6 is applicable in both cases since it could also be derived by substituting Equation 2.4 (instead of 2.5) into Equation 2.3. Hilltop curvature should thus scale with erosion rates beyond the critical erosion rate for producing steep, planar hillslopes, providing soil production rates on the hilltops can keep pace (i.e. the landscape isn't stripped to bedrock; soil/regolith must remain readily available for transport). The maximum attainable rate of soil production is critical to the application of hilltop curvature as a metric for erosion rate, because the ability of soil production on hilltops to keep pace with erosion rates is a prerequisite to the validity of Equation 2.6. Since Equations 2.4 and 2.5 allow soil transport to tend to infinity on steep slopes, soil may be stripped and bedrock may be exposed on hillslopes. Despite this, I require hillslope material to remain readily transportable such that hilltop morphology is controlled by the ability to transport material rather than the ability to generate material from underlying bedrock.

Critically, the application of Equation 2.6 to predict erosion rates does not require an entire drainage basin to be in steady state, but only that each hillslope is fully adjusted to the rate of incision of the adjacent channel (i.e. so that the hilltop curvature is adjusted to this lowering rate). Therefore, in a landscape where the response time of the hillslopes is short relative to that of the stream network, hillslope morphology should keep pace with channel erosion rates, permitting the use of hilltop curvature as a surrogate for erosion rate. The response times of hillslopes governed by Equation 2.5 are set primarily by hillslope length (longer hillslopes take longer to respond), and the transport coefficient $D$ (more efficient transport results in a more rapid response). The rate of base-level fall also plays a role since steep planar

hillslopes can respond more rapidly to changing rate of base-level fall than a gentle hillslope due to the nonlinearity in sediment transport rates with hillslope gradients (I discuss hillslope response times in more detail in section 2.6).

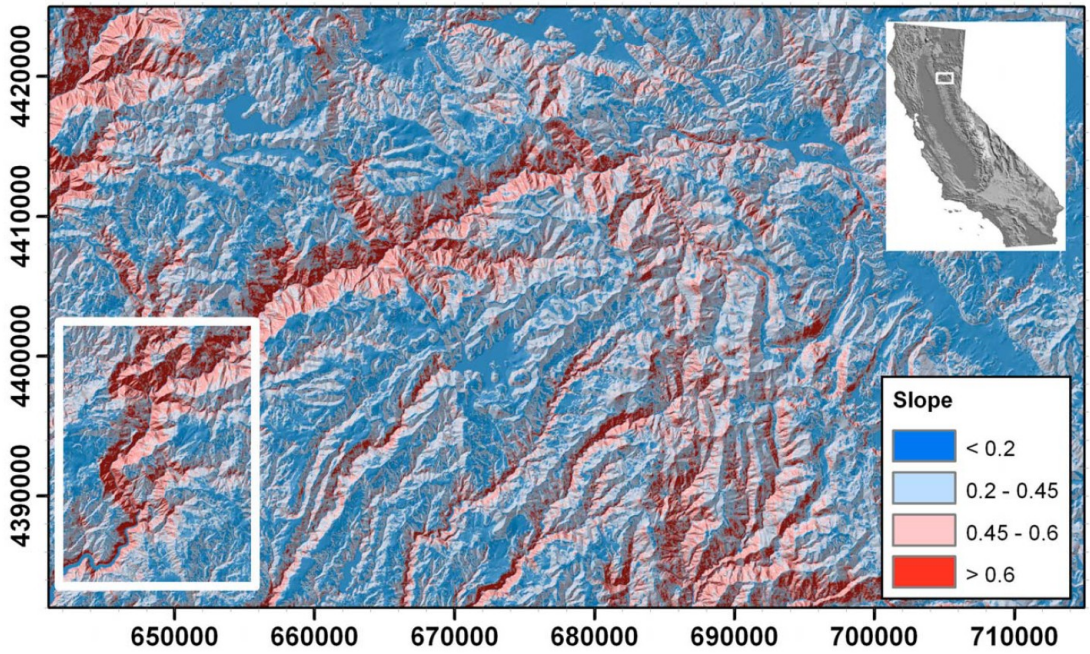


Figure 2.1: Shaded slope map for my study site in the Feather River (Middle Fork) basin, Sierra Nevada (inset map shows location of the study area in California). White box shows the extent of the ALSM-derived topographic dataset. The relict upland landscape with low slopes depicted in blue is dissected by the canyon of the Feather River and its tributaries with steeper slopes, depicted in red. The spatial reference system is UTM Zone 10N with spatial units in metres.

## 2.3 Field Setting

Our field site is located in the lower reaches of the Middle Fork Feather River, in the northern Sierra Nevada of California (Figure 2.1). The Sierra Nevada microplate is a west-tilted fault block of Mesozoic granites, granodiorites and tonalites of the Sierra Nevada batholith with emplacement occurring during Cretaceous arc volcanism. The microplate is bound to the west by the San Andreas Fault system and to the east by the escarpment of a transtensional (dextral) frontal fault system (Unruh, 1991). The westward tilting of the fault block is recorded in the topography by the tilting of a relict landscape, with the western side of the range sloping gently away from the summit crest line toward the Great Valley to the west (Saleeby et al., 2009). The relict surface is dissected by main river drainages which have incised deep canyons (Figure 2.1).

The relict surface is interpreted as the remnant of the western edge of an orogenic plateau surface (Nevadoplano) which existed into the early Cenozoic (Busby and Putirka, 2009). Apatite fission track (AFT) dates reveal an average erosion rate of 40 mm $ka^{-1}$ for the relict landscape, persisting until at least 32 million years ago (Ma) (Cecil et al., 2006). This is slightly higher than CRN-derived denudation rates (millennial timescale) reported for summit flats (2-19 mm $ka^{-1}$) (Riebe et al., 2000; Small et al., 1997) and for low relief basins on the relict surface (~20-40 mm $ka^{-1}$) (Riebe et al., 2000; Stock et al., 2005a) in the study area. Thermochronology studies suggest that the relief of modern catchments in the Sierra Nevada may have developed in the late Cretaceous (House et al., 1998; House et al., 2001) and thus the modern drainage pattern is likely to be antecedent. The Feather River traverses the northern Sierra Nevada, dissecting the relict surface to generate a deep canyon, providing an excellent natural laboratory for this study. This

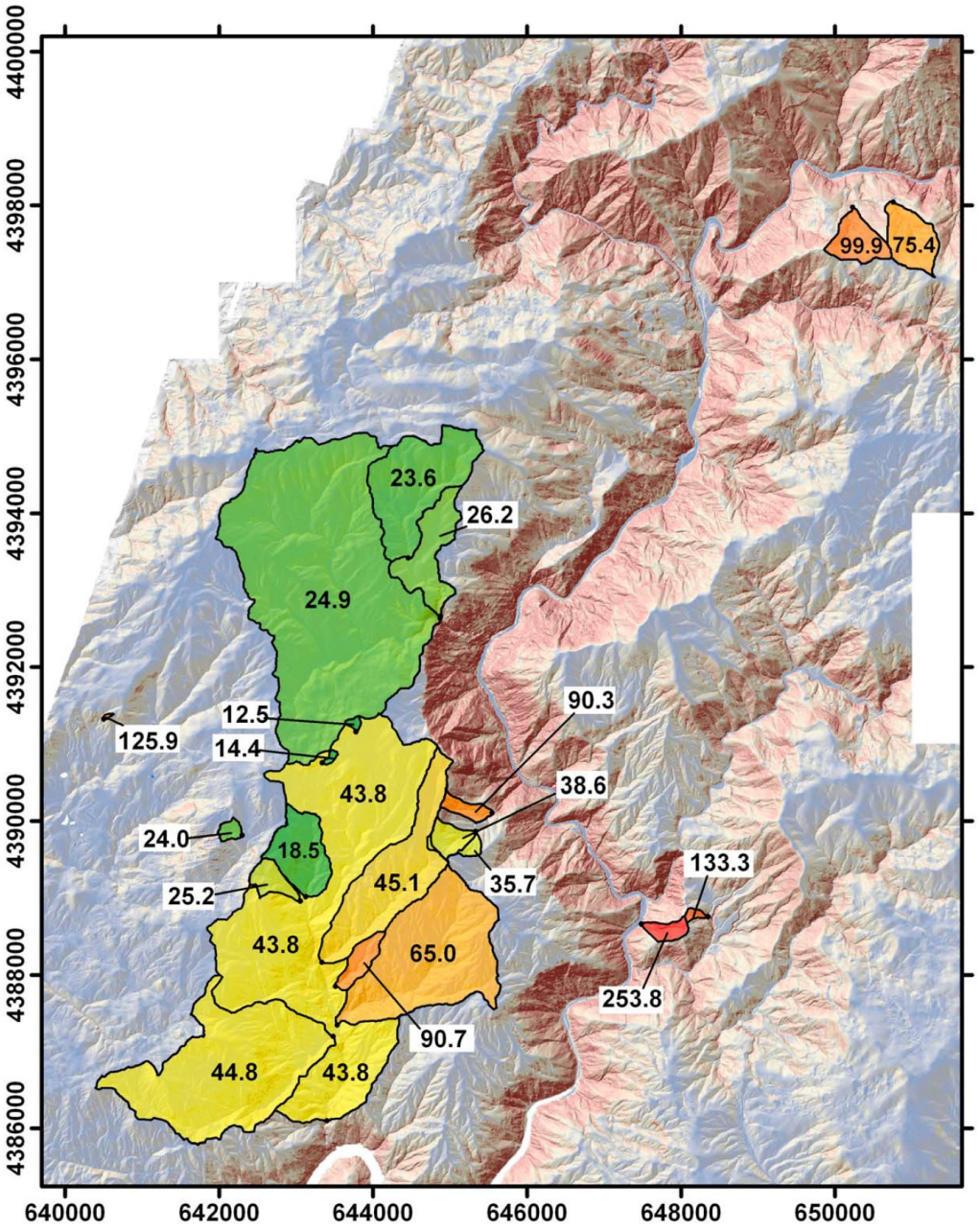


Figure 2.2: High resolution (ALSM-derived) shaded slope map of study site (low gradients are blue, steep slopes are red). Overlain are CRN sample sites with estimated basin-averaged erosion rates in mm $ka^{-1}$ (shaded green to red with increasing erosion rate). Samples were taken for basins exclusively in granitoid bedrock. Erosion rates vary over an order of magnitude from the canyon to the adjacent relict upland. The spatial reference system is UTM Zone 10N with spatial units in metres.

morphology is clear from the distribution of slope angles in the basin, with steep slopes (>~ 0.6) mainly occurring immediately adjacent to the Feather River and the largest tributaries (Figure 2.1). This relief structure is generally accepted to be the result of accelerated incision along the major river systems as recorded by elevation differences between recent (< 5 Ma) volcanic which filled major valleys and the current valley floor (Wakabayashi and Sawyer, 2001). Knickpoints in channel profiles throughout the Sierra Nevada are interpreted as a pervasive signal of accelerated channel incision (Clark et al., 2005; Figueroa and Knott, 2010). The landscape transience has been interpreted to have initiated by accelerated uplift c. 3.5-5 Ma (Stock et al., 2004; Wakabayashi and Sawyer, 2001), possibly caused by the delamination of an eclogite root beneath the mountain range (Jones et al., 2004; Saleeby and Foster, 2004). Isostatic unloading has been suggested as a possible uplift mechanism however such a means is unable to account for all uplift in the Sierra Nevada (Small and Anderson, 1995; Stock et al., 2005a).. Erosion rates in and adjacent to the canyon quantified by comsogenic radionuclide analysis (millennial timescales) and by dating of perched volcanic (rates averaged over their lifespan) significantly exceed those predicted by AFT (>200 mm $ka^{-1}$; (Riebe et al., 2000; Wakabayashi and Sawyer, 2001); Figure 2.2). Long term exhumation rates derived from (U-Th)/He ages fail to record late-Cenozoic acceleration in denudation, implying that less than 3 km of the crust has been exhumed since the acceleration (Cecil et al., 2006).

Despite rapid denudation rates, much of the landscape remains forested and soil-mantled (Figure 2.3). Yoo et al. (2011) documented that soil depth appears not to vary with erosion rates and instead argued that it is primarily set by the rooting depth of vegetation (see Appendix 1). The presence of a thick soil cover supports the assumption that hillslopes are in a transport-limited state, which is required by Equation 2.5 and subsequent derivations (particularly Equations 2.6 and 2.8). The analysis presented in this and the following chapter focuses on soil-mantled areas of the landscape. The modern climate is semi-arid with a strong precipitation gradient

from the dry Central Valley of California to the high elevations of the Sierra Nevada Mountains. In the vicinity of my study site (Figure 2.1, 2.2), mean annual temperature (MAT) is on the order 12.5°C and mean annual precipitation (MAP) is 1750mm (data from the PRISM Climate Group, Oregon State University, http://prism.oregonstate.edu (accessed 7th July 2011; Daly (1997)). The Feather River basin remained largely unglaciated during the Pleistocene, except for its uppermost reaches (Clark, 1995; Wahrhaftig and Birman, 1965). Erosion rates in the Sierra Nevada are insensitive to climatic variability but highly sensitive to tectonic forcing and Holocene erosion rates have seemingly been relatively uniform (Riebe et al., 2001a).

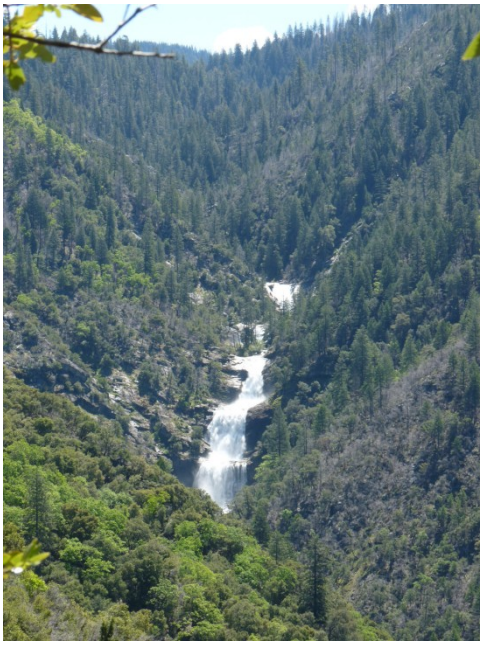

Figure 2.3: Photograph of Cascade River, a large tributary to Feather River. Channel is steep due to presence of a knickpoint associated with increased erosion rate in the channel. Hillslopes retain soil-mantle despite increased erosion rate.

## 2.4 Methods

### 2.4.1 Denudation rates from Cosmogenic Radionuclides

Cosmogenic radionuclides (CRNs) are chemical isotopes formed due to the bombardment of matter by cosmic rays (protons, neutrons, muons and α-particles). High energy cosmic ray particles collide with atoms, which split to produce cosmogenic radionuclides such as $^{3}$He, $^{10}$Be, $^{14}$C, $^{21}$Ne, $^{26}$Al and $^{36}$Cl. These reactions occur in the Earth's atmosphere and in the near-surface producing meteoric and *in situ* CRNs respectively. Understanding the rate at which these radionuclides are produced in the near-surface (i.e. in soil or rock) facilitates estimating how long the soil or rock has been accumulating CRNs, provided that the concentration of CRNs can be measured. The development of accelerator mass spectrometry (AMS) to measure the abundance of radionuclide isotopes lead to the rapid development of analysis of CRNs in the geosciences since pioneering studies appeared in the mid to late 1980's (e.g. Nishiizumi et al., 1986b; Phillips et al., 1986). CRNs now have a range of applications in the geosciences such as for dating rock exposures (e.g. Dunai et al., 2005; Ivy-Ochs et al., 1995), sedimentary deposits (e.g. Granger, 2006), and understanding process rates such as erosion (e.g. Bierman and Steig, 1996; Binnie et al., 2007; Brown et al., 1995; Codilean et al., 2008; DiBiase et al., 2010; Granger et al., 1996; Ouimet et al., 2009), sediment transport (e.g. Clapp et al., 2001; Riggins et al., 2011b), soil production (e.g. Clapp et al., 2002; Heimsath et al., 1997; Heimsath et al., 1999; Small et al., 1999; Wilkinson et al., 2005b) and chemical weathering (e.g. Kirchner et al., 2006; Riebe et al., 2004).

This thesis utilises the measurement of $^{10}$Be accumulated in quartz ($SiO_2$) in fluvial sediments to determine average erosion rates within a drainage basin (Bierman and Steig, 1996; Brown et al., 1995; Granger et al., 1996). $^{10}$Be is the most commonly utilised CRNs in geoscience studies, though $^{3}$He, $^{14}$C, $^{21}$Ne, $^{26}$Al and $^{36}$Cl are also used widely (Dunai, 2010; Gosse and Phillips, 2001). Here a brief outline of

the theory and physics behind the production of CRNs is presented, focused on $^{10}Be$ and its application to determining spatially and temporally averaged erosion rates within a river catchment. The approach requires the measurement of $^{10}Be$ concentrations in a sample of river sediment by AMS and the interpretation of this quantity given constraints on the expected rate of production in the sample catchment and consideration of any shielding to production the sample may have experienced. I present the physics behind cosmogenic nuclide production and discuss the controls on production including shielding. Details of sampling strategy and sample preparation in the laboratory are then presented before a detailed account of how a measured concentration is interpreted in terms of a basin averaged erosion rate.

#### *2.4.1.1 Theory and Physics of Cosmogenic Radionuclides*

CRNs are produced in the atmosphere and in the near-surface of the Earth due to the interaction of cosmic rays with matter. The Earth is under continual bombardment by cosmic radiation. This radiation consists of high energy cosmic rays (100 MeV - 10 GeV) comprising positively charged particles sourced from supernova events within my galaxy, and lower energy cosmic rays sourced from Earth's own sun (Dunai, 2010). The lower energy solar cosmic rays do not contribute significantly to CRN production (Masarik and Reedy, 1995). Upon reaching the top of Earth's atmosphere these primary cosmic rays typically consist of protons (87%) and α-particles (12%) plus some heavier nuclei (Simpson, 1983). This primary cosmic radiation interacts with the Earth's magnetic field and atmosphere to produce secondary cosmic rays.

Charged particles interact with the Earth's magnetic field such that only the highest energy particles can enter the Earth's atmosphere at low geomagnetic latitudes, since low energy particles are more likely to be deflected towards the poles (depending on their rigidity; a measure of momentum per unit charge). Whether an individual particle is deflected depends on its rigidity compared to the cut-off

rigidity, i.e. the minimum rigidity which permits penetration of Earth's magnetic field (Gosse and Phillips, 2001). Cut-off rigidity is a function of latitude, being highest at the equator where cosmic rays have an incident angle perpendicular to Earth's magnetic field. Therefore there is a pole-ward increase in the transmission of cosmic rays through the magnetosphere until ~60° latitude, beyond which cosmic rays at all energy levels are permitted to penetrate the geomagnetic field and thus the cosmic ray flux to the atmosphere is greatest (Dunai, 2010). As a result, CRN production rates must be scaled for latitude (Lal, 1991).

Upon entering the atmosphere primary cosmic rays react with atomic nuclei to produce secondary cosmic radiation. The energy of primary cosmic rays far exceeds the binding energy of atomic nuclei in the atmosphere resulting in spallation reactions in which material is ejected (from the target nucleus) due to the impact of a projectile (cosmic ray). The ejected particles cause subsequent collisions until their energies are reduced, producing a nuclear cascade (Gosse and Phillips, 2001). This process results in the cosmic ray flux changing from being proton to neutron dominated. The highest energy primary cosmic rays interact with the atmosphere to produce muons (Dunai, 2010). Whilst the production of CRNs is dominated by the nucleonic component, muogenic production can be significant, particularly in rapidly eroding landscapes as will be discussed further. Secondary cosmic rays are responsible for the production of CRNs both in the atmosphere (meteoric production) and in rock and sediment at the Earth's surface (*in-situ* production). The former, atmospherically produced $^{10}$Be has been used in studies of hillslope soil processes (McKean et al., 1993; Monaghan et al., 1992). Exposure age and erosion rate studies are concerned with *in-situ* produced rather than this 'garden-variety' $^{10}$Be. Since spallation reactions occur in the atmosphere, the secondary cosmic ray flux is attenuated before reaching the Earth's surface. Therefore, production rates must also be scaled for atmospheric depth, or equivalent surface elevation or air pressure (Desilets et al., 2006; Dunai, 2000; Lal, 1991; Lifton et al., 2005; Stone, 2000). Production by muons both in the atmosphere and *in-situ* has a much longer

attenuation length and can be modelled independently (Heisinger et al., 2002a; Heisinger et al., 2002b; Stone, 2000).

#### 2.4.1.2 Production of $^{10}$Be in Rock and Soil

Production of $^{10}$Be in the near-surface (mainly in the upper 1 m) is dominated by spallation reactions, with minor contributions occurring by negative muon capture and fast muon interaction. Muon contribution is often considered negligible for relatively erosion rates (> 10 mm $ka^{-1}$) (DiBiase et al., 2010). Calculating the production rate of cosmogenic radionuclides requires scaling for latitude and altitude. Production is scaled with respect to measured production rates at high latitude and low altitude (~5.1 ± 0.3 atoms $g^{-1}$ $yr^{-1}$) (Stone, 2000), and various scaling schemes have been proposed (Desilets et al., 2006; Dunai, 2000; Lal, 1991; Lifton et al., 2005; Stone, 2000). The decline in production as a function of depth within rock ot soil follows an exponential decline function with an *e*-folding depth of ~1 m with the rate of decline principally governed by the density of the material the cosmic rays are passing through (e.g. Quartz 2600kg $m^{-3}$).

Negative muon capture is a reaction in which an atom nucleus captures a negative muon ($\mu^-$) triggering the emission of radionuclides. Negative muon capture accounts for ~2% of $^{10}$Be production (Heisinger et al., 2002a). Fast muon reactions are similar to nucleonic (spallation) reactions but have a much longer attenuation length (Heisinger et al., 2002b). Muons penetrate much deeper into the Earth's subsurface and are the dominant producer of $^{10}$Be beyond c.3 m depth (Dunai, 2010). (Heisinger et al., 2002a; Heisinger et al., 2002b) provided scaling Equations for muogenic production by negative muon capture and fast muons which have not been directly applied in this study since muons were anticipated to contribute a negligible amount of $^{10}$Be to samples from the study site.

#### *2.4.1.3 Topographic Shielding*

Cosmic rays are attenuated by the atmosphere. The shortest path for cosmic rays through the atmosphere is vertical, therefore the cosmic ray flux is highest from zenith, with the intensity decreasing with higher incident angles measured from horizontal. Considering the cosmic ray flux received by a horizontal surface with no topographic shielding, the total incoming cosmic ray flux is thus attained by integrating through all incident angles ($\theta$ = 0-90°) from all azimuth directions ($\varphi$ = 0-360°). On a hypothetical flat surface a samples site is exposed to the full range of $\varphi$ and $\theta$, but where there is significant topography a samples site may be shielded from a portion of this hemisphere and will receive a lower cosmic ray flux. Such topographic shielding can significantly reduce CRN production, particularly in high relief landscapes where large portions of the sky may be obstructed. A sloped surface also receives a reduced radiation flux since the upslope will shield a portion of the horizon. As a result there will be foreshortening effects which change the effective surface area, and the effective attenuation length will be reduced by an increasing angle of incidence (Dunne et al., 1999; Gosse and Phillips, 2001). When modelling CRN production rates, both of these shielding effects must be accounted for.

Codilean (2006) presented a method using relief shadow modelling (RSM) to calculate shielding factors to correct for this effect and that of cast shadows (i.e. where a location is shielded from cosmic rays due to a nearby object such as a mountain or boulder). This identifies DEM cells that are in shadow when considering a radiation source (e.g. the Sun) with a given azimuth ($\varphi$) and elevation angle ($\theta$). RSM (or hillshade) algorithms are provided in most GIS software packages and thus the Codilean (2006) approach can be implemented with relative ease by integrating across $\varphi$ and $\theta$ through 360° and 90° respectively to determine a shielding factor as a percentage of the total radiation every cell in a DEM should receive (see Codilean, 2006).

Additionally a sloped surface experiences effective shielding due to a number of factors. Since the incoming radiation flux is dominated by vertical incidences, a slope will experience foreshortening, so that the radiation received is distributed over a larger surface area with increasing slope angle. In addition, for a non-vertical radiation source the effective surface area viewed parallel to the incident radiation will be reduced (Gosse and Phillips, 2001). Production rates on a sloped surface are also shielded geometrically due to an effective decrease in attenuation length due to the change in incidence angle of cosmic rays, and conveniently, this balances perfectly the foreshortening effects described above (Dunne et al., 1999).

#### *2.4.1.4 Sampling Strategy*

Fluvial sand was collected from the bed of the active channel during base flow conditions. The location of sample sites is shown in Figure 2.2. Catchment averaged denudation rates must be determined from sediment that is actively being transported so that it can be assumed it has not spent significant time in storage in the fluvial system. Derivation of a catchment-averaged erosion rate from the $^{10}$Be concentration in sampled quartz assumes that the sediment is sourced from throughout the upstream catchment and is well mixed, having not undergone any significant period of storage *en route* to the sample site. Care was taken to only sample from the upper 5cm of sandy deposits along the channel bed, with preference given to deposits nearest the thalweg and unrestricted by obstacles such as woody debris or large boulders.

#### *2.4.1.5 Sample Processing*

The samples were sieved in the laboratory later and only the size fraction 250-1000μm retained. Quartz separation and $^{10}$Be isolation was carried out at the University of Edinburgh's Terrestrial Cosmogenic Nuclide Laboratory following standard techniques (e.g. Bierman et al., 2002), with accelerator mass spectrometry

(AMS) performed at PrimeLab (Purdue University) to measure the concentration of $^{10}$Be in the samples.

#### *2.4.1.6 Interpreting Catchment-Averaged Erosion Rates*

If the rate at which $^{10}$Be is being produced can be predicted (see section 2.4.1.3), then the amount in a rock or sediment sample is a function of how long it has been exposed to cosmic rays. Hence the concentration of $^{10}$Be can tell you how long a sample has been exposed at the Earth's surface or how rapidly it has been exhumed through the near surface.

The interpretation of a catchment-averaged erosion rate from a stream sediment sample is based on the assumption that the sampled sediment comprises a mixture of material derived from throughout the upstream catchment that has been delivered rapidly to the channel once at the surface. Therefore the concentration of $^{10}$Be in the stream sediment reflects an average of the distribution of production rates and erosion rates throughout the upstream catchment (Bierman and Steig, 1996; Brown et al., 1995; Granger et al., 1996).

In this study the scaling scheme of (Dunai, 2000) was used to interpret concentrations of $^{10}$Be in terms of erosion rates. Production rates and topographic shielding factors were calculated for all pixels in a U.S. Geological Survey National Elevation Dataset 1/3 Arc second (approx. 10m) DEM [http://seamless.usgs.gov/; accessed 15/1/2009] of the study site. Concentrations of $^{10}$Be were interpreted in terms of an erosion rate using the CRONUS-Earth online calculator version 2.2 (http://hess.ess.washington.edu/, accessed September, 2010) to determine basin-wide erosion rates (Balco et al., 2008b). Whilst this tool is designed to calculate site specific denudation rates, it can also be used to calculate basin-wide denudation rates by using a production-weighted mean elevation and mean shielding factor for the catchment area. A production-weighted mean elevation was calculated by calculating

the production rate at every cell in a DEM following Stone (2000) and finding the mean production rate, which is inverted using the same production model to an equivalent elevation. The calculation of nuclide concentration varies slightly depending on the production model used. Here, production rates were scaled according to Dunai (2000) in calculating the catchment averaged denudation rate. A site may be shielded due to being sloped or due to shadow effects of surrounding topography. Topographic shielding was calculated following Codilean (2006) and scale production according to a basin averaged shielding factor.

Cosmic radiation can also be shielded from the surface through snow cover. Using snow fall data from 2002-2009 from the nearest and lowest observation station (Four Trees; elevation 1600 m) indicates that snow at water equivalent depths averaging 74 cm cover the ground for five months of the year (NOHRSC; data accessed 3rd March 2011). Following Gosse and Phillips (2001) this equates to a snow shielding factor of 0.73. Whilst such significant snowfall may shield the surface from incoming cosmic radiation, the observation station is >600 m higher than the maximum elevations at my field site and thus expect snow shielding to be significantly less. Therefore snow shielding was not accounted for which may result in overestimation of erosion rates. Overestimation will be most significant for the slowest eroding portions of the landscape, since these sample sites are highest in elevation (900-1000 m).

Riebe et al. (2000) used cosmogenic radionuclides to demonstrate that erosion rates are an order of magnitude higher adjacent to the Feather River canyon, compared to rates on the relict upland. Here I recalculate denudation rates determined from $^{10}Be/^{9}Be$ ratios reported by Riebe et al. (2000) given new shielding factors (Codilean, 2006) and refinement in scaling of spallogenic and muogenic $^{10}Be$ production (Dunai, 2000). I also calculate denudation rates for thirteen new catchments (Table 2.1).

### 2.4.2 Topographic Analysis

Topographic analysis was carried out on a gridded 1 m resolution DEM derived by airborne light detection and ranging (LiDAR). The LiDAR was collected by the US National Science Foundation's (NSF) Center for Airborne Laser Mapping (NCALM). This data was provided in both point cloud (xyz) and gridded format.

#### *2.4.2.1 Slope, Aspect and Curvature*

Here topographic curvature is defined as the two dimensional Laplacian ($C = \nabla^2\zeta$) of the function defining the surface $\zeta = f(x,y)$. Both 6-term quadratic and 9-term polynomial functions have been routinely fitted to elevation data to approximate the land surface (e.g. Evans, 1980; Moore et al., 1991; Zevenbergen and Thorne, 1987). Schmidt et al. (2003) compared methods for 10 meter resolution, gridded data, using both an analytical and real landscape. They concluded that fitting 9-term polynomials was appropriate where elevation data are reliable; however, quadratics were better fitted where the dataset quality is poor. I carried out a similar comparison for a sample area of the Feather River LiDAR topography for both gridded and point cloud data and found that the results were indistinguishable (near identical values of slope and curvature metrics everywhere). Consequently, a 6-term function was used working with gridded elevations to minimise computation time. An algorithm was created to fit a surface by least squares regression to a local window of elevations. The fitted surface has the form:

$$\zeta = ax^2 + by^2 + cxy + dx + ey + f \qquad [2.10a]$$

with curvature ($C$) and slope ($S$) calculated from the fitted coefficients (Evans, 1980) according to:

$$C = 2a + 2b \qquad [2.10b]$$

$$S = \sqrt{d^2 + e^2} \qquad [2.10c]$$

The length scale $L$ dictates the size of the moving window of elevations to which Equation 2.9a is fitted. Regression was performed on the gridded data using an un-weighted square window of size $L \times L$ in which the cell of interest is at the centre. High resolution DEMs tend to contain local metre-scale variability reflecting the roughness of real landscapes at such scales (see next paragraph). Since the least squares fitted surface does not necessarily pass through any DEM nodes, it is acting to smooth the surface and so no pre-processing to smooth the LiDAR data was performed. I tested this approach against performing regression on point cloud data (e.g. Roering et al., 2010) and found the results indistinguishable.

In forested landscapes, LiDAR-derived digital topography commonly exhibits strong local variability due to the presence of pits associated with the upheaval or decay of tree root clumps (e.g. Roering et al., 2010) or dense vegetation or 'brush' which has been misclassified as bare earth in the initial data processing to produce the DEM (Lashermes et al., 2007). Standard algorithms computing slope and curvature from 3x3 pixel moving windows produce noisy results. Thus the length scale $L$ over wich slope, curvature and aspect were calculated was chosen carefully. This length scale is reflected by a break in indicators of variability (i.e. variance or standard deviation) as a function of length scale and is expected to vary from landscape to landscape depending on the dominant processes of sediment transport. Lashermes et al. (2007) found that a length scale $L$ of 12 m was appropriate in the forested landscape of the South Fork Eel River in California, whilst Roering et al. (2010) demonstrated $L$ = 15 m in another forested landscape in

the Oregon Coastal Range (using a search radius of 7.5m, hence $L = 2 \times$ window radius). Figure 2.4 shows the standard deviation of curvature as a function of length scale for a 60 × 20 m portion of steadily denuding hilltop in a tributary to the Feather River basin ($E = 40$ mm ka$^{-1}$; sample BRB-6; see table 1). A scaling break exists at $L = 12$ m, above which curvature is independent of scale (up to 32 m) as shown by the grey region in Figure 2.4, and there is linear scaling of the standard deviation of curvature as a function of scale. This length scale is used to report slope, curvature and aspect across the entire landscape.

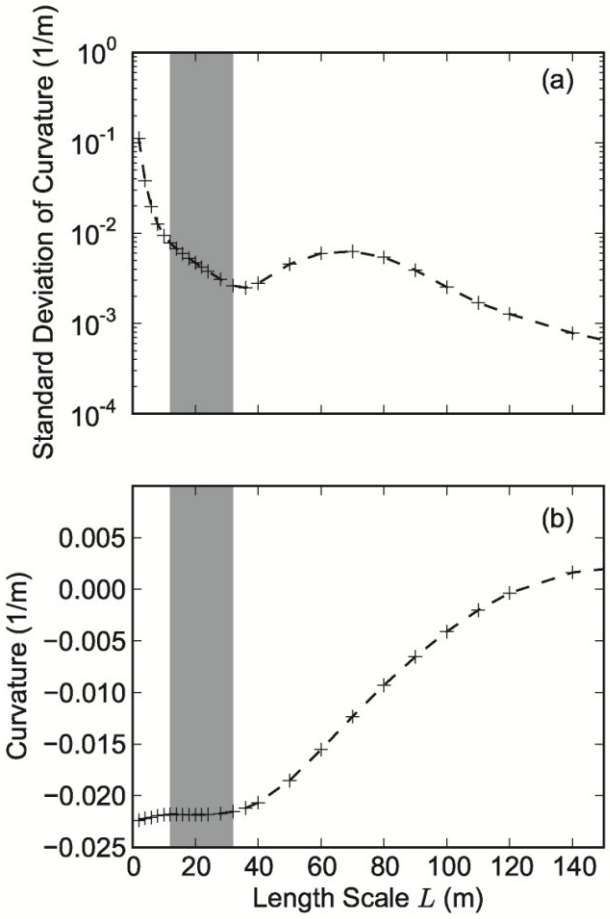


Figure 2.4: Influence of window size when calculating topographic curvature from gridded elevation data of a soil-mantled hillslope. (a) Standard deviation and (b) mean value of curvature for a 60 × 20m portion of a hilltop eroding at ~ 40 ± 5 mm $ka^{-1}$. Crosses indicate the scales at which the test took place. A scaling break occurs at $L$ = 12m separating the signal of pit-mound topography from that of hillslope morphology. Curvature values are consistent (b) and there is constant scaling of standard deviation of curvature (a) up to $L$ = 32m (grey band) at which point adjacent valley bottoms start to influence curvature.

#### 2.4.2.2 Mapping Hilltops

Hilltops were delineated from topographic data as the intersecting margins of basins at all stream orders using ArcGIS software and scripting with Python. Prior to this some pre-processing of the DEM was required. LiDAR DEMs are typically of such fine resolution (1 m) that the presence of trails and roads can significantly influence the inference of the distribution of water flow across the landscape, particularly where they are built across valleys and where pipes have been used to route water underneath. Therefore, identification of trails and roads was crudely automated by filtering the DEM for pixels with positive curvature and low slope which have extreme values of both positive and negative curvature within a 10 m radius. The resulting areas were preferentially smoothed using a Gaussian filter to aid extraction of the stream network and a mask created to exclude these areas from later hillslope analysis, since the topographic form does not reflect the natural processes operating in the landscape.

To define the extent of the valley network I implemented the Geonet tool (in MATLAB) made publicly available by Passalacqua et al. (2010a). This tool identifies the likely location of channel heads based on a curvature threshold following non-linear smoothing of the DEM. This filtering smoothes low relief, high-frequency noise yet preserves sharp features such as hillslope-to-valley transitions. Once likely channel heads were identified, a steepest descent trace was run from each to create a vector network of the valley system. Thus I ensured sampling of zero-order basins, regardless of the dominant valley-forming process. It is important to note here that the resulting valley network is defined as a series of 1-pixel wide lines, whilst valley floors are often greater than 1 m wide. Strahler stream order (Strahler, 1952) was calculated from the resulting valley bottom network, and drainage basins were mapped for the downstream termination of each stream segment with a given stream order. A vector network of intersecting basin margins was generated and filtered to exclude slopes of > 0.4 (beyond which sediment

transport typically has a > 15% non-linear component following parameterisation of (Roering et al., 1999) for Equation 2.5), since I am only interested in hilltops where I can assume that sediment transport is linearly proportional to hillslope gradient (Equation 2.6). A second filter excluded hilltop vectors within 10 m horizontal distance of identified roads/trails/valley bottoms, any of which might influence slope and curvature estimates and therefore invalidate Equation 2.6. The resulting network (Figure 2.5) was segmented to sample hilltop sections with length > 50 m. Traces to get hillslope profiles were initiated at every node adjacent to a hilltop vector and so 50 m segments ensured that the number of hillslope profiles samples per segment equalled or exceeded 100 when subsequently computing statistics on the sampled hillslope properties.

### 2.4.3 Sampling the Landscape

I adopted two approaches for exploring how topography varies with erosion rates. CRN-derived denudation rates dictate a basin-averaged approach to allow direct comparison between sampled topography (e.g. mean $S$ or mean $C_{HT}$ internal to a basin) and measured erosion rate. The second approach focused on the network of hilltop segments where topographic curvature was sampled only at locations defined as hilltops. The adjacent hillslopes were sampled to determine mean slope, relief and hillslope length. Because a hilltop has two adjacent hillslopes, it is responding to erosion rates in two separate catchments. If there is a significant difference in erosion rates between the two catchments then the resulting $C_{HT}$ will be some composite of the two erosion rates, since one side of the hillslope will be eroding faster than the other. In such a scenario a basin-averaged sampling approach may dampen or enhance the erosion rate inferred from curvature, since hilltops at the basin margin will reflect erosion rates in an adjacent basin as well as the basin of interest.

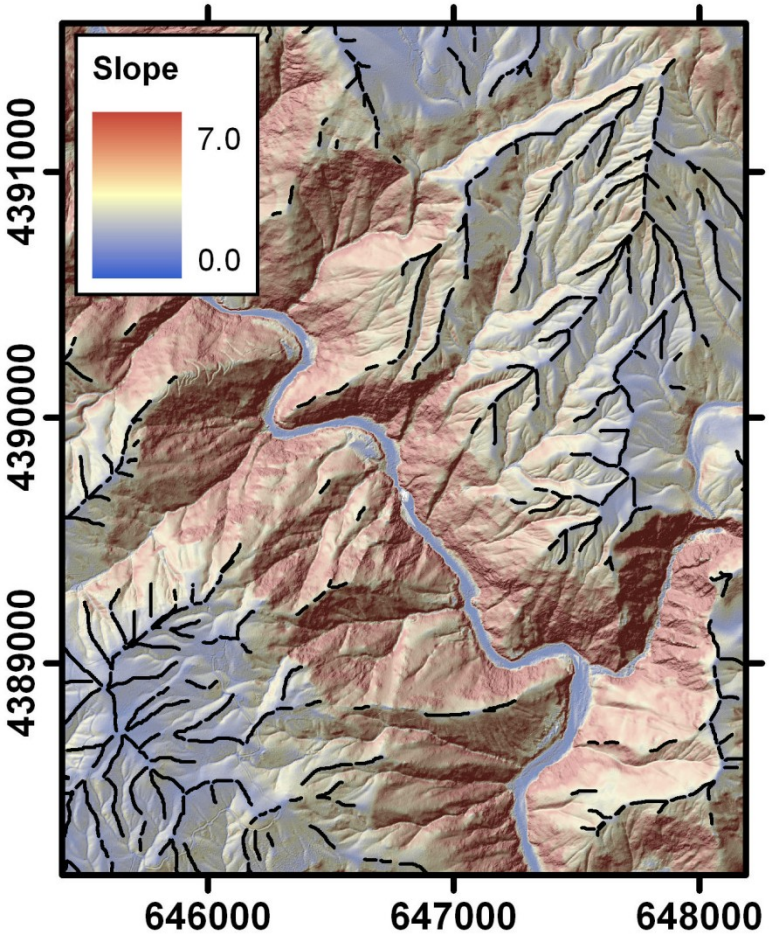


Figure 2.5: Shaded slope map for a subsample of the LiDAR adjacent to the Feather River canyon showing a network of mapped hilltops (black lines). Hilltops are defined at drainage divides where slope < 0.4. High slopes in legend due to the proximity to Feather Falls in the east of the area, a near vertical cliff face and waterfall. The spatial reference system is UTM Zone 10N with spatial units in meters.

#### 2.4.3.1 Basin-averaged Sampling

For comparison to CRN-derived denudation rates I extracted the mean slope (slope derived following methods outlined in section 2.4.2.1) of each sample basin (e.g. Binnie et al., 2007; DiBiase et al., 2010; Matsushi and Matsuzaki, 2010; Ouimet et al., 2009). Mean hilltop curvature was calculated from all hilltops internal to each basin. Hilltops at the basin margin were rejected if there was a noticeable difference in hillslope gradients either side of the divide for smaller catchments that were sampled for CRN. For extracting basin averaged topographic metrics *throughout* the landscape, hilltops at catchment boundaries were not included. Basins of ~50 000 $m^2$ were sampled; large enough that there were some hilltops internal to the basin (i.e. not zero-order basins) but small enough that I could capture spatial variation in landscape morphology between basins.

#### 2.4.3.2 Sampling Hillslopes

To explore relationships between hillslope gradient and hilltop curvature throughout the landscape, algorithms were developed to extract hillslopes associated with each hilltop (Figures 2.6). This approach is broadly similar to that of Gangodagamage et al. (2011). For a given hilltop segment, beginning at each hilltop pixel, a trace was run down the path of steepest descent. The trace algorithm created a vector route which crosses a DEM pixel according to the aspect direction. For the condition where two cells faced one another the trace continued down the margin between them (Lea, 1992). The trace continued until a pixel defined as a valley bottom was reached. Along the resulting profile, the mean slope ($S$), relief ($R$) and horizontal hillslope length ($L_H$) were recorded. Since the valley network is defined as a single cell wide, whilst valley floors may in reality be wider, it is possible that there may be slight overestimation of hillslope length which will vary depending on the nature of valley bottom. Hilltop curvature ($C_{HT}$) was recorded only at the top pixel (i.e. each trace that flows from the hilltop to the channel, is associated with a

curvature measured only at the hilltop). A mean value for each of these metrics was then determined for each hilltop segment (as defined in section 2.4.2.2).

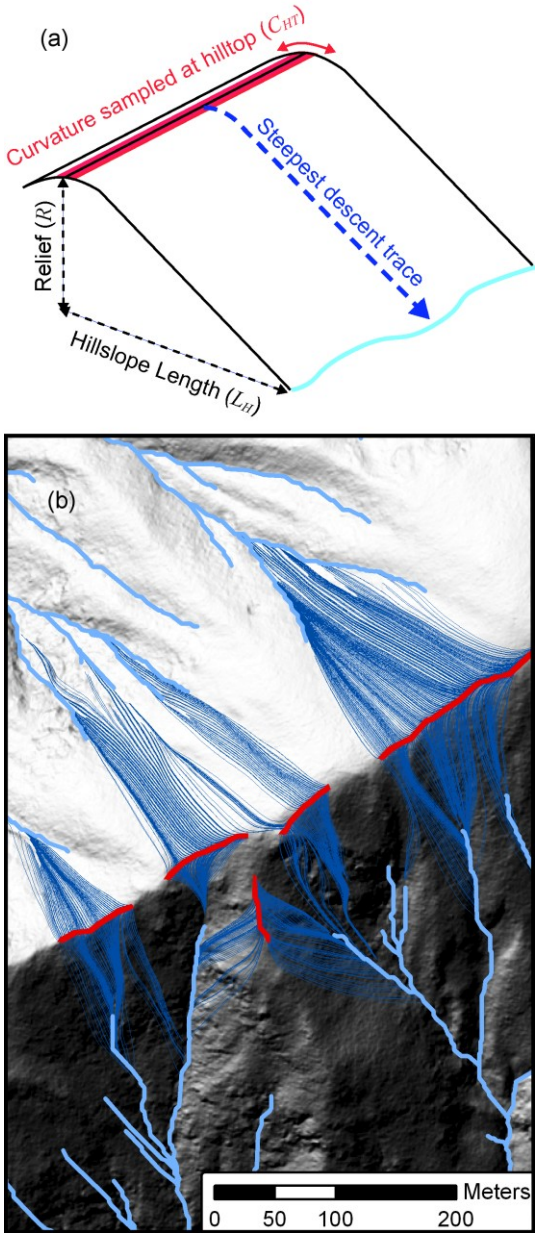


Figure 2.6: (a) Schematic illustration of sampling approach. For each DEM pixel defined as a hilltop (red) the curvature was recorded ($C_{HT}$). A steepest descent path was generated until a stream pixel (light blue) was reached. The slope of each pixel encountered was collected and a mean ($S$) then calculated. From this trace hillslope length ($L_H$) and relief ($R$) were calculated. Mean values of each variable associated with each hilltop segment were calculated. (b) Sampling approach illustrated in (a) applied to a real hillslope in the Feather River region showing a series of steepest descent traces between hilltops and valleys.

## 2.5 Results

### 2.5.1 CRN-derived Denudation Rates and Topography

Denudation rates vary from 10 to 250 mm $ka^{-1}$ from the basins on the plateau to those immediately adjacent to the Feather River (Figure 2.2). Erosion rates of 20-30 mm $ka^{-1}$ characterise the low relief relict surface. In some locations slightly faster erosion rates ~30-40 mm $ka^{-1}$ are associated with an intermediate landscape cut into the plateau (concave-up channel profiles and broad convex up hillslopes). These areas are dissected due to accelerated erosion rates downstream, immediately adjacent to the Feather River, as indicated by knick-zones and steepened reaches immediately upstream of the basin outlet (Figure 2.7).

Figure 2.8 shows mean basin slope and mean hilltop curvature as a function of CRN-derived denudation rate. Mean basin slope is best approximated by a non-linear curve (e.g. $R^2 = 0.78$ for asymptote compared to $R^2 = 0.69$ for linear fit; not shown on figure) suggesting that hillslope angles are approaching some limited value with increasing denudation rates. This sugests that as erosion rates increase, hillslopes may respond through an increasing frequency of mass wasting events (Burbank et al., 1996; Roering et al., 1999; Strahler, 1950). If mean hilltop curvature varies linearly with denudation rate ($R^2 = 0.83$) then Equation 2.5 is applicable to the landscape. An exponential function also provides a reasonable fit ($R^2 = 0.72$). I assume that a linear fit is appropriate in order to use Equation 2.5 to predict the coefficient of sediment transport, although there are theoretical reasons why this may not be the case in landscapes with thin soils (Roering, 2008) (see discussion).

| Sample | Location (Decimal °N/°W) | Weighted Mean Elevation (m) [a] | Shielding Factor [b] | Quartz Weight (g) [c] | Be Carrier Weight (mg) | $^{10}Be/^{9}Be$ ($\times 10^{-15}$) [d, e, f] | $^{10}Be$ Concentration ($10^5$ atoms $g^{-1}$ $SiO_2$) [e, f, g] | Denudation Rate (mm $ka^{-1}$) [h, i] |
|---|---|---|---|---|---|---|---|---|
| FR-2 | 39.6604 / 121.3607 | 909.0 | 0.995 | n/a | n/a | 48 ± 8 | 0.52 ± 0.08 | 125.9 ± 23.2 |
| FR-4 | 39.6359 / 121.2783 | 496.5 | 0.985 | n/a | n/a | 36 ± 9 | 0.20 ± 0.05 | 253.8 ± 66.6 |
| FR-5 | 39.6361 / 121.2714 | 571.0 | 0.994 | n/a | n/a | 33 ± 7 | 0.40 ± 0.09 | 133.3 ± 31.9 |
| FR-6 | 39.6385 / 121.3322 | 917.4 | 0.998 | n/a | n/a | 279 ± 12 | 2.56 ± 0.16 | 25.2 ± 2.7 |
| FR-7 | 39.6391 / 121.3311 | 907.0 | 0.992 | n/a | n/a | 341 ± 13 | 3.41 ± 0.22 | 18.5 ± 2.0 |
| FR-8 | 39.6586 / 121.3230 | 1055.7 | 1 | n/a | n/a | 556 ± 15 | 5.52 ± 0.31 | 12.5 ± 1.4 |
| FR-9 | 39.6552 / 121.3269 | 1032.5 | 1 | n/a | n/a | 473 ± 19 | 4.76 ± 0.31 | 14.4 ± 1.6 |
| FR-10 | 39.6465 / 121.3434 | 966.5 | 1 | n/a | n/a | 203 ± 9 | 2.75 ± 0.19 | 24.3 ± 2.7 |
| BRB-2 | 39.6491 / 121.3020 | 841.1 | 1 | 56.89 | 248 | 576 ± 32 | 1.57 ± 0.09 | 38.6 ± 3.4 |
| BRB-6 | 39.6463 / 121.3061 | 800.5 | 1 | 54.45 | 249 | 633 ± 22 | 1.76 ± 0.18 | 35.7 ± 4.7 |
| BRB-8 | 39.6483 / 121.3036 | 808.7 | 1 | 54.43 | 248 | 268 ± 13 | 0.71 ± 0.04 | 90.3 ± 8.5 |
| BEAN-1 | 39.6126 / 121.3295 | 782.2 | 0.997 | 47.84 | 249 | 422 ± 10 | 1.42 ± 0.04 | 43.8 ± 3.7 |
| BEAN-2 | 39.6225 / 121.3283 | 695.5 | 0.997 | 49.24 | 245 | 401 ± 9 | 1.31 ± 0.04 | 44.8 ± 3.7 |
| BEAN-4 | 39.6237 / 121.3273 | 717.9 | 0.997 | 54.47 | 243 | 314 ± 8 | 0.92 ± 0.03 | 65.0 ± 5.3 |
| BEAN-5 | 39.6312 / 121.3298 | 825.9 | 0.998 | 41.02 | 255 | 347 ± 8 | 1.42 ± 0.04 | 45.1 ± 3.8 |
| BEAN-7 | 39.6284 / 121.3277 | 671.7 | 0.995 | 45.70 | 246 | 184 ± 5 | 0.64 ± 0.02 | 90.7 ± 7.2 |
| FT-3 | 39.6714 / 121.3109 | 1065.9 | 1 | 19.82 | 249 | 858 ± 22 | 2.85 ± 0.09 | 26.2 ± 2.3 |
| FT-4 | 39.6712 / 121.3109 | 1007.6 | 1 | 52.17 | 249 | 906 ± 24 | 2.88 ± 0.09 | 24.9 ± 2.2 |
| FT-6 | 39.6784 / 121.3155 | 1097.0 | 1 | 50.86 | 249 | 994 ± 15 | 3.23 ± 0.10 | 23.6 ± 2.1 |
| BS-1 | 39.7184 / 121.2473 | 966.4 | 0.993 | 56.75 | 250 | 244 ± 14 | 0.70 ± 0.04 | 99.9 ± 9.7 |
| SB-1 | 39.7189 / 121.2411 | 1015.0 | 0.991 | 59.71 | 250 | 350 ± 15 | 0.96 ± 0.04 | 75.4 ± 6.6 |

Table 2.1: CRN sample information and calculated denudation rates. Samples with the prefix FR are from Riebe et al. (2000).

[a] Mean elevation weighted by spallogenic production in each DEM pixel in the basin (calculated following Stone (2000)).

[b] Calculated according to (Codilean, 2006).[c] A density of 2.6g/$cm^3$ was assumed.

[d] Isotope ratios were normalized to $^{10}Be$ standards prepared by (Nishiizumi et al., 2007)$^{10}Be/^{9}Be$ ratio of $2.85 \pm 10^{-12}$ (KNSTD07).

[e] Isotope ratios for FR-2 to FR-10 were normalised to National Institute of Standards and Technology standard material (NIST_certified) with $^{10}Be/^{9}Be$ ratio of $2.68 \pm 10^{-11}$ (Riebe et al., 2000). These data are scaled to the KNSTD07 standard using a factor of 1.0425 (Balco et al., 2008a).

[f] Uncertainties are reported at 1σ confidence.

[g] A blank value of $^{10}Be/^{9}Be = 35.63 \pm 10^{-15}$ was used to correct for background.

[h] Production rates were scaled according to (Dunai, 2000).

[i] Beryllium-10 erosion rates were calculated with the Cosmic-Ray Produced Nuclide Systematics (CRONUS) Earth online calculator (Balco et al., 2008a) version 2.2 (http://hess.ess.washington.edu/). Propagated error accounts for uncertainty in $^{10}Be/^{9}Be$ ratio measurement and production scaling only.

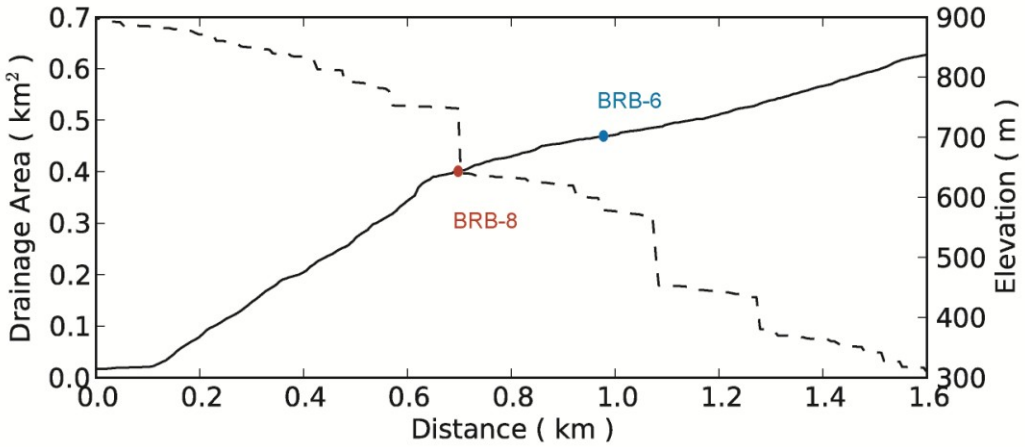


Figure 2.7: Long profile of a typical small basin immediately adjacent to the Feather River. Distance is upstream from the confluence with the Feather River. Solid line is the elevation profile and dashed line is drainage area along the channel. This basin is eroding at ~ 40 mm ka$^{-1}$ along its gentle upper reach upstream of the blue point (CRN sample BRB-6). Red point marks location where a sub-tributary eroding at ~ 90 mm ka$^{-1}$ joins this tributary (CRN sample BRB-8). The channel abruptly steepens as it approaches the rapidly incising Feather River, becoming linear and steep (mean slope 0.41).

### 2.5.2 Rates of Hillslope Sediment Transport

Based on the regression line in Figure 2.8 and observations from LiDAR and aerial photograph and in the field that hilltops analysed are all soil mantled I assume that Equation 2.5 is applicable to soil mantled hilltops throughout the landscape, and solved Equation 2.5 for the transport coefficient $D$. Assuming $\rho_s/\rho_r = 0.5$, a ratio that has been demonstrated for other granitic field sites (e.g. Heimsath et al., 2001; Riggins et al., 2011a), the transport coefficient is calibrated at $D = 0.0086$ m$^2$ yr$^{-1}$ for areas of granitic bedrock lithology. Recognising the dearth of data at erosion rates greater than ~100 mm ka$^{-1}$ I performed the regression with the highest rate (FR-4; see table 2.1) ignored and arrived at $D = 0.0077$ m$^2$ yr$^{-1}$.

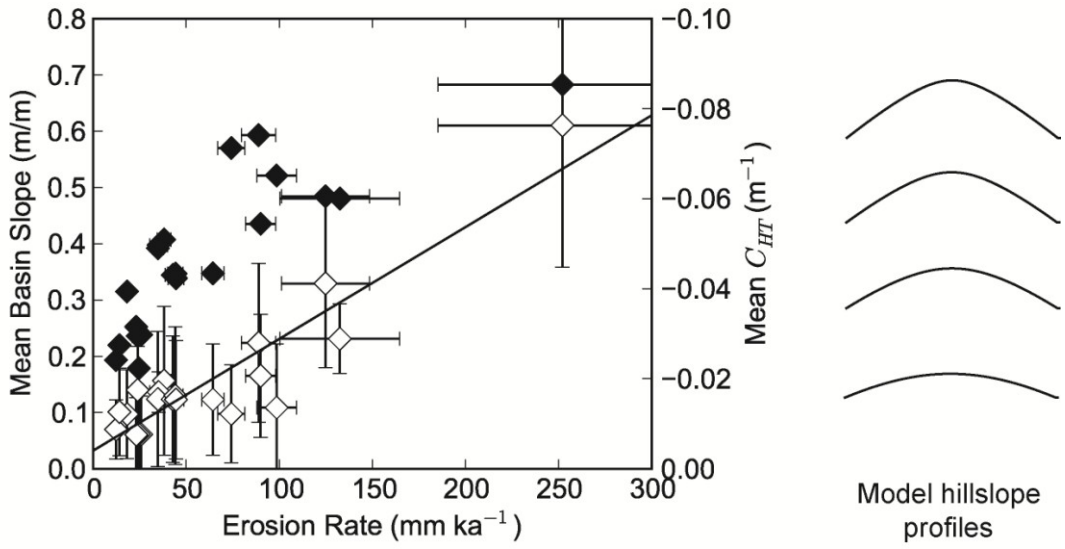


Figure 2.8: Plot showing variance of basin-averaged mean slope (filled symbols) and mean hilltop curvature (hollow symbols) with CRN derived erosion rates for sampled basins (see Figure 2.2). Note that curvature (Laplacian) on convex-up hilltops is negative by convention, so 'sharper' ridges have higher negative curvature. The solid line shows a linear relationship between erosion rate and hilltop curvature is predicted by Equation 2.6, suggesting $D$ = 0.0086 m$^2$ yr$^{-1}$. Error bars for hilltop curvature are one standard deviation about the mean. I do not include error bars for mean slope since I expect high variability in natural systems. Parabolas on the right represent steady state hillslope profiles (calculated following Roering et al. (2007) using $D$ = 0.0086 m$^2$ y$^{-1}$ and $S_C$ = 0.86 (see section 2.5.4) to illustrate sharpening of ridges with increased erosion rate, with $C_{HT}$ values corresponding to the adjacent axis.

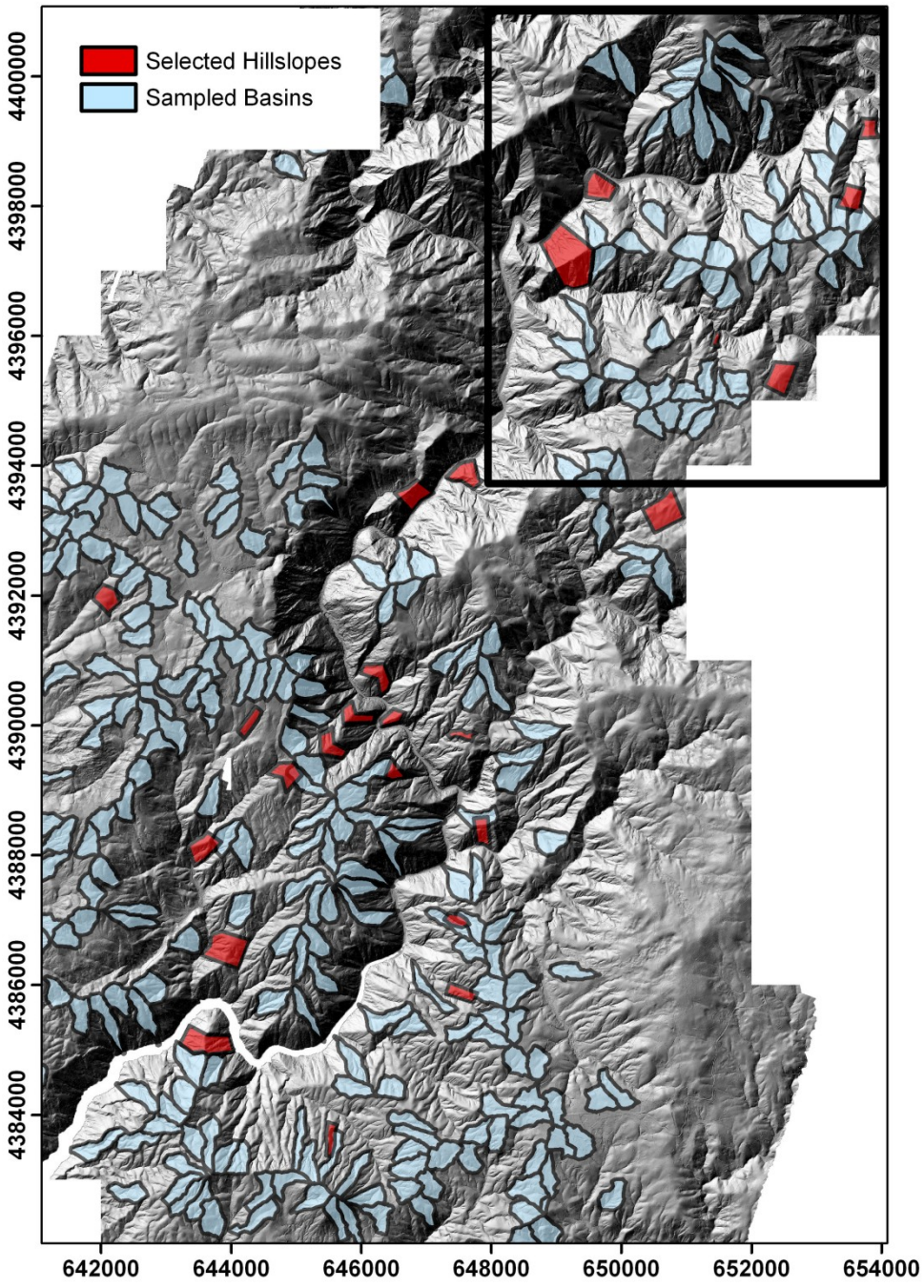


Figure 2.9: Shaded relief plot showing the location of all basins with a drainage area of c. 50 000 $m^2$ in granitoid basement and the location of hand selected ridges and their adjacent hillslopes used in Figure 2.11 (see text for description of sampling criteria). The black box indicates the location shown in Figure 2.13. The spatial reference system is UTM Zone 10N with spatial units in meters.

### 2.5.3 Topographic Relationships Across the Entire Landscape

I used my calibrated transport coefficient $D$ to predict erosion rates across the entire landscape by sampling hilltop segments and their associated adjacent hillslopes. Figure 2.9 shows basins that were sampled for topographic metrics, plus manually selected hilltop-hillslope areas (see below for rationale). A basin-averaged sampling approach failed to isolate rapidly eroding portions of the landscape, reflected by an approximately linear relationship between mean hilltop curvature and mean slope, and a dearth of data at high hilltop curvatures (Figure 2.10). The curvature of a hilltop is set by erosion rates in both adjacent channels. Rapidly eroding basins are limited spatially to being immediately adjacent to the Feather River; they are frequently adjacent to basins of lower relief. In such cases the mean curvature of hilltops at basin margins will be lower than the erosion rate in the basin should dictate. Values of hilltop curvature for basins of this size primarily come from the basin margins and therefore are influenced by erosion rates in adjacent basins. Manual sampling of hilltops and adjacent hillslopes distributed across the landscape can focus on hilltops with steep planar hillslopes on both sides of the divide. These areas were selected to sample hilltops and adjacent hillslopes down to nearest adjacent valley bottoms in order to demonstrate whether the expected nonlinearity between slope and hilltop curvature was present. For such hillslope areas shown in Figure 2.9, mean slope varies non-linearly with hilltop curvature (Figure 2.10).

Having automated the extraction of hilltop segments and adjacent hillslope properties (Figure 2.6), $C_{HT}$ and $S$ were compared (Figure 2.11a). Hillslopes steepen with increasing $C_{HT}$ but approach some limited value, such that $C_{HT}$ can continue to increase without an obvious associated change in $S$. This relationship is highlighted by calculating $S$ for regularly spaced bins in $C_{HT}$. The transition to invariantly steep mean hillslope gradients with increasing hilltop curvature occurs gradually, in that as hilltop curvature increases slope angle becomes less sensitive to the change.

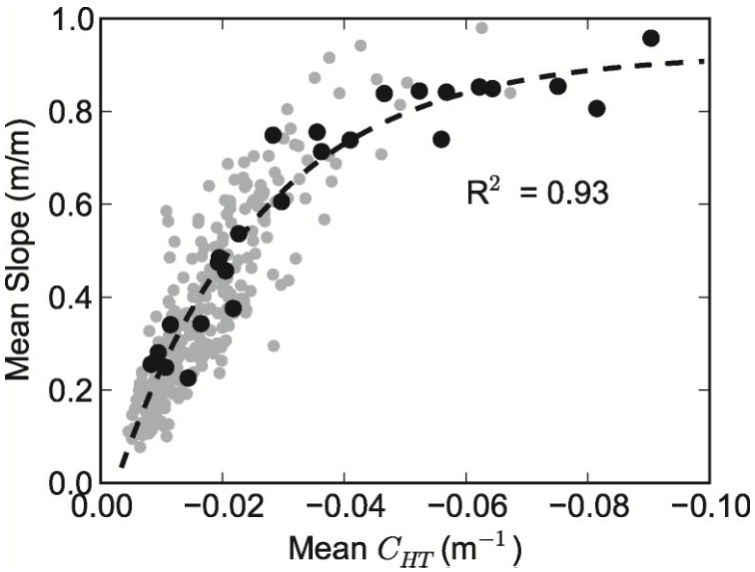


Figure 2.10: Relationships between topographic metrics of hilltop curvature and mean slope in areas sampled following Figure 2.10. A basin averaged sampling approach (grey circles) fails to sample hilltops with high curvature, whereas sampling of ridges and their adjacent hillslopes (black circles) reveals a nonlinear relationship (black dashed line fitted to black circles is an asymptote function) as hillslope gradient becomes limited whilst hilltop curvature continues to increase (black circles).

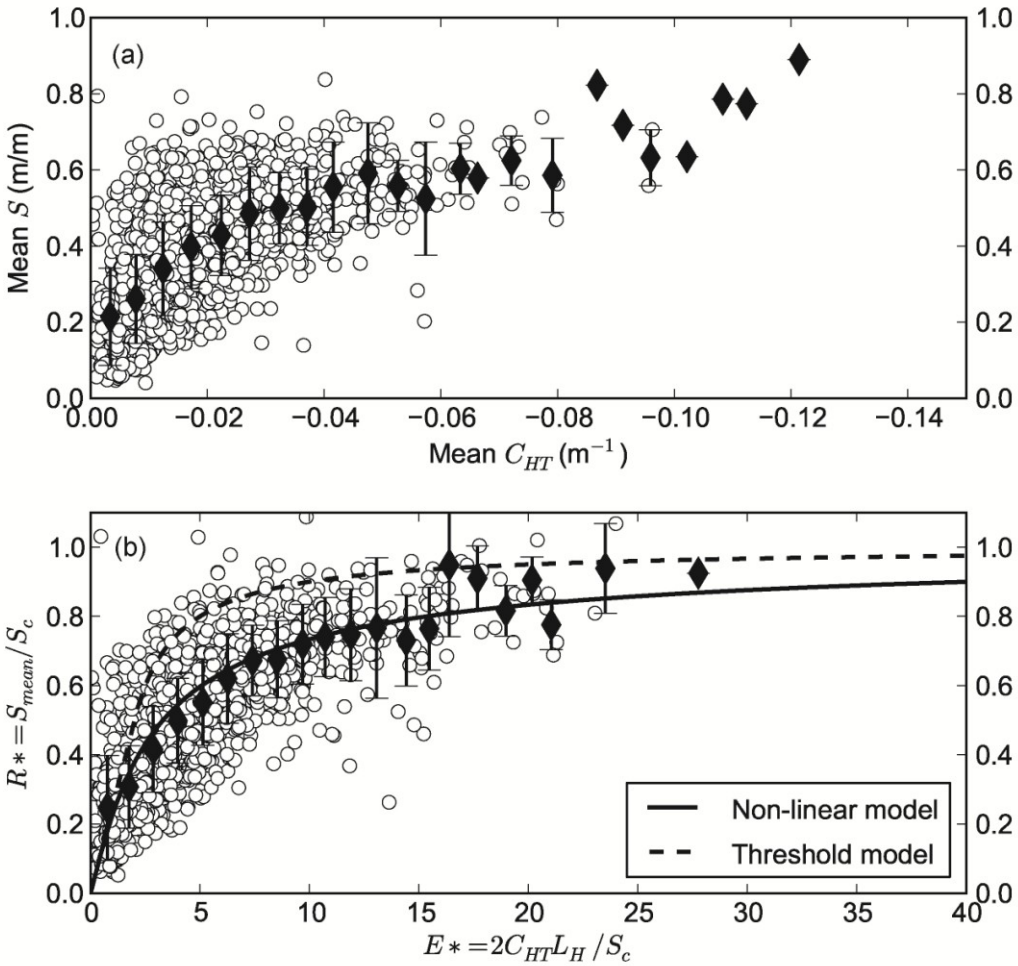


Figure 2.11: Topographic data generated by automated sampling of hilltops and their adjacent hillslopes. (a) Mean curvature verses mean slope for each hilltop segment and linearly spaced, binned averages (with ± one standard deviation error bars). Slope increases linearly with hilltop curvature up to a curvature of ~ -0.03, beyond which slope appears to be insensitive to changes in curvature. (b) Data from (a) used to calculate dimensionless erosion rate and relief using measured hillslope lengths (Equation 2.8a). Model predictions are shown for a non-linear sediment flux model (Equation 2.7) and linear-threshold model (Equation 2.8). Root mean square error is minimised between binned averages and the non-linear model (Equation 2.7) using a critical slope $S_C = 0.86$.

### 2.5.4 Comparison to Predictions of Geomorphic Transport Laws

I compare the results to hillslope morphology predicted by hillslope sediment models (Equations 2.7 and 2.8) by calculating dimensionless erosion rate and dimensionless relief (Figure 2.11b). I also plot the distribution of predicted hillslope morphology for the non-linear and threshold models for hillslope sediment transport (solid and dashed lines, Equations 2.7 and 2.8 respectively). Using regularly spaced bins in dimensionless erosion rate $E^*$ (bin size = 1), I find that my bin-averaged data offer a close fit to the non-linear transport model (Equation 2.7) which predicts the transition to steep, planar hillslopes to be gradual rather than marked. This further suggests that Equation 2.5 is applicable in this landscape, allowing us to predict the spatial distribution of erosion rates based on hilltop curvature (Figure 2.12).

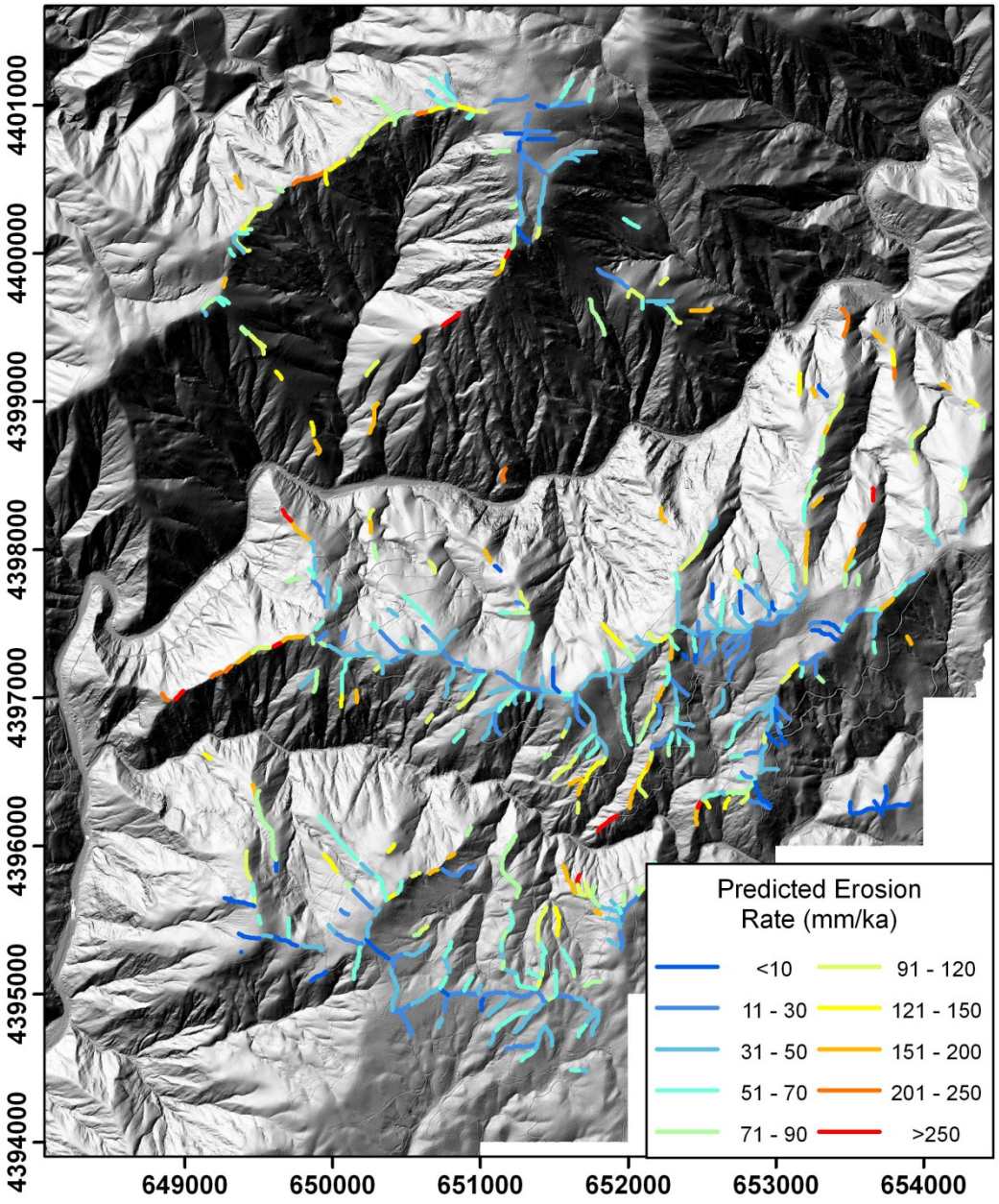


Figure 2.12: Shaded relief and hilltop map showing the spatial distribution of erosion rates predicted by hilltop curvature (using an estimated sediment transport coefficient $D = 0.0086$ m$^2$yr$^{-1}$, $\rho_s / \rho_r = 0.5$). Curvature is elevated on hilltops near to the Feather River and its larger tributaries, where the fluvial network has transmitted the signal of increased erosion, which is where the morphology of hillslopes becomes insensitive to changes in erosion rate. The spatial reference system is UTM Zone 10N with spatial units in meters.

## 2.6 Discussion

The intermediate zones between the plateau and the steepened landscape along the incised main river is common in the landscape and may be adjusted to a previous period of increased uplift prior to the late-Cenozoic acceleration, as observed elsewhere in the Sierra Nevada (Clark et al., 2005).

### 2.6.1 Climate Control on Hillslope Form and Process

This chapter has focused on tectonic-driven base-level change as the primary driver of morphological change in the Feather River. The influence of climate on hillslope form is primarily subsumed and time-averaged within *D*. This sediment transport coefficient combines the efficacy of all processes acting on a hillslope, including (but not limited to) expansion-contraction, freeze-thaw and wetting-drying cycles (Gilbert, 1909), root growth-decay (Gabet et al., 2003) and tree throw (Gabet and Mudd, 2010). The efficacy of these individual processes is likely to vary with climate, such that hillslope hydrology and temperatures may vary, influencing these processes directly or through changes in the type and distribution of biota (Gabet and Mudd, 2010; Gabet et al., 2003; Hughes et al., 2009; Pelletier et al., 2013; Roering et al., 2010; Yoo et al., 2005).

Measurement of CRN concentrations time-integrate sediment transport over the time period it takes material to reach the surface and be transported to the sampling sites. This timescale varies proportionally to erosion rates with high erosion rate sites integrating over ~2 ka and slow erosion rate sites over ~12 ka. Thus I consider the estimate of *D* presented in this chapter to be time averaged for this period of the Holocene, but may not be appropriate during glacial conditions. Indeed Roering et al. (2004) used tephra as a chemical tracer to demonstrate that *D* may have increased two fold as their landscape in New Zealand emerged from the last glaciations.

### 2.6.2 Steady State Assumption

Given the assumptions that hillslope lowering (and therefore conversion of bedrock to soil) is approximately uniform spatially and temporally (i.e. soil thickness and sediment flux are in steady state), and that sediment transport on hilltops is driven by creep-like processes, hilltop curvature can reveal the rates and distribution of erosion rates in a transient landscape at the scale of individual hillslopes. My methods require that these assumptions be met on both sides of the topographic divide in question, since hillslope pixels distributed across the divide are required for the calculation of hilltop curvature. Critically, the application of hilltop curvature as a predictor of erosion rates requires the response time of hillslopes to be shorter than that of the fluvial network, so that hilltops can track changes in channel erosion rates as they propagate through the landscape. I sought to verify this assumption since it is critical to the analysis presented in this study. A hilltop is the last part of the landscape to respond to a change in base-level lowering, since the signal propagates up the channel network and onto the hillslopes. Hence the assumptions above are most likely to be violated on hillslopes which are coupled with the channel network immediately downstream of knickpoints, and the downstream extent of such transient hillslopes will be set by the velocity of knickpoint propagation and the response time of the hillslopes. These assumptions may prove limiting in other transient landscape settings.

Given my constraints on erosion rates and the transport coefficient, I can predict response times for a range of realistic hillslope lengths for my landscape. Assuming hillslopes are transport limited and evolve following Equation 2.5, and that they adjust to a new equilibrium state following some exponential response function, Roering et al. (2001a) calculate the response time ($t$) according to:

$$t = -\tau \ln (P) \qquad [2.11]$$

where $P$ is a fraction set to define equilibrium and $\tau$ is an exponential timescale that defines how rapidly an equilibrium criterion approaches its asymptote [e.g.(Howard, 1988)]. For example consider a low gradient ($S$ < 0.4) hillslope responding to acceleration in erosion rate in the channel at its toe. The hillslope is expected to respond by increasing its relief. Using relief as a test criterion, by setting $P$ = 0.1 I consider the hillslope to have reached equilibrium when relief has increased to 90% (1-$P$) of its final value. The exponential timescale $\tau$ is approximated by:

$$\tau = \frac{{L_H}^2}{D} \frac{A}{(1+\psi)^B} \qquad [2.12]$$

where $A = 4/\pi^2$ (Mudd and Furbish, 2007), $B$ = 1.74 ± 0.02 is a constant (Roering et al., 2001a) and $\psi$ is the ratio of linear to non-linear transport components at the hillslope toe when the hillslope is evolving according to Equation 2.4. The response time of a soil-mantled hillslope is therefore primarily dependent on the length of the hillslope and the ratio of linear to non-linear components of sediment transport, which is set by the erosion rate and transport coefficient $D$. The linear/non-linear flux ratio can be described by:

$$\psi = \frac{\left\{ \frac{S_C}{2\varepsilon L_H} \left[ -D + \sqrt{D^2 + \left( \frac{2\varepsilon L_H}{S_C} \right)^2} \right] \right\}}{1 - \left\{ \frac{S_C}{2\varepsilon L_H} \left[ -D + \sqrt{D^2 + \left( \frac{2\varepsilon L_H}{S_C} \right)^2} \right] \right\}} \qquad [2.13]$$

where $\varepsilon = E\ (\rho_r/\rho_s)$ (see Roering et al., 2001a for derivations). Equation 2.13 predicts that as $\psi$ increases (e.g. due to an increase in erosion rate), hillslope response time is reduced. It also predicts that the response time is further dependent on hillslope length. Figure 2.13 shows the predicted response timescales according to Equation 2.11 for the range of hillslope lengths reported for my field site, within my constrained range of erosion rates. The response times for hillslopes given my calibrated parameters are predicted to be in the range 10-1000 ka, which is shorter than (but overlaps with) typical response time for detachment limited rivers (typically several million years, e.g. Hobley et al., 2010; Whipple, 2001; Whittaker et al., 2007a). The response time of the fluvial network in the Feather River must be >3.5 Ma since the landscape has not fully responded yet to the perturbation initiated sometime since3.5- 5 Ma (e.g. Wakabayashi and Sawyer, 2001). Yet, since erosion rates may be increasing to >200 mm $ka^{-1}$ hillslopes are expected to respond in less than 100 ka (Figure 2.13). The transport of sediment is relatively efficient in the Feather River (relative to other calibrated values of *D*, see section 3.1), which model predictions suggest should shorten the response time experienced by a hillslope adjusting to an increase in erosion rate (Fernandes and Dietrich, 1997; Mudd and Furbish, 2007; Roering et al., 2001a). Consequently I hypothesise that soil production and hilltop denudation should 'catch-up' with the distribution of channel erosion rates relatively quickly in this landscape, which is vital to the application of hilltop curvature for predicting erosion rates. Roering et al. (2001a) found a hillslope response time of ~50 ka in the Oregon Coast Range, similar to the minimum response time indicated for the most frequent hillslope length in my landscape (Figure 2.13).

Hillslope response is primarily driven by changes in the fluvial network; hence hillslopes will always lag behind transient signals in the channel network. However, since the hillslope relaxation time is anticipated to be short compared to that of the river network, hilltop curvature can offer insight into the distribution of erosion in the channel network. This response timescale will dictate the spatial extent

of hillslopes whose morphology does not reflect channel erosion. Where hillslopes are unable to keep pace with channel incision, the hillslope may be effectively decoupled from the channel network (e.g. Korup and Schlunegger, 2007; Norton et al., 2008), and hilltop curvature will bear no relation to erosion rates in the channel.

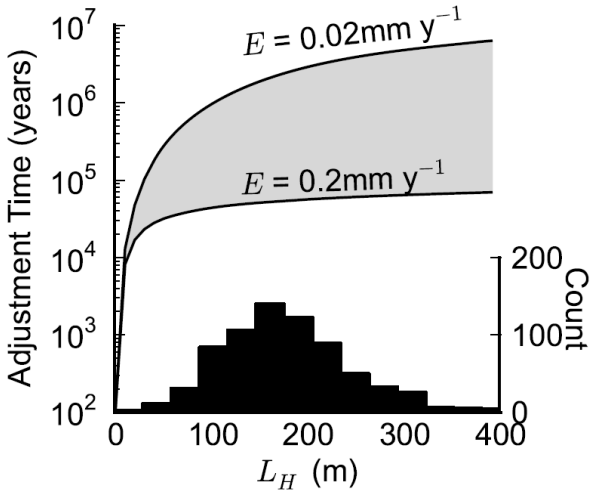


Figure 2.13: Predicted adjustment timescales for hillslopes modelled using a non-linear sediment flux law (Equation 2.6; parameters used are $D$ = 0.0086 m$^2$ yr$^{-1}$, $S_C$ = 0.86), responding to a step increase in erosion rate. Response time decreases with increasing erosion rates and increases with hillslope length. For the range of estimated erosion rates in the area in Figure 2.12, and the distribution of hillslope lengths (histogram), adjustment time ranges between 10 and 1000 ka (grey). From this, given that erosion rates are increasing to > 200 mm ka$^{-1}$, based on highest values from CRN analysis and highest values of $C_{HT}$ (Figure 2.12), we expect the adjustment time in this landscape to be <100 ka.

Hillslope response times calculated here are significantly greater than timescales over which climate is considered to vary. Climatic variability is thought to control the efficiency of sediment transport on hillslopes through changing the type and distribution of biota, the amount of moisture in the soil, the length of winters and growing seasons, and the efficiency of rainsplash erosion and sediment transport by overland flow. The style and timescale of hillslope response to climate fluctuations remains poorly understood (Roering et al., 2007; Tucker et al., 2011). Hence there is an implicit assumption that $D$ represents some time-averaged sediment transport efficiency, which in the case of this study is time-averaged over the timescale at which CRNs have accumulated ($10^3 – 10^4$ years), since $D$ is calibrated to these basin averaged erosion rate estimate.

The assumption of steady state is also critical to the application of CRN to determine basin-averaged denudation. Most critically, denudation in the basin must be assumed spatially and temporally constant for the period over which denudation rate is calculated (or at least any spatial variation cannot be resolved). Where the basin is still responding to acceleration in channel incision, sediment with a $^{10}$Be inventory indicative of the previous, slower erosional regime may contribute to the measured signal until the basin is fully adjusted. Bierman and Steig (1996) demonstrated that such heterogeneity should not mask a basin averaged erosion rate. However, the stochastic nature of landsliding may result in the mobilisation and contribution of sediment with low $^{10}$Be inventories from well below the surface, which could result in overestimated erosion rates in small catchments (Niemi et al., 2005).

### 2.6.3 Comparison to Other Topographic Metrics

Our new technique for mapping the spatial distribution of erosion rates across a landscape not only predicts erosion rates above those at which mean hillslope angles become insensitive, but also allows prediction of rates at the scale of a single

hillslope. The use of normalised steepness indices in the channel network is reliant on a basin-averaged sampling approach in basins large enough that it can be confidently assumed that fluvial processes are the dominant valley-forming process. Many of the Feather River's tributary valleys might be described as hanging valleys (e.g. Crosby et al., 2007; Wobus et al., 2006b) and their upper reaches are effectively decoupled from erosion rates in the main Feather River (Figure 2.7). Valley profiles are commonly linear approaching their outlet, exhibiting channel bed slopes >0.4. As such, the valley forming process may not be fluvial, but rather debris flow dominated (e.g. Sklar and Dietrich, 1998; Stock and Dietrich, 2006). In such settings normalised steepness indices may be decouple from erosion rates and in such settings hilltop curvature may offer an alternative way to estimate erosion rates.

All topographic metrics currently used to infer erosion rates cease to predict rates above some limited value. Invariantly steep, planar hillslopes emerge when erosion rates exceed ~200-300 mm $ka^{-1}$ (e.g. Binnie et al., 2007; DiBiase et al., 2010), though this value is likely to vary between settings. Such limits are probably dependent on lithology and climate. In my landscape the transition may occur at erosion rates as low as ~150 mm $ka^{-1}$ (Figure 2.8), yet the landscape remains predominantly forested and soil-mantled. Normalised channel steepness indices may allow inference of higher erosion rates, possibly up to 600 mm $ka^{-1}$, but also seem to be limited (Ouimet et al., 2009), perhaps by down-valley extension of debris flow-dominated erosion. In order to use hilltop curvature to predict erosion rates, a hilltop must be soil-mantled such that creep-like processes (e.g. expansion-contraction, freeze-thaw, root growth-decay, tree throw) can be assumed to be the dominant conveyor of soil. Therefore the application of techniques described in this contribution is limited to landscapes where erosion rates do not exceed the maximum soil production rates on hilltops. In my field site, soils are present on slopes where hilltop curvatures approach $C_{HT}$ = -0.08, suggesting soils can persist in this landscape at erosion rates as high as 250 mm $ka^{-1}$. Others have reported maximum soil production rates in the San Gabriel Mountains, California range 200-400 mm $ka^{-1}$

(DiBiase et al., 2010; Heimsath et al., 2012). In addition, some soil production mechanisms, such as overturning of bedrock during tree throw, appear to be able to maintain a patchy soil cover at high erosion rates (~500 mm $ka^{-1}$) (Gabet and Mudd, 2010; Heimsath et al., 2012). Given that hilltops in some rapidly eroding terrains are able to retain a patchy soil mantle, I feel that the mechanisms of soil production in such landscapes, particularly on ridges, require further investigation (e.g. Roering et al., 2010). My results highlight that the maximum soil production rate (>250 mm $ka^{-1}$) may not necessarily coincide with the erosion rate at which hillslope gradients become limited (100-150 mm $ka^{-1}$) as suggested by Heimsath et al. (2012). It is the ability of soil production *on hilltops* to keep pace with erosion rates which is critical to the outcomes of this study. Given this result, analysis of in situ CRN sampled in soil on hilltops, which has not yet been carried out, would allow direct comparison of soil production rates to hilltop curvature to further test the results presented here.

I have restricted my analyses to portions of the landscape where hilltops were observed to be soil-mantled, overlying granitoid lithologies. However, there are significant bedrock exposures elsewhere within the part of the landscape underlain by granitoids. These occur either (i) in broad patches on the gently eroding relict surface or (ii) immediately adjacent to the Feather River, in large single patches of exposure below the break in slope separating the steepened landscape from the relict topography. This may be attributed to particularly resistant patches of granitoid and/or a negative feedback whereby stripping of soil inhibits further soil production. The conversion of bedrock to soil follows a 'humped' function with soil production dependent on soil depth (Gabet and Mudd, 2010). Above some optimal soil thickness at which soil production is highest, soil production rate declines exponentially with soil depth (Heimsath et al., 1997). The maximum attainable soil production rate is itself dependent on erosion rate (Heimsath et al., 2012). Yet in order to convert bedrock to soil, a covering soil layer is required to trap water and allow plant colonisation (Gabet and Mudd, 2010; Roering et al., 2010; Wilkinson et al., 2005a). When soil becomes too thin or is removed altogether, bedrock hillslopes will emerge.

Sediment flux may have some dependence on soil depth (Mudd and Furbish, 2007; Roering, 2008) in which case any relationship between hilltop curvature and erosion rates may be non-linear. However soil depths measured in the Feather River do not depend on erosion rate and the depth of sediment transport penetration seems to be set by the rooting depth of the vegetation (Yoo et al., 2011) (see Appendix 1). Such conditions are more likely to be approximated by Equation 2.4.

The application of hilltop curvature, in concert with other topographic metrics for erosion rate such as channel steepness indices (e.g. DiBiase et al., 2010) will allow for comparison of predicted erosion rates between different metrics, and at different spatial scales within landscapes. Additionally this may provide insight into the scale of spatial heterogeneity in erosion rates in both steady state and transiently adjusting landscapes.

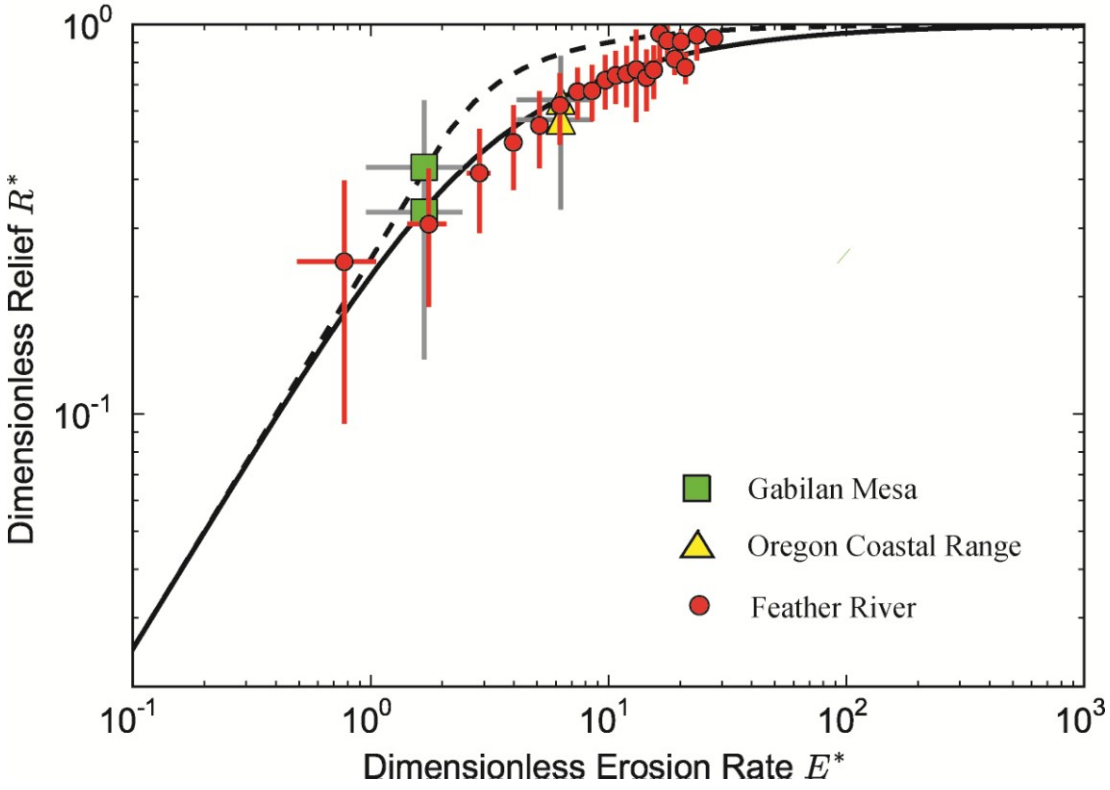


Figure 2.14: Modelled relationship between dimensionless erosion rate and dimensionless hillslope relief predicted by Equation 2.7 (solid) and 2.8 (dashed). Plot shows results reported byRoering et al. (2007) for Gabilan Mesa (green) and Oregon Coastal Range (yellow). Results from the Feather River (red) are binned averages of values calculated from individual hillslopes (Figure 2.11) and span a range of erosion rates and relief. Error bars are based on one standard deviation of binned values for $E^*$ and $R^*$.

### 2.6.4 Influence of Landscape Transience

Many tributary basins in my field setting contain steepened reaches immediately upstream of their outlet into the Feather River (Figure 2.7). Such hanging valleys (Crosby et al., 2007; Wobus et al., 2006b) prevent the recent tectonic signal and subsequent increase in erosion rate from being 'felt' by parts of the landscape upstream. The result is that few hilltops adjacent to the Feather River are being forced by the new incision rate in the channels that flank them on both sides. Hilltops with hillslopes responding to incision on both sides are restricted to areas dividing the Feather River from a large tributary, with close proximity to the Feather River itself (Figure 2.12). Previous quantification of dimensionless erosion rate and relief have focused in landscapes that can be assumed to be at topographic steady state (Roering et al., 2007), but despite landscape transience, hillslope morphology in the Feather River closely matches theoretical predictions made by Equation 2.8 (Figure 2.14; see also Figure 2.11).

The transience of the Feather River is important for the interpretation of my findings. Consider, as such, a mature hillslope responding to an increase in erosion rate. The transience will first be manifest as an increase in slope at the toe of the hillslope, causing increased sediment flux. A wave of increasing slope will propagate to the divide, with associated changes in soil thickness and production rates(Mudd and Furbish, 2005; Roering et al., 2001a). A transient hillslope is therefore predicted to deviate from model predictions (Equation 2.8) since $S$ may increase whilst $C_{HT}$ remains constant, plotting above the line predicted by Equation 2.8 (Figure 2.15). These criteria may allow us to identify the spatial extent of adjusting portions of the landscape in future contributions (Figure 2.15). Such transient relationships may be increasing the apparent non-linearity between $C_{HT}$ and $S$ in Figure 2.11a if there are hilltops with elevated $S$ and low $C_{HT}$. Given estimates for hillslope response time, I would expect there to be portions of individual hillslopes still undergoing adjustment.

## 2.7 Conclusions

The topographic form of hillslopes in a landscape undergoing a transient response to a rapid drop in base-level can be quantified through the extraction of hilltops and their adjacent hillslopes. My study shows that (negative) hilltop curvature increases with CRN-derived erosion rates that vary over an order of magnitude (20-250mm $ka^{-1}$). The suggested linear nature of this relationship facilitates calibration of the hillslope transport coefficient, allowing denudation rates to be predicted across the landscape using hilltop curvature. Following the framework of Roering et al. (2007), the distribution and covariance of hilltop curvature and slope angles appear to best replicate hillslope evolution models in which the transition from creep-dominated to landslide-dominated hillslopes is continuous and gradual, rather than a threshold model. In landscapes where hillslopes can respond relatively quickly to adjustment in the channel network, if the efficiency of sediment transport on hillslopes can be estimated, hilltop curvature can be used to predict erosion rates at the scale of individual hillslopes.

**A: Hilltop curvature and hillslope relief reflect erosion rates prior to increase in rate of base-level fall.**
**B: Hilltop curvature reflects erosion rates prior to increase in rate of base-level fall but hillslope relief is higher than predicted by Equation 2.8 due to the progressive steepening of the hillslope.**
**C: Hilltop curvature and hillslope relief reflect erosion rates after adjustment to increase in base-level fall.**

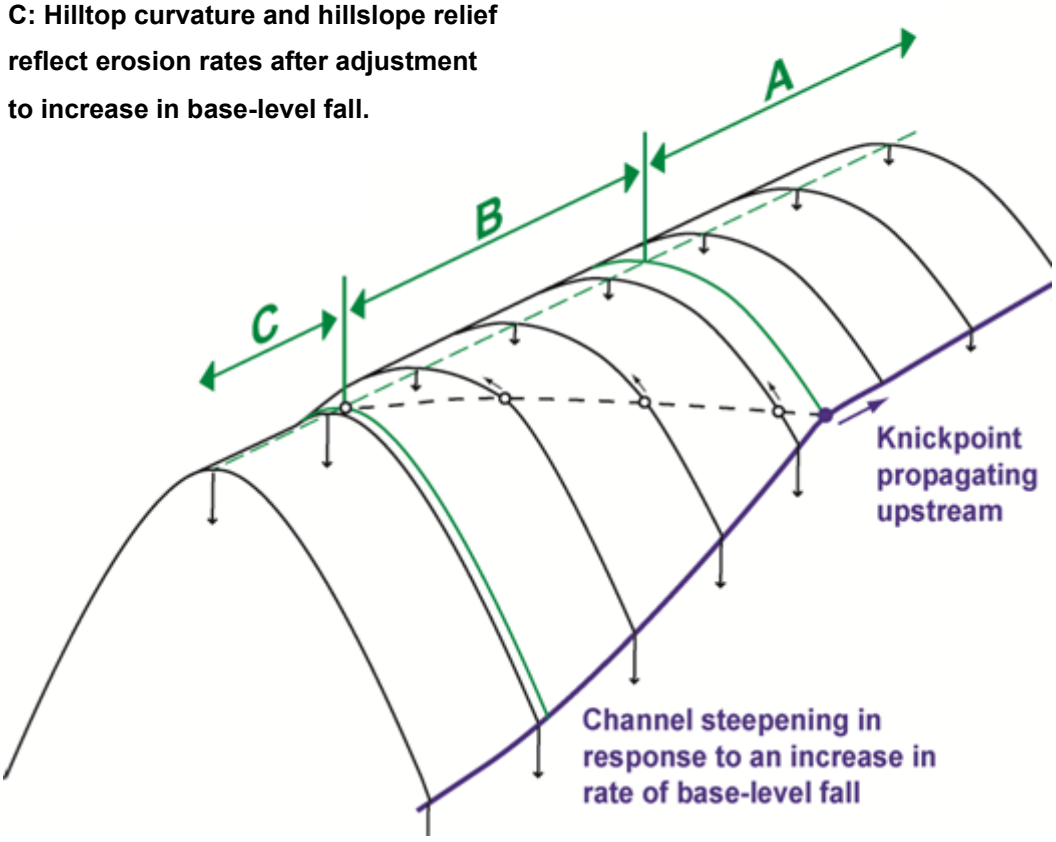


Figure 2.15: schematic illustrating the predicted response of the landscape to an increase in the rate of base-level fall. A knickpoint propagates upstream along the channel, separating the steepened landscape from the relict topography. In response to the increase in erosion rate along the channel, a wave of increasing slope and surface lowering propagates up the hillslopes (dots with black arrows), leading to the alteration of the relationship between hilltop curvature and hillslope relief and the differentiation of three domains (A, B and C). The width of domain B is a function of the response time of the hillslopes (the shorter the response time, the narrower the domain B).

# 3 INFLUENCE OF LITHOLOGY ON HILLSLOPE MORPHOLOGY AND RESPONSE TO TECTONIC FORCING IN THE NORTHERN SIERRA NEVADA OF CALIFORNIA

A version of this chapter has been published:

Hurst, M. D., S. M. Mudd, M. Attal, K. Yoo, and R. Walcott (*2013*), Influence of lithology on hillslope morphology and response to tectonic forcing in the northern Sierra Nevada of California, *Journal of Geophysical Research,* doi:10.1002/jgrf.20049.

## *Chapter Abstract*

Many geomorphic studies assume that bedrock geology is not a first-order control on landscape form in order to isolate drivers of geomorphic change (e.g. climate or tectonics). Yet underlying geology may influence the efficacy of soil production and sediment transport on hillslopes. I performed quantitative analysis of LiDAR digital terrain models to examine the topographic form of hillslopes in two distinct lithologies in the Feather River catchment in northern California, a granodiorite pluton and metamorphosed volcanics. The two sites, separated by <2km and spanning similar elevations, were assumed to have similar climatic histories, and are experiencing a transience in landscape evolution characterised by a propagating incision wave in response to accelerated surface uplift c. 5 Ma. Responding to increased incision rates, hillslopes in granodiorite tend to have morphology similar to model predictions for steady state hillslopes, suggesting that they adjust rapidly to keep pace with the incision wave. By contrast hillslopes in metavolcanics exhibit high gradients but lower hilltop curvature indicative of ongoing transient adjustment to incision. I used existing erosion rate data and the curvature of hilltops proximal to the main channels (where hillslopes have most likely adjusted to accelerated erosion rates) to demonstrate that the sediment transport coefficient is higher in granodiorite (8.8 $m^2$ $ka^{-1}$) than in metavolcanics (4.8 $m^2$ $ka^{-1}$). Hillslopes in both lithologies get shorter (i.e. drainage density increases) with increasing erosion rates.

## 3.1 Introduction

Climate and tectonics act in concert to control the morphology of the Earth's surface. The ability to quantify relationships between topography and climatic or tectonic driving processes is dependent on understanding how efficiently, and by which processes, sediment is generated and transported on hillslopes and in valleys (e.g. Ahnert, 1970; Dietrich et al., 2003; Gilbert, 1909; Gilbert et al., 1877). Such knowledge is vital for ongoing modelling efforts which help link empirical observations to theoretical predictions (e.g. Tucker and Hancock, 2010) and for quantifying the flux and calibre of sediment supplied to streams (Whittaker et al., 2010), the latter of which influences fluvial incision rates (Sklar and Dietrich, 2004) and the rate at which sediment is delivered to basins (Armitage et al., 2011; Duller et al., 2010).

Tectonic processes redistribute rock mass within the lithosphere and control the type and flux of rock material exhumed to the surface. This material may be weakened at depth via mechanical fracturing due to tectonic processes (Molnar et al., 2007) and later disrupted at or near the surface by physical and chemical weathering processes (e.g. penetration and growth of tree roots (Gabet and Mudd, 2010; Roering et al., 2010), frost wedging (Small et al., 1999) and chemical alteration and weakening (Burke et al., 2007; Dixon et al., 2009). These processes generate soil/regolith (here used synonymously and defined as readily mobilized material at or near the Earth's surface) which can be subsequently transported away. The physical properties (composition, rock mass strength (RMS), degree of fracturing) of bedrock will thus influence the physical properties of the resulting soil e.g. composition, grain size distribution (GSD), degree of weathering, porosity, cohesion; Yoo et al. (2005). The physical characteristics of soil are in turn expected to influence the efficacy at which sediment transport occurs on hillslopes (Culling, 1963; Furbish et al., 2009). Chemical properties also play a role: the mineralogical composition of parent material influences both the susceptibility to, and nature of, chemical alteration that

occurs prior to the onset of biophysical activities that generate and transport sediments (Burke et al., 2007; Dixon et al., 2009). Thus there is the potential for bedrock lithology to influence topography even in soil-mantled landscapes.

Several studies have attempted to quantify relationships between rock strength and topography, or have considered the role that spatially variable rock type may have in controlling processes which generate and redistribute sediment at the Earth's surface. Schmidt and Montgomery (1995) demonstrated that hillslope relief is limited by the material strength of bedrock. Similarly Burbank et al. (1996) suggested that hillslope gradients were limited at their internal friction angle, despite variation of over an order of magnitude in denudation rates in the north-west Himalayas (1-12 mm $a^{-1}$). Hillslopes were thus interpreted to evolve in response to variable erosion rates by adjusting the frequency of landslides rather than by steepening. The distribution of slope angles may serve as a proxy for rock mass strength in landslide dominated terrain (Korup, 2008; Korup and Schlunegger, 2009). Clarke and Burbank (2010) however, were not able to distinguish rock mass strength from hillslope gradients in distinct lithologies in Southern New Zealand. They attributed the similarities in slope distributions between low grade metamorphics of the Southern Alps and high grade and igneous units of the Fiordland to the nature of bedrock fracturing. Both sites are susceptible to landsliding but different styles of fracturing were interpreted to control the type of mass wasting process operating. In Fiordland fracturing occurs primarily due to near surface processes and thus drives frequent shallow landslides, whilst pervasive tectonic fracturing in the Southern Alps facilitates larger, deeper landsides (Clarke and Burbank, 2010; Clarke and Burbank, 2011). Although links between bedrock lithology and topography have been explored in bedrock landscapes, no studies have explored the role that lithology may play in controlling topography in soil-mantled landscapes.

Lithology may play an important role in controlling the efficiency of sediment transport on hillslopes. McKean et al. (1993) showed that the sediment

transport coefficient *D*, which relates hillslope gradient to sediment flux, is an order of magnitude larger in weak clay-rich soils than in strong, granular soils, presumably due to variation in the efficiency of shrink-swell cycles as a transport process. This is at least partially controlled by the parent lithology through the nature of jointing and susceptibility to weathering. Furbish et al. (2009) described the sediment transport coefficient *D* as a function of the material properties of soil including thickness, grain size distribution and cohesion which may directly influence the efficiency of sediment transport. The presence of coarse material in the soil may result in a boulder lag which armours underlying soil from erosion (Granger et al., 2001). Owen et al. (2011) showed that hillslope erosion rates across a climate gradient in Chile were sensitive to precipitation, which influences transport processes, with more rapid erosion rate attributed to wetter climate and biologically-driven sediment transport. To assess whether there is any existing evidence that *D* might be influenced by lithology, I compiled published values of *D* to search for global trends with lithology (Figure 3.1a; Table 3.1). Simplifying to cohesionless, clastic, volcanic and crystalline lithologic groups, I was not able to observe any trends between lithology and the sediment transport coefficient (Figure 3.1b). However, isolating for values derived from cohesionless substrate (i.e. alluvium; $n$=24) I observed that *D* increases with precipitation and seasonality (Figure 1b,c; seasonality defined here as the standard deviation about mean annual precipitation), as suggested by Hanks (2000). Yet it seems likely that both substrate lithology and climate will control *D*, since lithology will influence the production of, and material properties of the soil, and climate will control the style and efficiency of processes which mobilise the soil. If lithology can significantly influence hillslope sediment transport, I anticipate differences in landscape morphology for adjacent areas (with similar climate) overlying distinct bedrock types, even if the mechanisms of sediment transport are similar.

Table 3.1: Reported values of the sediment transport coefficient *D* and associated crude climate data; includes descriptions of vegetation type and substrate material and landforms.

| Study | Site | Climate* | | Vegetation | Brief Description | *D* ($m^2$ $ka^{-1}$)† |
|---|---|---|---|---|---|---|
| | | MAT (°C) | MAP (mm) | | | |
| Almond et al. (2008) | Charwell Basin, New Zealand | 10.6 ± 3.6 | 1159 ± 35 | Grassland/Shrubland | Fluvial gravel terraces | 3.0 ± 1.0 |
| | | | | Podocarp/Beech forest | | 5.0 ± 2.0 |
| Almond et al. (2008) | Ahuriri, New Zealand | 11.8 ± 3.9 | 662 ± 22 | Grassland/Shrubland<br>Recent pasture grasses | Thick loess deposits (underlain by altered basalt) | 3.1 ± 0.4<br>7.0 ± 2.0 |
| Arrowsmith et al. (1998) | Carrizo Plain, CA, USA | 14.5 ± 6.2 | 475 ± 73 | Grasses and shrubs | Fault scarps in alluvial gravel | 8.6 ± 0.8 |
| Avouac et al. (1993) | Tien Shan, China | 9.5 ± 14.2 | 138 ± 13 | Grasses and shrubs | Fault scarps in alluvial gravel | 5.5 ± 2.0 |
| Avouac and Peltzer (1993) | Hotan Region, Xinjiang, China | 1.8 ± 10.7 | 33 ± 6 | Not vegetated | Fault scarps in alluvial gravel | 3.3 ± 1.4 |
| Begin (1992) | Northern Negev, Israel | 19.6 ± 5.0 | 193 ± 36 | Not vegetated | Fluvial gravel terraces | 0.4 ± 0.3 |
| Bowman and Gerson (1986) | Lake Lisan, Dead Sea | 24.3 ± 6.5 | 142 ± 27 | Not vegetated | Lake terraces | 0.4 |
| (Bowman and Gross, 1989) as reported in Hanks (2000) | Northern Arava, Israel | 18.8 ± 5.5 | 198 ± 37 | Not vegetated | Fault scarps in alluvial gravel | >0.4 |
| Carretier et al. (2002) | Gurvan Bugd fault system, Mongolia | 0.3 ± 12.2 | 160 ± 33 | Not vegetated | Fault scarps in alluvial gravel | 3.3 ± 1.7 |
| Colman and Watson (1983) | Lake Bonneville, UT, USA | 9.5 ± 9.2 | 456 ± 19 | Grasses and shrubs | Alluvial shoreline scarps | 0.9 |
| Constantine et al. (2012) | Simulated Douglas Fir Forest | N/A | N/A | Douglas Fir | N/A | 0.1 - 3.5 |
| Enzel et al. (1996) | Southern Arava Valley, Israel | 24.2 ± 6.3 | 32 ± 6 | Not vegetated | Fault scarps in alluvial gravel | 0.2 – 0.3 |
| Gabet (2000) | Transverse Ranges, CA, USA | 15.0 ± 4.0 | 498 ± 83 | Coastal Sage | Plio-Pleistocene fanglomerates. Process specific: gopher bioturbation | 7.4 |
| Gabet (2003) | Transverse Ranges, CA, USA | 15.0 ± 4.0 | 498 ± 83 | Coastal Sage | Plio-Pleistocene fanglomerates. Process specific: dry ravel | 0.17 |
| Hanks et al. (1984) | Lake Bonneville, UT, USA | 9.5 ± 9.2 | 456 ± 19 | Grasses and shrubs | Alluvial shoreline scarps | 1.1 |

| | | | | | | |
|---|---|---|---|---|---|---|
| Hanks et al. (1984) | Santa Cruz sea cliffs, CA, USA | 13.8 ± 2.8 | 693 ± 111 | Lower terraces are farmed, upper terraces grassland | Quaternary wave-cut terraces cut into Pliocene mudstone | 11 |
| Hanks et al. (1984) | Raymond Fault Scarp, LA. CA, USA | 18.1 ± 4.2 | 450 ± 76 | Not reported | Fault scarps in alluvial gravel | 16 |
| Hanks et al. (1984) | Drum Mtns. UT, USA | 10.1 ± 9.9 | 192 ± 10 | Low shrubs (sagebrush and shadscale) 7-20% cover | Fault scarps in alluvial gravel | 1.1 |
| Hanks and Wallace (1985) | Lake Lahonta, NV, USA | 10.0 ± 8.5 | 202 ± 9 | Not reported | Alluvial shoreline scarps | 1.1 |
| Hanks (2000) | Lost River, ID, USA | 3.3 ± 9.1 | 270 ± 16 | Not reported | Fault scarps in alluvial gravel | 0.9 - 1.0 |
| (Heimsath et al., 2000) | Nunnock River, SE Australia | 12.8 ± 4.4 | 827 ± 32 | Schlerophyll forest | Soil-mantled granite | 4.0 |
| (Heimsath et al., 2005) | Nunnock River, SE Australia | 12.8 ± 4.4 | 827 ± 32 | Schlerophyll forest | Soil-mantled granite | $D_d$ = 5.5 m ka$^{-1}$ |
| | Tennessee Valley, CA, USA | 13.8 ± 2.8 | 794 ± 125 | Coastal grassland and scrub | Soil-mantled deep marine metasedimentary | $D_d$ =1.25 m ka$^{-1}$ |
| | Point Reyes, CA USA | 12.9 ± 2.9 | 977 ± 153 | Bishop pine forest | Soil-mantled granite | $D_d$ =0.5 m ka$^{-1}$ |
| Hughes et al. (2009) | Charwell Basin, New Zealand | N/A | N/A | Shrubland/Grassland (late-Pleistocene) | Fluvial gravel terraces (underlain by greywacke) | 4.7 ± 2.0 |
| | | 10.6 ± 3.6 | 1159 ± 35 | Podocarp and Beech forest | | 8.8 ± 3.0 |
| Hurst et al. (2012) | Feather River, CA, USA | 13.2 ± 6.5 | 1508 ± 217 | Mixed conifer forest | Soil-mantled granitoids | 8.0 |
| Jungers et al. (2009) | Great Smokey Mountains, NC, USA | 8.4 ± 7.3 | 1855 ± 24.1 | Deciduous forest | Soil-mantled quartzite | 6.5 - 10 |
| Martin and Church (1997) | Various | N/A | N/A | Various | From field measurements of volumetric creep rates | 0.2 |
| Mattson and Bruhn (2001) | Lake Bonneville, UT, USA | 9.5 ± 9.2 | 456 ± 19 | Grasses and shrubs | Alluvial shoreline scarps | 1.2 ± 0.3 |
| Mattson and Bruhn (2001) | Wasatch Fault Zone, UT, USA | 9.5 ± 9.3 | 420 ± 17 | Not reported | Fault scraps in alluvial gravel | 2.8 ± 1.1 |
| McKean et al. (1993) | East Bay Regional Park, CA, USA | 14.9 ± 5.4 | 522 ± 79 | Grasses, clay rich soil. | Soil-mantled eocene marine shale. | 36 ± 5 |
| Nash (1980a) | Emmet County, MI., USA. | 5.7 ± 10.1 | 825 ± 35 | Mixed Pine, Oak, Beech forest | wave-cut terraces in moraine | 12 |
| Nash (1980b) | Drum Mtns., UT, USA | 10.1 ± 9.9 | 192 ± 10 | Low shrubs (sagebrush and shadscale) 7-20% cover | Fault scarps in alluvial gravel | 0.4 |
| Nash (1984) | Hebgen Lake, MT USA | 1.9 ± 9.6 | 615 ± 22 | Not reported | Fault scarps in alluvial gravel and fluvial gravel terraces | 2.0 ± 0.4 |

| | | | | | | |
|---|---|---|---|---|---|---|
| Nivière and Marquis (2000) | Upper Rhine Graben, Germany | 10.2 ± 6.6 | 707 ± 32 | Forested | Fluvial gravel terraces | 1.4 |
| Pelletier et al. (2006) | Lake Bonneville, UT, USA | 9.5 ± 9.2 | 456 ± 19 | Grasses and shrubs | Alluvial shoreline scarps | 1.0 |
| Pelletier and Cline (2007) | Lathrop Wells, NV, USA | 17.6 ± 8.9 | 109 ± 8 | Little vegetation | Loose vesicular scoria lapilli | 3.9 |
| Pelletier et al. (2011) | Banco Bonito lava flow, Valles Caldera, NM, USA | 4.9 ± 8.4 | 482 ± 25 | Pine, oak and mixed conifer forest | Soil-mantled rhyolite lava flow | $D = 0.5 \pm 0.2$<br>$D_d = 0.55 \pm 0.35$ |
| Petit et al. (2009) | Wasatch Mtns., UT, USA | 8.4 ± 9.3 | 599 ± 31 | Not reported | Soil-mantled gniess (Precambrian) | 120 ± 10 |
| Pierce and Colman (1986) | Big Lost River Valley, ID, USA | 5.2 ± 10.0 | 271 ± 13 | Not reported | Alluvial fan scarps | $D = 0.2 \rightarrow 7.0^{+}$ |
| Reneau (1988) reported in (Heimsath et al., 2005) | Tennessee Valley | 13.8 ± 2.8 | 794 ± 125 | Coastal grassland and scrub | Soil-mantled deep marine metasedimentary | 5.0 |
| | Point Reyes | 12.9 ± 2.9 | 977 ± 153 | Bishop pine forest | Soil-mantled granite | 3.0 |
| Reneau et al. (1989) | Clearwater River, WA, USA | 9.0 ± 4.5 | 3316 ± 344 | Western hemlock and Pacific silver fir forest | Soil-mantled deformed tertiary silts, sandstones and conglomerates | 4.7 ± 2.5 |
| Riggins et al. (2011a) | Bodmin Moor, Cornwall, UK | 9.2 ± 4.5 | 1134 ± 52 | Grasses, (previously hazel and oak woodland) | Soil-mantled coarse-grained granite (Permian) | 46 ± 16 |
| Roering et al. (1999) | Sullivan Creek, OR, USA | 10.8 ± 3.5 | 1671 ± 205 | Douglas fir, mixed conifer forest | Soil-mantled turbidite beds | 3.0 |
| Roering et al. (2001b) | Experimental | N/A | N/A | N/A | Sand pile disturbed by acoustics | 0.27 ± 0.02 |
| Roering et al. (2002)<br>Roering et al. (2004) | Charwell River, South Island, New Zealand | 10.6 ± 3.6 | 1159 ± 35 | Podocarp and Beech forest | Fluvial gravel terraces (underlain by greywacke) | 12 ± 8<br>16 ± 6 |
| Roering and Gerber (2005) | Sullivan Creek, OR, USA | N/A | N/A | N/A | Same site as *Roering et al*. [1999] but post-wildfire | 11 ± 3.5 |
| Roering et al. (2007) | Gabilan Mesa, CA, USA | 14.7 ± 5.1 | 278 ± 44 | Oak Savannah | Soil-mantled shallow marine and alluvial sediement | * $D$ in range<br>38 ± (+40/-24) |
| Rosenbloom and Anderson (1994) | Santa Cruz, CA, US. | 13.5 ± 2.6 | 713 ± 114 | Lower terraces are farmed, upper terraces grassland | Marine terraces cut into Miocene marine mudstone | 10 |
| Small et al. (1999) | Wind River Range, WY, USA | -4.4 ± 7.7 | 651 ± 13.3 | Not vegetated | Soil-mantled crystalline bedrock | 17.5 ± 2.7 |
| Spelz et al. (2008) | Laguna Salada, Baja California, Mexico | 21.6 ± 6.3 | 87 ± 10 | Not vegetated | Fault scarps in fluvial gravel terraces | 0.051 – 0.066 |

| | | | | | | |
|---|---|---|---|---|---|---|
| Tapponnier et al. (1990) | Qilian Shan, China | 5.9 ± 10.8 | 137 ± 24 | Not vegetated | Fault scarps in Quaternary fanglomerates | 3.3 ± 1.7 |
| This study | Feather River, CA, USA | 13.2 ± 6.5 | 1508 ± 217 | Mixed conifer forest | Soil-mantled intermediate metavolcanics<br>Soil-mantled granodiorite | 4.8 ± 1.8<br>8.8 ± 3.3 |
| Walther et al. (2009) | Blue Mountains, WA, USA | -0.7 ± 15.6 | 305 ± 60 | Coniferous forest | Soil-mantled basalt | 4.8 ± 0.7 |

[*] Mean annual temperature (MAT) and mean annual precipitation (MAP) calculated over the period 1950-2000. Data from the WorldClim global climate 30 arc-second dataset (http://www.worldclim.org accessed 6th August 2011) (Hijmans et al., 2005). Error ranges are 1σ of monthly means as an indicator of seasonality.

[†] I report absolute values, range constraints and/or error estimates as they appear in the literature

[**] Pierce and Colman (1986) found that *D* ranged over two orders of magnitude depending on the scarp aspect.

[††]Large range due to poor constraints on boundary erosion rate

In soil-mantled, forested landscapes the dominant mechanism of sediment flux is often via tree throw and the growth and decay of tree roots (Constantine et al., 2012; Gabet and Mudd, 2010; Roering et al., 2010). The efficiency of sediment transport may therefore be strongly linked to the amount and type of vegetation acting to disturb sediment. Hughes et al. (2009) inferred that sediment transport increased at the start of the Holocene due to colonization by forests, replacing previous grassland in the Charwell Basin, New Zealand (see table 1). Light Detection and Ranging (LiDAR) allows for quantification of metrics for above-ground biomass, such as vegetation density or mean canopy height (e.g. Donoghue and Watt, 2006; Holmgren et al., 2003; Lefsky et al., 1999; Naesset, 1997; Nilsson, 1996), which can be compared to topographic attributes to explore whether $D$ may vary systematically as a function of vegetation (Pelletier et al., 2011).

The morphology of soil-mantled hillslopes reflects the processes which create and redistribute sediment downslope, and the erosion rate in the adjacent channels. Where estimates of erosion rates have been made within a landscape, one may infer the nature of sediment transport based on the morphological properties of hillslopes such as hilltop curvature $C_{HT}$, mean hillslope gradient $S$, and hillslope length $L_H$ (Hurst et al., 2012; Riebe et al., 2000; Roering, 2008; Roering et al., 2007). In this contribution I extract these properties from high resolution (1 m grid) topography, derived from airborne LiDAR, to compare the topographic signature of landscapes in two distinct lithologies, the granodiorite of the Cascade pluton and the metavolcanic rocks of the Central Belt in the northern Sierra Nevada of California. In this region I have constraints on rock uplift rates and associated transient erosion rates (Hurst et al., 2012; Wakabayashi and Sawyer, 2001), present day climate, and current vegetation. Hence there is an opportunity to quantitatively analyse the morphological properties of rapidly denuding, soil-mantled hillslopes in two distinct lithologies in order to investigate the control bedrock type plays in a soil-mantled landscape. I sought to quantify the efficiency of sediment transport processes on hillslopes in two

distinct lithologies and identify whether any differences could be attributed to climate, the type and distribution of vegetation or underlying lithology. I investigated differences in the distribution of hillslope gradients between bedrock types. Finally I documented differences in the length of hillslopes between the two lithologies, and a tendency for hillslope lengths to shorten with increasing erosion rate, suggesting that drainage density may be controlled by erosion rate.

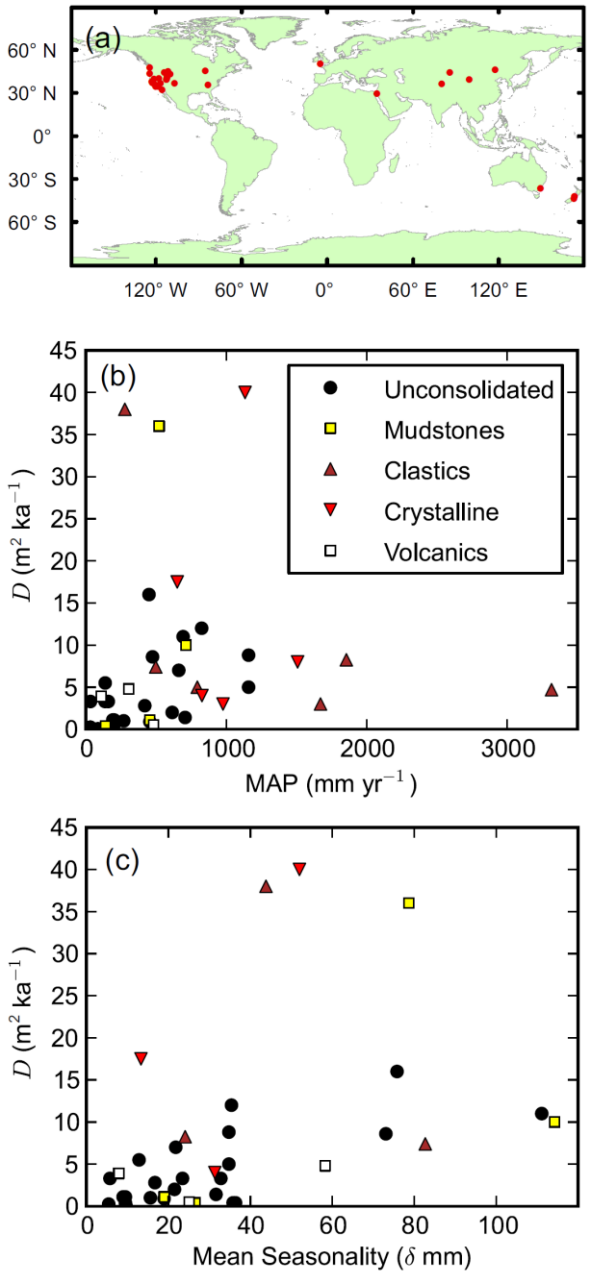


Figure 3.1: (a) Global distribution of calibrated sediment transport coefficients (red) (see table 1) (b) Sediment transport efficiency vs. mean annual precipitation (MAP) for lithologic groups. In unconsolidated substrate there is a weak tendency for $D$ to increase with wetter climate ($R^2 = 0.27$ for linear regression). (c) Sediment transport efficiency vs. annual variability of precipitation ($2\sigma$ about mean monthly precipitation). There is a trend for $D$ to increase with more variable intra-annual precipitation ($R^2 = 0.51$ for linear regression). There were no trends observed when comparing $D$ to mean annual temperature.

## 3.2 Theory on Hillslope Morphology and Evolution

### 3.2.1 Hillslope Mass Balance and Sediment Transport Equations

The spatial and temporal evolution of soil-mantled landscapes can be examined using principles of mass conservation (Culling, 1960; Dietrich et al., 2003; Gilbert, 1909) where the surface elevation $\zeta$ [L] changes in time $t$ relative to a moving reference elevation $\zeta_0$ [L] (e.g. Mudd and Furbish, 2005). The surface elevation evolves according to:

$$\frac{\partial \zeta}{\partial t} = -\frac{\partial \zeta_0}{\partial t} - \nabla \cdot q_s \,, \qquad [3.1]$$

where $q_s$ [$L^2$ $T^{-1}$] is volumetric sediment flux per unit contour width. I equate the lowering rate of the reference elevation $\zeta_0$ to the rate of local bedrock lowering (i.e. valley incision) at the base of the hillslope ($E$ [L $T^{-1}$]) such that $\partial\zeta_0 / \partial t = -(\rho_r/\rho_s)E$ where $\rho_r$ and $\rho_s$ [M $L^{-3}$] are the densities of bedrock and dry soil respectively. If the entire hillslope lowers at the same rate as the channel then Equation [3.1] reduces to:

$$\frac{\rho_r}{\rho_s} E = \nabla q_s \,. \qquad [3.2]$$

Equations 3.1 and 3.2 assume that all mass transport is the result of physical processes and mass/volume change due to aeolian and chemical weathering processes is negligible.

Most processes which act to transport sediment down a hillslope are gravity driven, and are therefore dependent on hillslope angle. Both grain displacement

during disturbance (normal to the surface) and subsequent gravitational settling (vertical) increase with steeper slopes (Furbish et al., 2009; Roering et al., 1999). On gentle, soil-mantled hillslopes, sediment flux, $q_s$, is often attributed to slope dependent creep-like processes (Davis, 1892; Gilbert, 1909). However, in landscapes with high relief, hillslopes often become planar away from topographic divides, commonly inferred to be driven by a process transition to landslide-dominated sediment flux (Binnie et al., 2007; Howard, 1994; Roering et al., 1999) and/or an increase in particle displacement distances (Foufoula-Georgiou et al., 2010; Tucker and Bradley, 2010). Roering et al. (1999) formulated a disturbance-driven transport law allowing sediment flux to increase in a non-linear fashion with hillslope gradient to account for this process transition. As slope approaches a critical angle $S_C$, which field studies have shown to vary between 0.8 (DiBiase et al., 2010; Hurst et al., 2012) and 1.25 (Roering et al., 1999), sediment flux asymptotically approaches infinity (Anderson, 1994; Andrews and Bucknam, 1987; Roering et al., 1999):

$$q_s = -D\nabla\zeta\left[1-\left(\frac{|\nabla\zeta|}{S_C}\right)^2\right]^{-1} \qquad [3.3]$$

where $D$ [$L^2$ $T^{-1}$] is a transport coefficient. Equation 3.3 has empirical and experimental support (Gabet, 2000; Pelletier and Cline, 2007; Roering et al., 2001b). I do not consider similar depth-dependant models (e.g. Heimsath et al., 2005) since soil depth does not vary systematically with erosion rate at my field site (Yoo et al., 2011) (see Appendix 1).

In Equation 3.3 the combined influences of climate and lithology on a suite of processes are lumped into a single parameter, $D$. These processes include freeze/thaw, wet/dry and shrink/swell cycles (Gilbert, 1909), bioturbation due to tree throw (Gabet and Mudd, 2010; Roering et al., 2010) or burrowing organisms (Gabet,

2000; Yoo et al., 2005) and rainsplash grain displacement (Dunne et al., 2010). Hanks (2000) documented that $D$ increases systematically with climate from $D$ = 0.1-0.7 $m^2$ $ka^{-1}$ in the arid Middle East (Begin, 1992; Bowman and Gerson, 1986; Bowman and Gross, 1989) through to 0.5-2.0 $m^2$ $ka^{-1}$ and 3.3-5.5 $m^2$ $ka^{-1}$ in the semi-arid regions of the western U.S. (Hanks, 2000; Hanks and Andrews, 1989; Hanks et al., 1984; Hanks and Wallace, 1985) and western China (Avouac, 1993; Avouac and Peltzer, 1993; Tapponnier et al., 1990) respectively, to 8.5-16 $m^2$ $ka^{-1}$ in more humid coastal California (Arrowsmith et al., 1998; Hanks et al., 1984) and Michigan (Nash, 1980a). Several studies have postulated increased hillslope sediment transport rates at the glacial-interglacial transition between the late Pleistocene and early Holocene in New Zealand, attributed to changes in vegetation density and type (Almond et al., 2008; Hughes et al., 2009; Roering et al., 2004; Walther et al., 2009). Variation in the type and density of vegetation may also occur as soil conditions and nutrient availability changes at lithologic boundaries.

### 3.2.2 Hillslope Morphology

When hillslope gradient ($\nabla\zeta$) is small, the bracketed term in Equation 3.3 approaches unity. Substituting Equation 3.3 into Equation 3.2 I can therefore solve for erosion rate where slope angles are low (i.e., on hilltops):

$$E = -\frac{\rho_s}{\rho_r} D\, C_{HT}\,, \qquad [3.4]$$

where $C_{HT}$ is the hillslope curvature, i.e.$\nabla^2\zeta$, at the hilltop, since this is where I expect hillslope gradients to be the gentlest. Equation 3.4 predicts that the erosion rate on a steadily denuding hillslope should be linearly proportional to hilltop curvature $C_{HT}$ and $D$. I adopt the sign convention that convex up surfaces (i.e., hilltops) have negative curvature and erosion is a positive quantity (i.e. a positive

value of $E$ indicates a lowering of the land surface). Equation 3.4 predicts erosion rates as a function of $C_{HT}$ only if $(\nabla\zeta/S_C)^2$ (Equation 3.3) is negligible.

Hillslope relief may also be used to estimate $E$, but once $E$ exceed ~100-300 mm $ka^{-1}$, further increases in $E$ have been inferred to be accommodated by increased landsliding frequency on threshold slopes and hillslope gradients or hillslope relief become poor predictors of $E$ (e.g. Binnie et al., 2007; Burbank et al., 1996; DiBiase et al., 2010; Ouimet et al., 2009). Larsen and Montgomery (2012) mapped recent (1974-2007) landslides in the eastern Himalayas to document that rates of landsliding vary by an order of magnitude despite little variation slope gradients across a zone of high uplift. Roering et al. (2007) provided a framework for analysing relationships between denudation and hillslope topography (i.e. relief, slope, curvature and hillslope length) when Equation 3.3 is combined with the mass balance Equation (Equation 3.2). Non-dimensionalization allows comparisons between landscapes with distinct process rates. Erosion rate and Relief are cast in non-dimensional form as functions of topographic parameters $C_{HT}$, $L_H$ and mean hillslope gradient $\overline{S}$ :

$$E^* = \frac{E}{E_R} = \frac{\rho_r}{\rho_s} \cdot \frac{2\,E\,L_H}{D\,S_C} \qquad [3.5a]$$

$$E^* = \frac{2\,C_{HT}\,L_H}{S_C} \qquad [3.5b]$$

$$R^* = \frac{1}{E^*}\left\{\sqrt{1+(E^*)^2} - \ln\left[\frac{1}{2}\left(1+\sqrt{1+(E^*)^2}\right)\right] - 1\right\} \qquad [3.6a]$$

$$R^* = \frac{\overline{S}}{S_C} \qquad [3.6b]$$

Equation 3.6a predicts a non-linear relationship between $E^*$ and $R^*$, which all hillslopes with a morphology that is adjusted to its boundary conditions should obey (provided that Equation 3.3 gives a reasonable approximation of sediment transport processes on the hillslope). Similarly to Equation 3, the prediction of Equation 6a only holds when the hillslope is denuding in concert with the adjacent channel. However Equations 5b and 6b allow us to calculate $E^*$ and $R^*$ even where the steady state assumption is violated, to compare to the model predictions for steady state encapsulated in Equation 6a. In such a scenario, hillslope morphology is expected to vary from the model prediction in a manner that reflects the style of transience (Hurst et al., 2012). I therefore developed techniques to quantify the spatial distribution of $C_{HT}$, $L_H$ and $S$ within a landscape from LiDAR derived topography in order to explore the spatial distribution of $E^*$ and $R^*$ and their relationship to bedrock type.

## *3.3 Methods*

### 3.3.1 Hillslope Morphology

In forested landscapes, high resolution LiDAR DEMs commonly exhibit high local variability due to the presence of pits associated with the upheaval or decay of tree root clumps (Roering et al., 2010) or dense vegetation or 'brush' which has been misclassified as bare earth (Lashermes et al., 2007). Thus standard algorithms computing slope and curvature from 3x3 pixel moving windows produce noisy results. Assuming a diffusion-like model for sediment transport requires slope to be calculated at a larger scale than that at which the disturbance forces operate (Furbish et al., 2009; Jyotsna and Haff, 1997). Lashermes et al. (2007) found that a length scale or search radius of 6 m was appropriate for LiDAR from the South Fork Eel River, CA., whilst Roering et al. (2010) demonstrated a scale of 7.5 m in their forested landscape in the Oregon Coast Range. At my field site the appropriate scaling was 6m (Hurst et al., 2012). Here I calculated the slope, curvature and aspect

from a 6-term quadratic surface fitted to a 12×12 m window (length scale = 6 m) in the gridded elevation data, centred on the pixel of interest (see section 2.4.2 for further details).

A hillslope can be considered to begin at a topographic divide and extend to a valley bottom, at which a transition from hillslope processes (i.e. diffusive processes and landslides) to valley forming processes occurs (e.g. debris flow and/or fluvial erosion). I extract hilltops from the LiDAR DEM as the intersecting margins of zero-order and upward drainage basins, where slope ($\nabla\zeta$) < 0.4. The valley network was defined using the Geonet algorithm of Passalacqua et al. (2010a). Hilltop curvature $C_{HT}$ was sampled as all pixels within 2 m of these hilltops. Adjacent hillslopes were sampled using an aspect-driven routing algorithm (Lea, 1992) to trace from each hilltop pixel to an adjacent valley bottom. Along the resulting profile, the mean slope ($S$), relief ($R$) and horizontal hillslope length ($L_H$) were recorded. A mean value for each of these metrics was then determined for each hilltop segment (see Hurst et al. (2012), or section 2.4.4 for a detailed description of methods).

### 3.3.2 Quantifying Vegetation Properties

Sediment transport in forested, soil-mantled landscapes is driven, in part, by tree turnover through growth and decay of tree roots and the upheaval of tree root wads (Dietrich and Perron, 2006; Gabet and Mudd, 2010; Gabet et al., 2003; Schaetzl and Follmer, 1990). Therefore it has been suggested that the sediment transport coefficient $D$ in Equation 3.3 may vary with above ground biomass (AGB) (Roering et al., 2004; Walther et al., 2009). Airborne derived LiDAR data collected from forested landscapes contain a wealth of information about vegetation, with last/lowest returns being generally classified as the ground surface and all above-ground returns being reflected from vegetation surfaces (leaves, branches etc.). Properties of the canopy elevation structure such as the mean and standard deviation of the height of canopy returns ($V_{mean}$ and $V_{sd}$ respectively) can be readily extracted

from LiDAR (Lefsky et al., 1999; Naesset, 1997; Nilsson, 1996) and may provide useful indicators of AGB [e.g. (Clark et al., 2011; Hall et al., 2005; Pelletier et al., 2011; Saatchi et al., 2011). Clark et al. (2011) found that LiDAR derived metrics $V_{mean}$ and $V_{max}$ provided robust indicators of measured AGB. Pelletier et al. (2011) used a 1m resolution canopy height map derived from LiDAR to demonstrate a negative relationship between mean $C_{HT}$ and $V_{mean}$, suggesting that vegetation cover may be controlling the sediment transport coefficient $D$.

Here I investigated how vegetation cover varies on ridgetops as a function of lithology between my two study areas to assess whether variation in the quantifiable vegetation metrics derived from LiDAR could account for differences in the efficacy of sediment transport. The approach is limited by the assumption that modern vegetation accounts for the current shape of hillslopes, yet others have attributed change in biologically-driven sediment transport to change in vegetation cover at the end of the last glaciations (Roering et al., 2004; Walther et al., 2009).

I analysed point cloud density and height above the ground surface for returns classified as vegetation (LiDAR data acquisition and processing completed by the National Center for Airborne Laser Mapping (NCALM - http://www.ncalm.org). NCALM funding provided by NSF's Division of Earth Sciences, Instrumentation and Facilities Program. EAR-1043051). To estimate canopy height, the heights of above-ground point returns were de-trended by subtracting the elevation of the ground surface interpolated to a 1-m grid. The resulting canopy heights were analysed to compute values for $V_{mean}$ and $V_{sd}$ in each grid cell in 4-m-resolution grids (coarsened to avoid data gaps where there were no LiDAR returns). Although the low relief portions of the landscape have been heavily logged, there is no evidence of recent logging (i.e., no cut stumps and numerous trees with diameters exceeding 1 meter). Canopy height data from the LiDAR appears to qualitatively agree with satellite imagery (i.e., bare patches apparent on satellite images correspond to absent or minimal canopies from LiDAR). I defined a vegetation density ratio $V_{dens}$ as the ratio

between the points classified as above ground and points classified as ground, normalised to the total number of returns within a 4-m-resolution grid. A ratio $V_{dens}$ = 1 indicates that all points returned were above ground and the canopy is dense, whilst a ratio $V_{dens} \rightarrow 0$ indicates little/no vegetation cover. I consider this a crude approach since the results are limited by the average point spacing of LiDAR returns (~ 4 $m^{-2}$) and may be influenced by any variation in leaf structure and tree spacing.

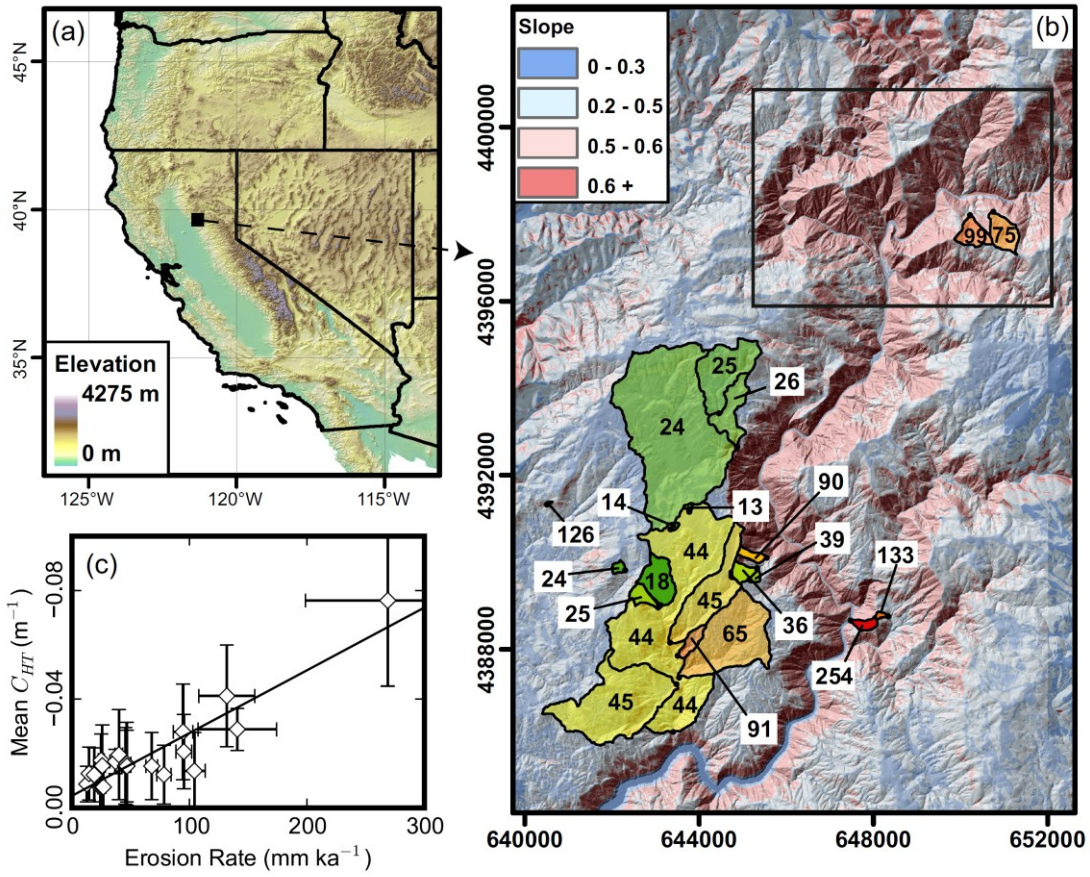


Figure 3.2: (a) Location of study area in Sierra Nevada of northern California. (b) High resolution (LiDAR) shaded slope gradient map of the study area along the Feather River (Middle Fork); low gradients are blue, steep slopes are red. Overlain are CRN sample sites with estimated basin-averaged erosion rates in mm $ka^{-1}$ (shaded green to red with increasing erosion rate; uncertainties on these estimates are shown in (c)) (Hurst et al., 2012). Samples were taken for basins exclusively in granitoid bedrock. Erosion rates vary over an order of magnitude from the canyon to the adjacent relict upland. (c) Plot of mean hilltop curvature compared to denudation rate in each of the basins sampled. Solid line represents a linear relationship between hilltop curvature and denudation ($R^2 = 0.83$), as predicted by Equation 3.4, allowing the sediment transport coefficient to be constrained at 8.6 $m^2$ $ka^{-1}$ (Hurst et al., 2012). The black box in (b) shows the location of Figure 3.3. The spatial reference system is UTM Zone 10N with spatial units in meters.

## 3.4 Study Sites

I explore hillslope morphology in two lithologies in the lower reaches of the Middle Fork Feather River, in the northern Sierra Nevada of California (Figure 3.3). My study is focused on an area where granitoid plutons are intruded into the Central Belt terrain which consists of Upper Triassic-Jurassic ophiolitic, volcanic and sedimentary units of the Fiddle Creek Complex (Day and Bickford, 2004).

The landscape comprises a low-relief, relict surface characterised by concave up channel profiles and broad "diffusive" hillslopes which is likely adjusted to some previous erosional regime. This landscape is dissected by the incised canyons of the Middle Fork Feather River and its tributaries (Figure 3.2b). Canyon incision was initiated by accelerated uplift c. 3.5-5 Ma (Stock et al., 2004; Wakabayashi and Sawyer, 2001), possibly caused by the delamination of an eclogite root beneath the mountain range (Jones et al., 2004; Saleeby and Foster, 2004). Apatite fission track dates reveal an average erosion rate of 40 mm $ka^{-1}$ for the relict landscape, persisting until at least 32 million years ago (Ma) (Cecil et al., 2006). Long term exhumation rates derived from (U-Th)/He ages fail to record a late-Cenozoic acceleration in denudation, implying that less than 3 km of the crust has been exhumed since the acceleration (Cecil et al., 2006). Incision rates for the Feather River canyon have been reconstructed for the last 5 Ma from the presence of late-Cenozoic volcanics capping ridges/divides. Minimum incision rates were found to vary between 100 and 240 mm $ka^{-1}$, with the Feather River having an estimated minimum incision rate of 170 mm $ka^{-1}$ over the last 5 Ma (Wakabayashi and Sawyer, 2001). Erosion rates measured within the Feather River basin vary by over an order of magnitude from the relict surface (~20 mm $ka^{-1}$) to the canyons (~250 mm $ka^{-1}$) (Hurst et al., 2012; Riebe et al., 2000; Wakabayashi and Sawyer, 2001) (Figure 3.2b). For several Sierra Nevada catchments > 200 km to the south of the Feather River, Stock et al. (2004) established canyon erosion rates of ~200 mm $ka^{-1}$ between 1.5 and 2.7 Ma, compared with ~30 mm $ka^{-1}$ since 1.5 Ma, from CRN dating of cave sediments now suspended

above the valley floor. They attributed this change to an incision wave propagating upstream 2-5 Ma ago due to accelerated tectonic uplift.

The modern climate is semi-arid with a strong precipitation gradient from the dry Central Valley of California to the high elevations of the Sierra Nevada Mountains. At my study site, mean annual temperature (MAT) is 12.5 °C and mean annual precipitation (MAP) is 1750 mm (data from the PRISM Climate Group, Oregon State University, http://prism.oregonstate.edu, accessed 7th July 2011; Daly, 1997). The Feather River basin remained largely unglaciated during the Pleistocene, except for its uppermost reaches (Clark, 1995; Wahrhaftig and Birman, 1965). Erosion rates from low-relief areas in the Sierra Nevada are insensitive to spatial variations in climate (Riebe et al., 2001a).

Hurst et al. (2012) extended the dataset used by Riebe et al. (2000) and demonstrated that as basin-averaged erosion rates increase, hilltops get sharper (i.e., curvature becomes more negative) in granitoid portions of the landscape (Figure 3.2c). A linear relationship provides the best fit ($R^2 = 0.83$) but Hurst et al. (2012) could not rule out the possibility of an exponential relationship ($R^2 = 0.72$). Mean slope angles vary non-linearly with erosion rate suggesting that some hillslopes in the field area approach the critical gradient (i.e., $S_C$) and thus their mean gradient may be insensitive to increases in erosion rate. Hillslope gradients rarely exceed 0.9, and occasional landslide scars can be in the steepest parts of the landscape. This is consistent with a sediment transport law in which flux increases to infinity as slopes approach some limiting angle (approximating the effect of increased landslide frequency), as in Equation 3.3, as previously demonstrated in other landscapes (Binnie et al., 2007; DiBiase et al., 2010; Ouimet et al., 2009).

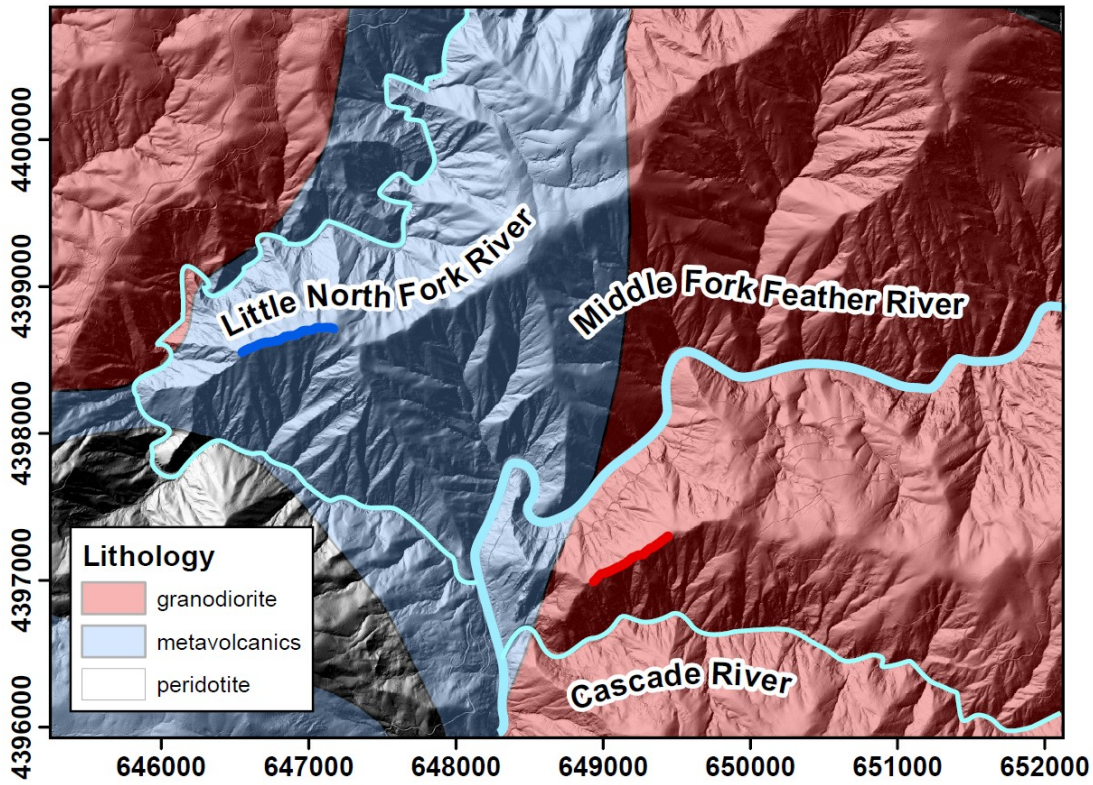


Figure 3.3: Shaded relief image of study site with lithology super imposed (Moosdorf et al., 2010). Topographic metrics from all hillslopes in granodiorite in the east and metavolcanics to the east were retrieved, with vegetation analysis focused on the two ridge transects highlighted in red and blue respectively. The principle drainage conduits are highlighted in light blue. The spatial reference system is UTM Zone 10N with spatial units in meters.

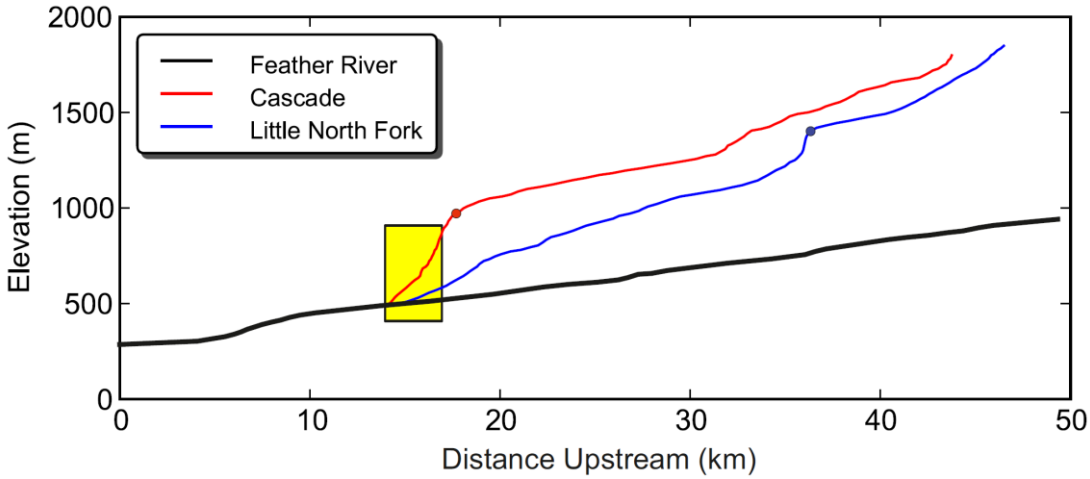


Figure 3.4: Longitudinal profiles for Little North Fork (blue) and Cascade (red) rivers relative to the lower reaches of the Feather River (black) which sets base-level. Distance is upstream from the outlet into Oroville Reservoir. Profiles were generated from U.S. Geological Survey National Elevation Dataset 1/3 Arc second (approx. 10m) DEMs [http://seamless.usgs.gov/; accessed 15/1/2009] following (Wobus et al., 2006a). Knickpoints on the Cascade River and Little North Fork River profiles are marked with red and blue dots respectively. Shaded region indicates area in which the landscape is interpreted to be adjusting/adjusted to the rapid incision rate of the Feather River along both the Little North Fork and Cascade Rivers and hillslope morphology may reflect this erosion rate. The lower reaches of the Cascade and Little North Fork rivers cross the Cascade Pluton (granodiorite) and Central Belt (metavolcanics) respectively.

I focus my analysis on the area near the confluences of the Little North Fork and Cascade rivers with the Feather River (Figure 3.3). In the east of the area shown in Figure 3.3 the bedrock is the granodiorite of the Cascade Pluton; in the west, intermediate volcanics of the Fiddle Creek complex. With the Feather River down-cutting rapidly, the Little North Fork and Cascade rivers are undergoing a transient adjustment to acceleration in base-level lowering. I studied hilltops and adjacent hillslopes near the confluences where they were most likely to be adjusting/adjusted to base-level lowering, since adjacent valleys are downstream of major knickpoints (location of a sudden increase in slope downstream;. Figure 3.4). The studied hillslopes, separated by less than 5 km and spanning similar ranges in elevation, can be assumed to have similar climatic histories, and their proximity to the Feather River implies similar denudation history. Based on field observations, the dominant driver of sediment transport in this forested landscape is growth/decay of tree roots and the upheaval of root wads and associated soil by tree throw. Soil pits dug on steep slopes in both lithologies reveal thick (60cm+) soils (Figure 3.5); however the spatial variation in soil thickness was not explored extensively. Thick soils are developed on steep slopes in both areas (Figure 3.5). The two areas lie in the Plumas National Forest and vegetation consists of the California mixed conifer forest type, which includes Douglas fir, incense-cedar and sugar pine (Warbington and Beardsley, 2002).

Figure 3.5: Example soil profiles in (a) granodiorite and (b) metavolcanics. Pit in granodiorite comes from hilltop along cascade ridge (red line in Figure 3.4) with hilltop curvature $C_{HT}$ = -0.062; pit depth is 65cm. Pit in metavolcanics on steep slope (c. 40°), pit depth is 85 cm.

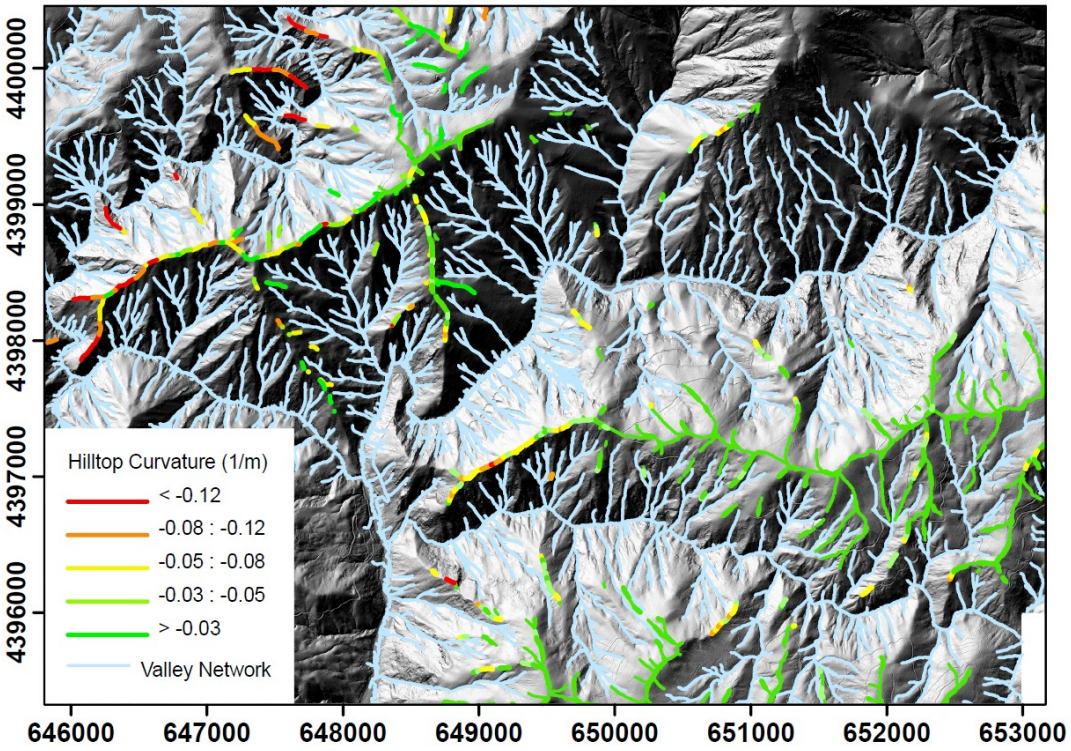


Figure 3.6: Map of channel and hilltop networks in the study region. Hilltops are colour coded by hilltop curvature, with the highest values of hilltop curvature occurring mainly in the metavolcanics and near to the main rivers. Channel network extracted using the Geonet tool (Passalacqua et al., 2010a), hilltops defined as the adjoining edges of drainage basins extracted at all stream orders (see text).

## *3.5 Results*

### 3.5.1 Morphology of Hillslopes as a Function of Lithology

Figure 3.6 shows the spatial distribution of hilltops sampled and their hilltop curvature. The highest values of hilltop curvature (i.e., the most convex or sharpest hilltops) occur on hilltops most proximal to the Feather River, the Cascade River and the Little North Fork River, downstream of the main knickpoints (Figure 3.4). High values of hilltop curvature are more distributed in the north west of the study area since the knickpoint has propagated further up the Little North Fork tributary than along Cascade River. In Figure 3.7 the relationship between hilltop curvature and hillslope gradient is compared in the granodiorite and metavolcanics. I found a non-linear relationship between mean hilltop curvature and mean hillslope gradient. Where there is low hilltop curvature, hillslope gradients are also low. As hilltop curvature increases so too does hillslope gradient; however beyond $C_{HT} \sim$ -0.03 $m^{-1}$ (i.e. more negative values) hillslope gradients do not continue increasing as rapidly. This relationship occurs in both lithologies, however the two datasets are offset such that in the metavolcanics, for low values of hilltop curvature (> -0.03 $m^{-1}$) hillslopes tend to be steeper, and hillslopes in the metavolcanics approach their limiting gradient at lower hilltop curvatures than in the granodiorite. Since hillslope gradients appear to be limited, they will not reflect the erosion rates driving their evolution, however following Equation 4 hilltop curvature may better reflect the distribution of erosion rates if the hillslope has fully responded to the change in boundary conditions (Hurst et al., 2012).

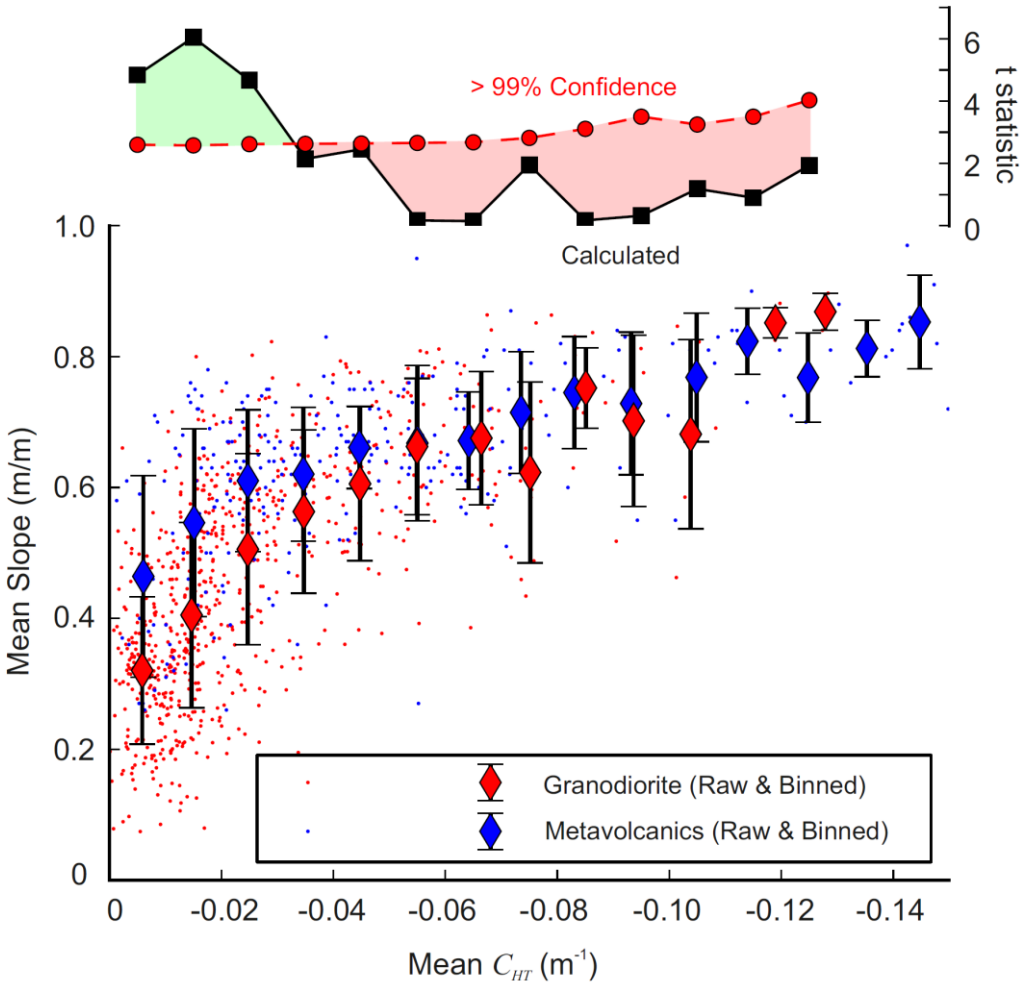


Figure 3.7: Relationship between mean hilltop curvature ($C_{HT}$) and mean adjacent slope ($S$) for hilltops in the granodiorite (red) and metavolcanics (blue), with Students t-statistic used to compare between the two data sets. Where the calculated t-statistic (black) falls above the 99% confidence level (red dashed) the two datasets can be interpreted as originating from different populations (area shaded green). Data are binned into regularly spaced bins in $C_{HT}$. $C_{HT}$ is expected to be a good indicator of relative erosion rate whilst at high erosion rates $S$ becomes insensitive to baselevel fall. Note we plot bin-mean averaged $C_{HT}$ and $S$. In both lithologies $C_{HT}$ continues to vary despite $S$ becoming limited. For low $C_{HT}$, hillslopes are steeper in the metavolcanics (at 99% confidence level). $S$ in both lithologies appears to be limited to ~0.85.

I cast these results in non-dimensional form to compare them to the expected form of model hillslopes governed by Equation 3.3, calculating dimensionless erosion rate as a function of hilltop curvature and hillslope length, and dimensionless relief as a function of mean slope (Equation 3.5b and 3.6b) (Roering et al., 2007). Despite considerable scatter, I find that the distribution of binned $R^*$ and $E^*$ is of a similar form to that predicted by Equation 3.6a (as depicted by the dashed line in Figure 3.8). Note from Equations 5b and 6b that $S_C$ is required to quantify both $E^*$ and $R^*$ based on measureable topographic properties and hence the value of $S_C$ used can alter the position of the data relative to the dashed steady state line (see section 3.5.2). Despite non-dimensionalization there is still a tendency for hillslopes in the metavolcanics to be steeper when $E^*$ is low. $E^*$ was calculated as a function of hilltop curvature and hillslope length (Equation 3.5b).

Frequency distributions of hillslope lengths (Figure 3.9a) reveal that hillslopes are slightly longer in the metavolcanics (peak at 175-200m, and a larger proportion of long hillslopes) than in the granodiorite (peak at 150-175m, with a larger number of short hillslopes). I carried out a *t-test* to test the equality of the two sample means and concluded at 99% confidence ($p < 0.01$) that the samples were drawn from different populations. This is also shown by plotting $C_{HT}$ (controlled by $E$) versus $L_H$ (Figure 3.9b), which indicates that hillslope lengths have a tendency to shorten in response to increased erosion rates (assumed to be signified by increased $C_{HT}$). The tendency of hillslopes to be steeper in the metavolcanics is therefore not the result of hillslopes being longer (and consequently having a larger proportion of their length that is steep and planar), since non-dimensionalising normalises for hillslope length. The tendency for hillslopes to be steeper in the metavolcanics may relate to a difference in the limited slope angle that hillslopes can reach in the two lithologies, or to differences in the transient development of the hillslopes in response to base-level fall. Hillslopes with high hillslope gradient but low hilltop curvature (or high $R^*$ but low $E^*$) are expected to develop when a hillslope is

adjusting to an increase in erosion rate, or the passing of a knickpoint at its toe (Hurst et al., 2012). Hillslopes in metavolcanics tend to be steeper than in granodiorite for similar values of $C_{HT}$ which might suggest there are more transient hillslopes in the metavolcanics.

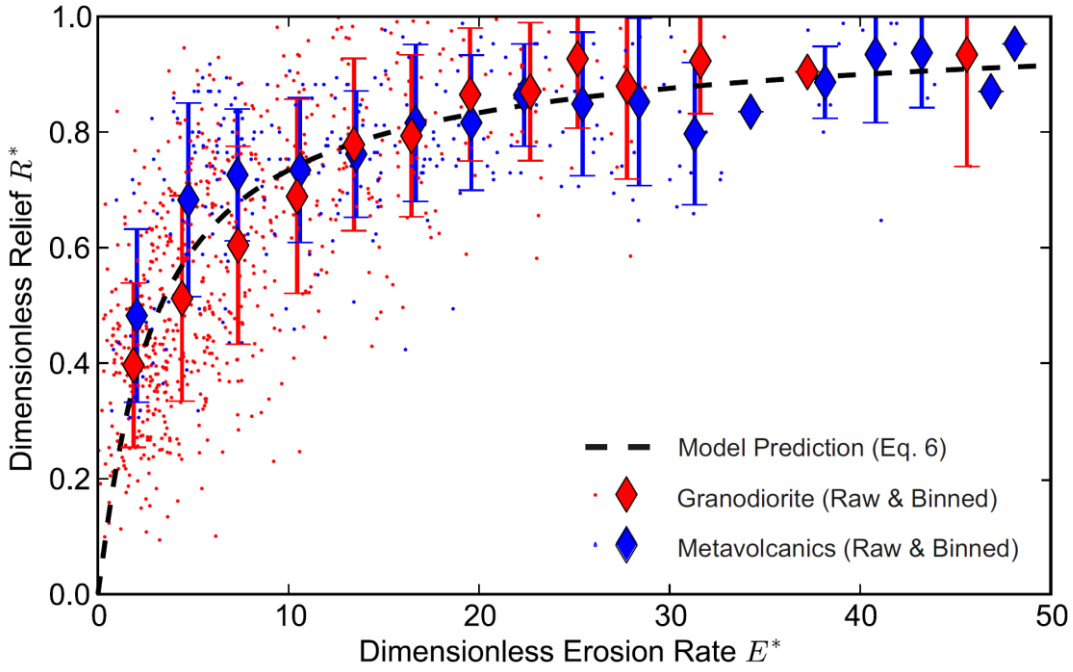


Figure 3.8: Non-dimensional erosion rate ($E^*$) and relief ($R^*$) calculated from topographic metrics following Equations 3.5 and 3.6 for hilltops in the granodiorite (red) and metavolcanics (blue), using maximum likelihood estimated values for $S_C$ of 0.79 and 0.85 respectively. Data is binned into regularly spaced bins in $E^*$. Black dashed line shows theoretical relationship predicted by Equation 3.6 for steadily eroding hillslopes. Non-dimensional analysis effectively normalises the data from Figure 3.7 for variation in hillslope length. Hillslopes in the metavolcanics tend to be steeper for a given erosion rate despite correcting for hillslope length, suggesting a greater number of hillslopes undergoing transient adjustment were sampled in the metavolcanics (see text for further discussion).

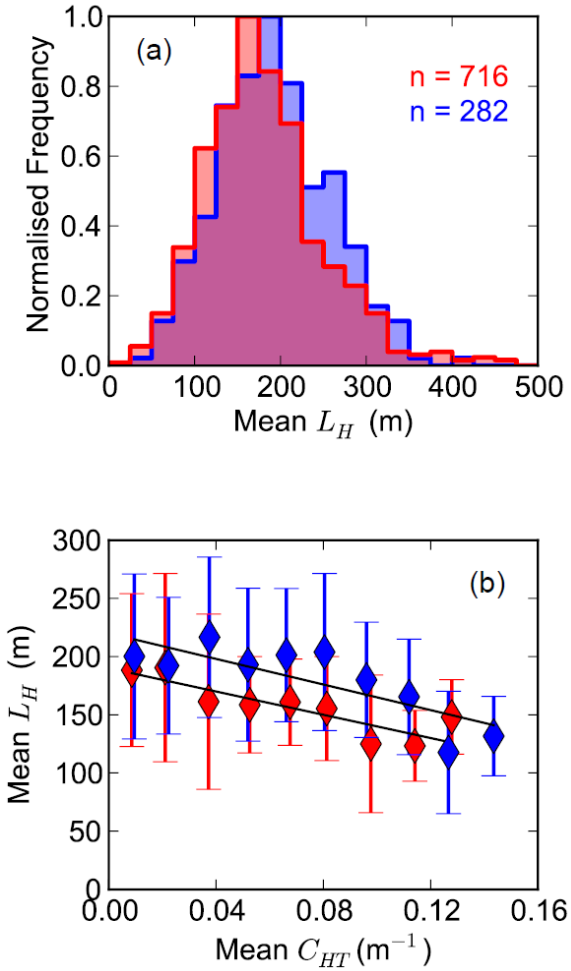


Figure 3.9: (a) Frequency of hillslope length $L_H$ for the granodiorite (red) and metavolcanics (blue), normalised by the maximum frequency. Maximum frequency occurs at $L_H$ = 150-175m in the granodiorite and $L_H$ = 175-200m in the metavolcanics. Additionally, there are more short hillslopes in the granodiorite and more long hillslopes in the metavolcanics. A *t-test* reveals at 99% confidence that these two datasets are drawn from different populations. (b) Plot of $C_{HT}$ (indicating relative erosion rate) verses $L_H$ in granodiorite (red) and metavolcanics (blue). Black lines represent linear least-square fits to binned averages with $R^2$ = 0.74 and 0.66 respectively. Hillslope lengths tend to shorten with increasing hilltop curvature (an indicator of erosion rates).

### 3.5.2 Constraining $S_C$

Critical slope $S_C$ is used when calculating both $E^*$ and $R^*$ from topographic metrics. I estimated $S_C$ by finding the maximum likelihood estimator (MLE) between the hillslope data and model predictions for $R^*$ as a function of $E^*$ (Equation 3.6a) with varying $S_C$. It is important to highlight here that the model fitted applies to steady state hillslope morphology, yet the landscape analysed spans a range of erosion rates (Figure 3.2) and there are knickpoints in the channel system (Figure 3.4). Thus it is likely that some hillslopes may have transient morphology. Nevertheless, the tendency of the asymptote created by Equation 3.6a (see dashed line in Figure 3.8) is controlled by $S_C$, and the highest values of $R^*$ contained in the datasets should reflect $S_C$. The MLE was calculated as follows, reporting error range at one standard deviation of the normalised probability distribution:

$$MLE = \prod_{i=1}^{n} \exp\left[\frac{\left(R^*_{meas} - R^*_{mod}\right)^2}{2\sigma_p}\right] \qquad [3.7]$$

Where $n$ is the number of hillslopes sampled, the subscripts *meas* and *mod* refer to measured and modelled values, respectively, and $\sigma_p$ is the variance in measured $R^*$ values, which will alter the magnitude of MLE calculated, but will not change the most likely value of $S_C$. The MLE for $S_C$ was 0.79 -0.07/+0.38 for the granodiorite and 0.85 -0.08/+0.53 for the metavolcanics. This indicates that the maximum attainable gradient on hillslopes in the metavolcanics may be slightly higher. I interpret the large range in error values as due to a significant proportion of hillslope data having low $E^*$ (<10) and $R^*$ (<0.8) (Figure 3.8), at which the model predictions are insensitive to changes in $S_C$. Having more data points at high $E^*$ would significantly reduce the error range since it is at high erosion rates that hillslopes become steep and planar and are most likely to reflect $S_C$. The likelihood that $S_C$ is 0.85 and 0.79 in the granodiorite and metavolcanics (i.e. that my result is reversed) is

over a factor of two less likely. As hillslopes become steep and planar, mean hillslope gradient $S$ should approach $S_C$. Mean hillslope gradients presented in Figure 3.7 rarely exceed 0.8 suggesting that the values calculated here are appropriate, however I also note that I was unable to demonstrate a statistical difference in $S$ between the two lithologies at high $C_{HT}$, which might otherwise have corroborated my calibrated values.

Slope histograms were computed for hillslope areas nearest to the tributary junctions with the Feather River, i.e. the parts of the landscape with the steepest slope. I avoided sampling where there were obvious remnants of the relict upland, concentrating instead on hillslopes adjacent to canyons. Figure 3.10 shows slope histograms sampled for both granodiorite and metavolcanics portions of the landscape which are downstream of convexities in the channel profile. The two lithologies have similar mean (0.84 and 0.85) and median (0.83 and 0.86) slope values for granodiorite and metavolcanics respectively.

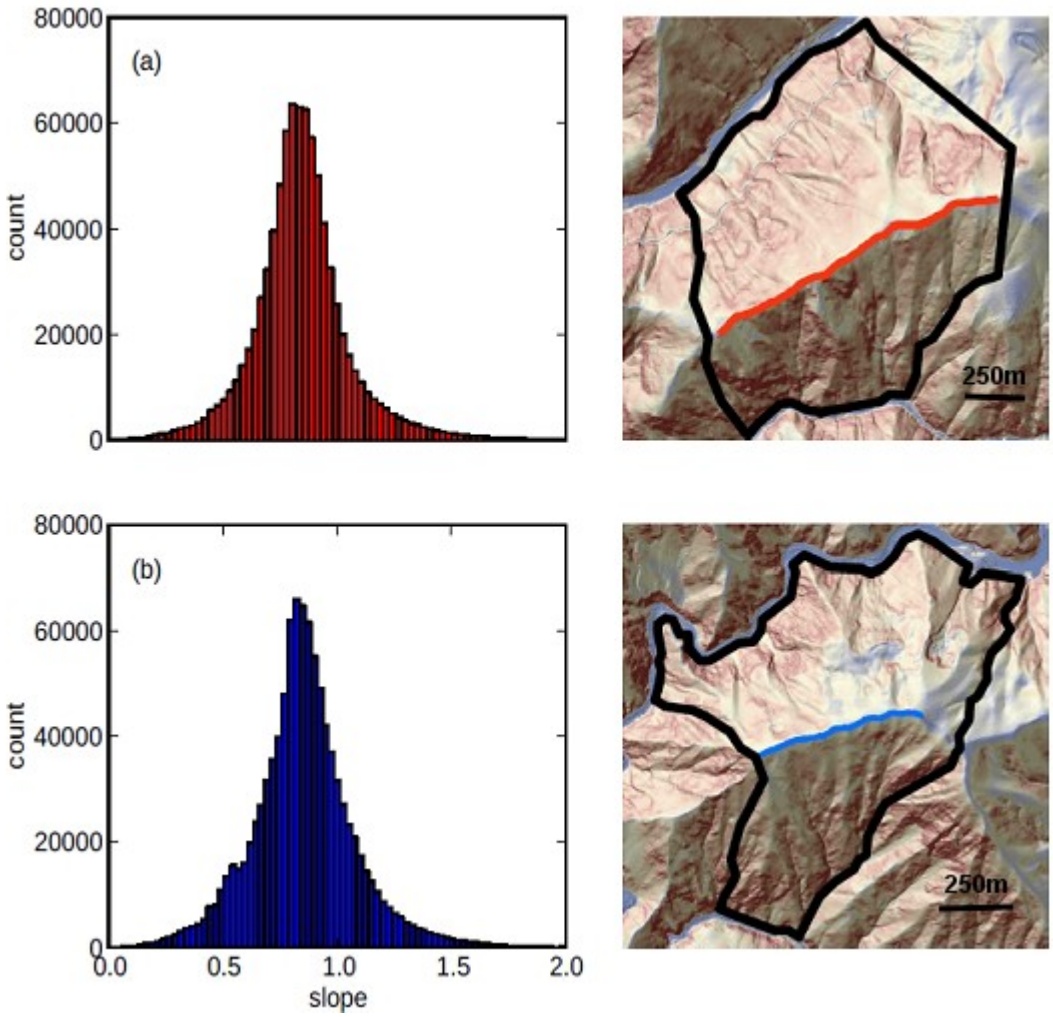


Figure 3.10: Distribution of hillslope gradients and area sampled for hillslopes in (a) Cascade Pluton and (b) Little North Fork metavolcanics. Slope was calculated over 12x12 m window (Hurst et al., 2012). For the area in metavolcanics mean slope = 0.85, median slope = 0.86. In granodiorite mean slope is 0.84 and median slope is 0.83.

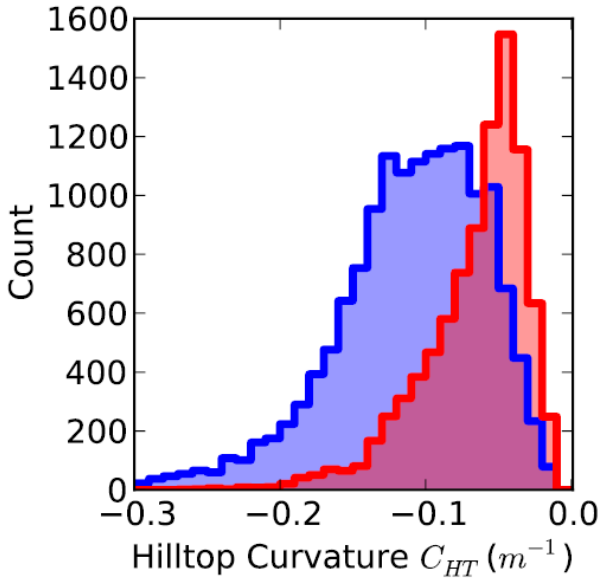


Figure 3.11: Histogram of hilltop curvatures extracted from hilltops adjacent to the Feather River, Cascade River and Little North Fork River. Distributions are negatively skewed, median values (median absolute deviation reported as error range) are -0.105 ± 0.034 and -0.057 ± 0.019 for hilltops in the metavolcanics (blue) and granodiorite (red) respectively.

### 3.5.3 Calibrating the Sediment Transport Coefficient

To compare estimates of the sediment transport coefficient $D$ between lithologies I sampled hilltop curvature on all ridges within 500 m of reaches of the Feather River, Cascade River or Little North Fork River, downstream of knickpoints, where the long-term erosion rate is estimated to be c. 250 mm $ka^{-1}$ (Hurst et al., 2012; Riebe et al., 2000; Wakabayashi and Sawyer, 2001). The results were binned to produce histograms of hilltop curvature by lithology (Figure 3.11). Hilltops tend to be much sharper (curvature more negative) in the metavolcanics than in the granodiorite. Following Equation 3.4 sharper hilltops can result from increased erosion rate $E$ or reduced sediment transport efficiency $D$. I assumed that proximal to the Feather, Cascade and Little North Fork Rivers, downstream of knick zones (see Figure 3.4), the landscape has responded to accelerated incision such that erosion rates are equilibrated. I used median values and median absolute deviation to estimate $D$. Assuming $\rho_s / \rho_r = 0.5$ (a ratio that has been demonstrated for some other granitic field sites, e.g. Heimsath et al., 2000; Riggins et al., 2011a) and $E$ = 250 mm $ka^{-1}$, we solved Equation 3.4 for $D$. In the granodiorite $D = 8.8 \pm 3.3$ $m^2$ $ka^{-1}$. In the metavolcanics hilltop curvature tends to be higher (more negative) (Figure 3.11), predicting a lower diffusivity of $D = 4.8 \pm 1.8$ $m^2$ $ka^{-1}$ The result from the granodiorite is similar to the value of $D = 8.0$ $m^2$ $ka^{-1}$ reported by Hurst et al. (2012) for granitoid lithologies in this field site based on data in Figure 3.2. The sediment transport rates reported here are dependent on the assumption that erosion rates are the same in parts of the landscape that are most likely to be adjusted to increased incision.

### 3.5.4 Estimates of Above Ground Biomass

In the field I observed mixed A soil horizons of fairly uniform depth (Yoo et al., 2011) and no evidence of overland flow or ravelling processes, even during the 2009 field season when I visited the site after a fire. The entire area studied is forested and I observed a number of uprooted trees and associated surface pits. These field observations suggest that slope-dependent sediment transport on hilltops is dominated by vegetation turnover in the Feather River region, although I cannot rule out rheologic creep as a contributing mechanism (McKean et al., 1993).

Vegetation properties were compared along two prominent ridges in the granodiorite and the metavolcanics to determine whether the differing distributions of hilltop curvature could be explained by vegetation controlling the sediment transport coefficient. These ridgelines were selected as the only hilltops bound on both sides by the main tributary channels. On these ridges hilltops are sharp (more negative $C_{HT}$ values indicate sharper hilltops and imply more rapid erosion): mean $C_{HT}$ for granodiorite is -0.067 $m^{-1}$ and -0.12 $m^{-1}$ for metavolcanics (Figure 3.12), indicating that these sites have likely responded to base-level lowering (though they may still be adjusting). I find that vegetation on the two ridges have remarkably similar density ratios $V_{dens} \sim 0.8$ yet exhibit differences in canopy height (Figure 3.12). The mean height values from profiles along the length of each ridgeline are similar on both ridges ($V_{mean}$ = 7.9 ± 4.9 m and 8.0 ± 3.5 m for ridges in the the granodiorite and metavolcanics respectively).

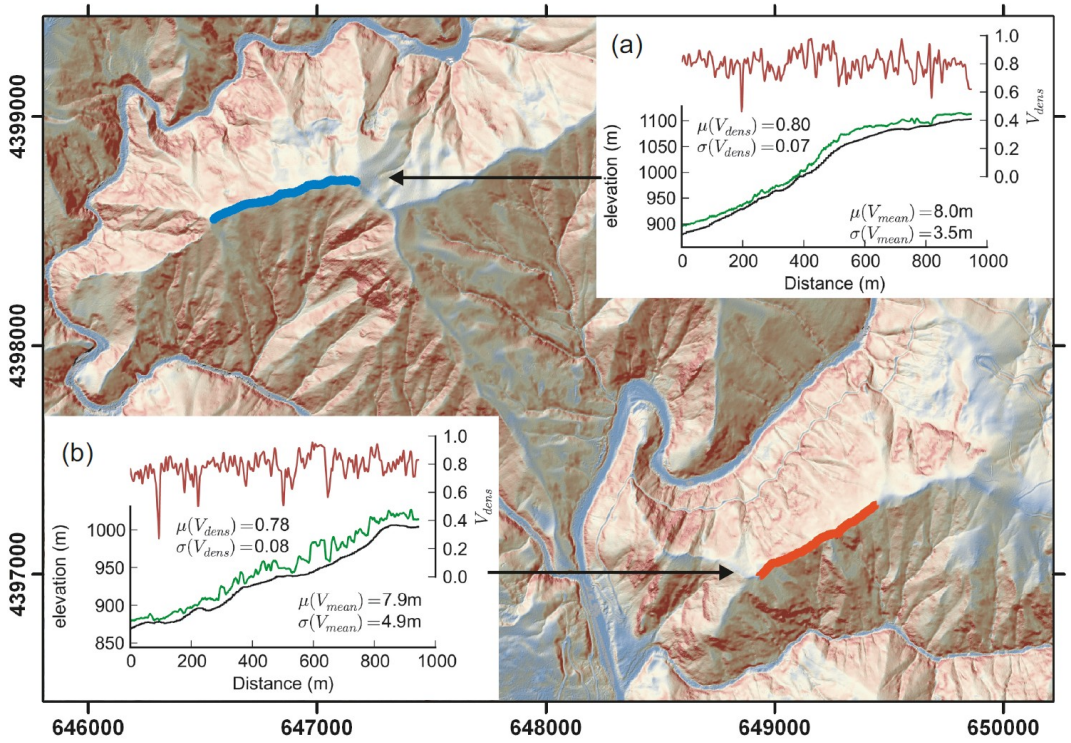


Figure 3.12: Comparison of vegetation properties for (a) Little North Fork ridge and (b) Cascade ridge. Vegetation density ($V_{dens}$) is plotted in red, and mean canopy height ($V_{mean}$) is the difference in elevation between the ground surface (black) and mean vegetation elevation (green). Both vegetation parameters are similar between the two sites, but canopy height is more variable on Cascade ridge due to the presence of several large trees. Background image is shaded slope map similar to Figure 3.2. The spatial reference system is UTM Zone 10N with spatial units in meters.

## *3.6 Discussion*

### 3.6.1 Applicability of Sediment Transport Models

Much of the topographic analysis above has been carried out assuming hillslope sediment transport is well approximated as a non-linear function of local slope (Equation 3.3). This model is assumed to be applicable to the Feather River since hilltop curvature varies linearly with erosion rate and the distribution of dimensionless erosion rate and relief quantified from topography in the granodiorite closely matches model predictions (Hurst et al., 2012). Models similar to Equation 3.3 in which sediment flux is also a product of soil depth (i.e. $D = D_d \times h$, where $D_d$ [L $T^{-1}$] is the transport coefficient for depth-dependent transport and $h$ [L] is soil depth) predict that hilltop curvature will vary non-linearly with erosion rate, becoming extremely sensitive to changes in $E$ when $E$ is relatively high (Roering, 2008). Field measurements of soil depth were invariant on hillslopes above, at and just below a prominent break in slope that separates the relict landscape from the steep topography in an area of tonalite ~10 km to the south of the study area (Yoo et al., 2011). This implies that soil thickness seems to be set primarily by the depth of root action in this forested landscape. However there are local patches of bare bedrock on upland surfaces underlain by granitoids. These occur either (i) in broad patches on the gently eroding relict surface, or (ii) immediately adjacent to the Feather River, in large single patches of exposure below the break in slope separating the steepened landscape from the relict topography. This may be attributed to particularly resistant patches of granitoid and/or a negative feedback whereby stripping of soil inhibits further soil production (Furbish and Fagherazzi, 2001). There is patchy bedrock outcrop below knickpoints in the channel system, even in the predominantly soil-mantled areas this study has focused on, and a recent study has demonstrated that the amount of rock exposure on hillslopes increases with

erosion rate across a wide range of erosion rates (10-1000 mm $ka^{-1}$) (DiBiase et al., 2012). The extent to which patchy bedrock emergence limits the application of non-linear (and/or depth-dependent) hillslope sediment transport models remains unclear. DiBiase et al. (2012) also demonstrated that mean hillslope gradient measured from high resolution topography may continue to increase with erosion rates beyond those at which studies using coarser DEMs have that suggested hillslope gradients become limited (e.g. Binnie et al., 2007; DiBiase et al., 2010; Ouimet et al., 2009). The relationship between $C_{HT}$ and $S$ presented in Figure 3.7 supports this since $S$ continues to increases slightly even at high $C_{HT}$, though I have limited data at high erosion rates (high $C_{HT}$). I however stress that $E^*$ vs $R^*$ curves in this landscape closely match predictions based on the non-linear sediment transport model suggesting this model provides a good description of hillslope morphology in the Feather River.

Previously reported values for critical slope $S_C$ in Equation 3.3 vary between 0.8 and 1.25. Roering et al. (1999) performed forward modelling of a real landscape in the Oregon Coastal Range to calibrate a best fit value of 1.25. DiBiase et al. (2010) found that $S_C$ = 0.81 provided a better fit in the San Gabriel Mountains, California by fitting hillslope morphology to the theoretical $E^*$ vs $R^*$ curve. Mattson and Bruhn (2001) reported $S_C$ = 0.95 in cohesionless sediment cut by fault scarps in the Wasatch Fault Zone, Utah, by comparing numerically modelled scarp profiles to modern scarp morphology. Through analysing the non-dimensional form of hillslopes, best fit values for $S_C$ in the Feather River region were 0.79 and 0.85 in granodiorite and metavolcanics respectively, and similar to the median values of hillslope gradient in rapidly denuding regions of the landscape (Figure 3.10). In the context of Equation 3.3, $S_C$ represents a slope angle that cannot be attained since sediment flux becomes infinite at $S_C$. As such there is discrepancy between my fitted $S_C$ and the distribution of slope angles in the landscape shown in Figure 3.10. I hypothesise that my sampling approach may under-sample the steepest parts of the landscape, with hillslope traces terminating in debris flow channel heads, whilst the

steepest hillslope gradients occur where there is patchy emergent bedrock on hillslopes proximal to the main stem channels. Equation 3.3 applies only to soil-covered hillslopes whereas emergent bedrock will be capable of maintaining steeper slopes, limited by the mechanical strength of the rock face.

### 3.6.2 Transient Landscape Response

In Figure 3.4 it can be observed that the transient erosion rate signal, represented in this case by a distinct convexity in the channel profile, has migrated further along the Little North Fork River than the Cascade River. All else being equal I would expect knickpoints to propagate faster into weaker/less resistant lithologies (Whipple and Tucker, 1999) suggesting that the metavolcanics may be less resistant to fluvial erosion than the granodiorite. However the Little North Fork is a slightly larger basin (120km$^2$ compared to Cascade River 85km$^2$). The tendency for hillslopes in the metavolcanics to have steep slopes at low hilltop curvature however results in them plotting above the steady state line in Figure 3.8 and therefore they may still be responding to accelerated incision (Hurst et al., 2012). Hillslope morphology in the granodiorite conforms better to the steady state predictions (Figure 3.8). Hillslopes in the granodiorite may be able to keep pace with channel incision due to having a higher sediment transport coefficient (Roering et al., 2001a) and since the knickpoint has not migrated as far into the granodiorite and therefore must be propagating slower than in the metavolcanics. Gallen et al. (2011) demonstrated that the passing of a knickpoint results in hillslope steepening and an increase in hillslope relief immediately downstream; these results mirrored the theoretical predictions of Mudd and Furbish (2007). However with increasing distance downstream from the knickpoint these metrics begin to reduce again suggesting hillslopes are relaxing following the passing of a knickpoint and initial hillslope steepening. In the Feather River I have been unable to observe such relaxation on hillslopes, and are as yet unable to assert whether the increased erosion rates that have carved the Feather River canyon are persistent or reflect a base-level

adjustment similar to that observed by Gallen et al. (2011). Such a problem has important bearing on the calibrated values of $D$, since I have assumed in section 6.1 that erosion rates are the same, and persistently high, in order to solve Equation 4 to derive $D$. Analysis of cosmogenic radionuclides in cave sediments elsewhere in the Sierra Nevada suggest that the erosion history in the late Cenozoic is characterised by a pulse of incision moving through the landscape (Stock et al., 2004). Incision is inferred to be a response to accelerated uplift in the late-Cenozoic (Wakabayashi and Sawyer, 2001). The likely mechanism of uplift is an isostatic response to delamination of an eclogite root beneath the mountain range (Jones et al., 2004; Saleeby and Foster, 2004). Therefore it seems likely that uplift rates will decrease through time as new isostatic equilibrium is approached.

### 3.6.3 Hillslope Lengths and Drainage Density

Hillslope lengths tend to be longer in the metavolcanics than in the granodiorite (Figure 3.9). A recent study by Perron et al. (2008) postulated that drainage density and its inverse, hillslope length, should be set by the relative efficiency of diffusive (hillslope) and advective (valley forming) processes. Their analysis focused on low relief settings, where hillslope processes could be assumed to be diffusive and sediment flux linearly related to slope, whilst valley forming processes were dominated by channelization of overland flow. However the present study is focussed on a landscape responding to an order of magnitude increase in erosion rates, where zero order basins may be predominantly eroded by debris flows and hillslopes approach a threshold gradient as a process transition to landslide-dominated sediment transport occurs. Perron et al. (2009) demonstrated that such a relationship breaks down in rapidly denuding landscapes with steep planar hillslopes such as the Oregon Coastal Range.

Hillslope length $L_H$ in part controls slope steepness through setting the proportion of a hillslope that is planar and experiencing non-linearity in sediment

transport (Roering et al., 2001a) (i.e. The longer the hillslope, the longer the proportion of its length that will be steep and planar). In the Feather River region, hillslope length decreases with erosion rate (assuming $C_{HT}$ is a surrogate) (Figure 3.9). Mudd and Furbish (2005) demonstrated that hilltops may migrate when subject to differential erosion rate on either flank such that when erosion rate is raised on one side the hillslope on that side increases its length. However in their model the extent of the drainage network was fixed and an increase in hillslope length by divide migration was accommodated by shortening of the adjacent, low erosion rate hillslope. Contrary to the results presented here, drainage density (inverse of $L_H$) has been demonstrated to vary negatively with relief in steep, mountainous landscapes (Montgomery and Dietrich, 1988; Oguchi, 1997). Such a result has been supported by analytical and numerical modeling studies which predict that where hillslope sediment transport is dominated by landsliding there should be an inverse relationship between drainage density and topographic relief (Howard, 1997; Tucker and Bras, 1998). These studies have focused on landscapes (real or otherwise) that are assumed to be adjusted to their boundary conditions. The Feather River is still responding to a transient erosion signal and as such the patterns observed here may only be associated with processes of landscape response. In landscapes experiencing rapid erosion, where coupled landslide and debris-flow processes are likely to be the dominant erosion processes on hillslopes and in valleys respectively, drainage density is likely to be influenced by factors governing the frequency and magnitude of landslide events and the potential for these events to erode valleys as they translate into debris-flows and scour the substrate (Stock and Dietrich, 2006). In such settings, it may therefore be difficult to isolate the relative efficiencies of hillslope and valley forming processes. I find that hillslopes tend to get shorter with increased erosion rate in the Feather River and speculate that this may be due to an increase in debris flow frequency, allowing the valley forming process to be more efficient at high erosion rates, so that valley heads migrate further into the landscape.

### 3.6.4 Mechanisms for Lithologic Control on Hillslope Sediment Transport

Several workers have suggested that lithology may be important in setting *D* (e.g. McKean et al., 1993; Yoo et al., 2005) but as yet we lack quantitative understanding of such a relationship (c.f. Furbish et al., 2009). This is in part due to an inability to isolate lithologic control from that of climate, vegetation and bioturbation. Here I have demonstrated that *D* varies by a factor of two between two landscapes underpinned by different lithologies, despite similarity in vegetation, and presumably climate given their spatial proximity and similar range in altitude. The sediment transport coefficient is not directly controlled by lithology, but rather by the characteristics of the soil produced and the processes that act to transport sediment, which are both in turn be influenced by lithology. I have demonstrated that LiDAR metrics for AGB are similar between the two lithologies on hilltops; therefore energy expended in root growth/decay and tree throw should be similar, yet the amount of soil moved per transport event must differ. Future research should attempt to quantify mechanical properties of bedrock and chemical weathering in settings where *D* can be determined, and a number of possible mechanisms by which lithology may influence sediment transport can be anticipated.

The chemical and physical properties of soils are set by lithology, which influence the efficacy of sediment transport. Disparity in the degree of chemical and physical weathering in soil and saprolite may result in different volume of material mobilized by tree throw and root growth. Furbish et al. (2009) derived a diffusion-like Equation through describing the disturbing and settling motions of individual particles within a soil. They parameterized *D* as controlled by active soil depth, characteristic particle size, porosity (partially set by particle size) and a rate of particle activation (frequency of disturbance per unit time). The grain size distribution in a soil may then exert control on sediment transport efficiency by adjusting the mean free path length a grain can travel when disturbed or settling.

Coarser grain size distributions have larger pore spaces and therefore facilitate longer travel distances per disturbance event. Rapid erosion rates lead to shorter residence times of soil material and therefore less time is available for the production of fine grained weathering products such as clays and pedogenic crystalline iron (Mudd and Yoo, 2010; Yoo et al., 2011), and accelerated erosion rates are expected to result in a greater proportion of rock fragments in soils (Marshall and Sklar, 2012). Furthermore, variation in grain size distributions may influence the hydrology (Poesen and Lavee, 1994), potentially impacting upon cyclical wetting/drying expansion/contraction within the soil. Because grain size distributions in soils are likely to be positively correlated with erosion rates, I also expect that $D$ may increase with erosion rates. Therefore the common assumption that $D$ is independent of $E$ (which I apply in Equation 3.4) may not hold for disturbance-driven sediment transport; if true, this would introduce significant complexity to efforts to utilise hillslope topography to predict erosion rates.

## 3.7 Conclusions

Despite similar vegetation, the hillslope morphology in two distinct lithologies in the Feather River region of California varies significantly, with hillslopes in metamorphosed volcanic rocks tending to be steeper and longer than those in a granodiorite pluton. Variation of the sediment transport coefficient is inferred from hilltop curvature in rapidly eroding portions of the landscape, with the sediment transport coefficient being lower in metavolcanics ($4.8 \pm 1.8$ m$^2$ ka$^{-1}$) than in the granodiorite ($8.8 \pm 3.3$ m$^2$ ka$^{-1}$). The study area is undergoing a transient adjustment to accelerated base-level fall and therefore exhibits a large range in hilltop curvature (considered an indicator of erosion rate at steady state). Hillslope gradient increases monotonically with hilltop curvature until approaching a critical hillslope gradient $S_C$. The range of erosion rates facilitates estimation of $S_C$ at 0.79 and 0.85 in the granodiorite and metavolcanics, respectively. In metamorphosed volcanics hillslopes

tend to have a steeper mean gradient at low hilltop curvature, indicating that they are in a transient stage of adjustment to increased erosion rate. Hillslope lengths get shorter as hilltop curvature increases suggesting that drainage density is increasing with increasing erosion rates during the adjustment to a new erosion rate. I conclude that lithologic variability in a landscape can influence rates of sediment transport, influencing the topographic form of hillslopes, and that lithology influences the degree of landscape dissection.

# 4 HILLSLOPES RECORD HYSTERESIS IN THE GROWTH AND DECAY OF TECTONICALLY ACTIVE LANDSCAPES

A version of this chapter has been submitted to *Nature Geoscience*

## *Chapter Abstract*

The shape of the terrestrial Earth surface results from the interaction of tectonics and erosion which roughen landscapes, and sediment transport and deposition which smooth them. These processes compete to raise or lower the land surface relative to some datum, leaving their mark on the landscape and thus offering insights into the history of landscape change. One of the grand challenges in geomorphology is to understand the processes that modify the Earth surface to an extent that I can reconstruct the time evolution of the driving forces behind landscape evolution (Processes, 2010). In tectonically active regions, fault activity that results in relative uplift drives erosion and topographic evolution. Thus there exists the tantalizing prospect of using topography to reconstruct the temporal and spatial history of fault activity. This inversion, however, is only possible if we understand how tectonic forcing drives topographic evolution (Kirby and Ouimet, 2011; Whittaker, 2012). Here I analyse a tectonically active landscape where the spatial and temporal evolution of tectonic forcing is well constrained through geological mapping (Hilley and Arrowsmith, 2008): the Dragon's Back Pressure Ridge (DBPR) along the San Andreas Fault (SAF) in California. Via ergodic substitution, I show that the time evolution of a sensitive indicator of erosion rate, hilltop curvature, can be predicted using a nonlinear sediment flux law. Further, I demonstrate that the temporal evolution of relief and hilltop curvature experiences hysteresis as the landscape grows and decays; hence I demonstrate how landscapes growing due to fault activity can be distinguished from those with quiescent faults undergoing topographic decay.

## 4.1 Introduction and Theory

Hillslope morphology is a first order indicator of landscape change, with great potential for interrogating landscapes in tectonically active settings (Hurst et al., 2012). The information contained in hillslope morphology may be invaluable for identifying earthquake prone faults with no historic movement or for identifying landslide prone terrain. Observations that hillslope gradients are limited in rapidly eroding landscapes (Binnie et al., 2007; Burbank et al., 1996) have resulted in geomorphologists focusing on properties of the channel network as an indicator of erosion rates, and by inference, tectonic processes (DiBiase et al., 2010; Kirby and Ouimet, 2011; Ouimet et al., 2009). However the advent of high-resolution light detection and ranging (LiDAR) topographic data has led to studies revisiting hillslopes as potential indicators of landscape change (DiBiase et al., 2012; Hurst et al., 2012).

Predicting erosion rates at the scale of individual hillslopes is vital to ongoing landscape evolution modelling efforts (Tucker and Hancock, 2010). Physically-based models for long term sediment transport in high relief landscapes have only recently emerged (Roering et al., 1999) and my ability to interpret hillslope morphology is bound to the assumption that such models are an appropriate representation of real conditions. Hillslope morphology evolves over millennial timescales and therefore validation of sediment transport models are limited to observations of modern topography (Hurst et al., 2012; Roering et al., 2007) and experimental modelling (Roering et al., 2001b). Here I revisit a landscape where the assumption of ergodicity facilitates interpretation of temporal changes in hillslope morphology in response to surface uplift. The Dragon's Back Pressure Ridge (DBPR) in central California consists of a series of small basins (<400 m in length) trending sub-perpendicular to the San Andreas Fault. These catchments developed in poorly consolidated sediments of the Paso Robles formation on the south-west side of the SAF (Pacific Plate) (Hilley and Arrowsmith, 2008).

Hilley and Arrowsmith (2008) performed geological mapping to reconstruct uplift rate and demonstrate that dextral strike slip motion carried the catchments over a zone of focused uplift, which is pinned to the North American plate on the north-eastern side of the SAF (Figure 4.1a). Geological mapping reveals that these sediments are progressively uplifted and also folded into a monocline whose amplitude increases to the northwest, and this structure can be unravelled to reveal the cumulative uplift along the DBPR. This structure implies uplift occurring in the south-east of the landform which terminates roughly 2000 m along the landform to the north-west (Figure 4.2b) and allows a kinematic history of deformation to be inferred (Hilley and Arrowsmith, 2008). Furthermore, surface structures exposed within the North American Plate and magnetotelluric profiles across the area suggest that the SAF is offset in the shallow subsurface beneath the DBPR, and that this offset remains stationary with respect to the North American Plate (Hilley, personal communication). Taken together, these observations indicate that flat-lying sediments southwest of the DBPR are progressively deformed as strike-slip motion moves them into and through the deformation zone created by this shallow offset (Figure 4.1a). As such, the distribution of topography along the DBPR records material entry into and exit from the fixed uplift zone at a rate equal to the slip rate along the SAF. Accordingly the distribution of topography along strike records the temporal history of onset and cessation of uplift. A space-for-time substitution was therefore made using a mean slip rate of 33 mm $a^{-1}$ (Hilley and Arrowsmith, 2008).

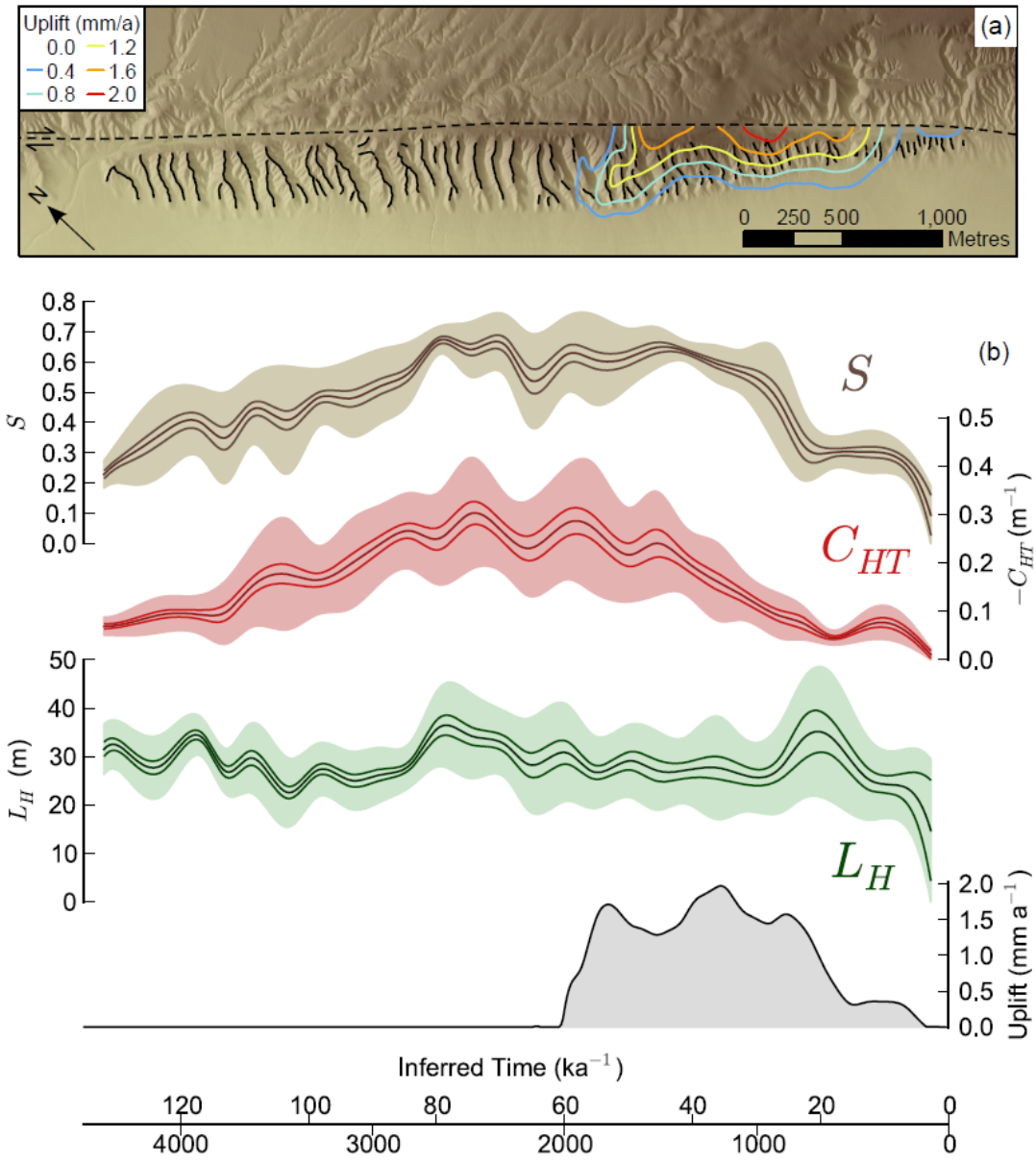


Figure 4.1: (a) Shaded relief image of the DBPR adjacent to the SAF. Contours show distribution of surface uplift rate (Hilley and Arrowsmith, 2008) and black lines depict the 509 hilltops used for this study. Dashed black line shows the San Andreas Fault which is experiencing dextral strike-slip at 33 mm a$^{-1}$. (b) The distribution of surface metrics mean slope $S$, mean hilltop curvature $C_{HT}$ and mean hillslope length $L_H$ sampled from the hilltops in (a). Shaded regions show standard deviation about binned averages, solid lines are standard errors about the bin means. $S$ becomes limited by ~800 m along the ridge whilst $C_{HT}$ continues to increase, suggesting that erosion rates are still rising as predicted by Equation 4.1. A transect of surface uplift rate created from the contours in (a) is also shown (solid line) as well as an assumed, simplified (Gaussian) uplift history (dashed line) used for generating modelling results shown in Figure 4.3.

The DBPR offers a remarkable opportunity to explore the temporal style of adjustments in hillslope morphology to initiation and termination of surface uplift and associated valley erosion. Hilley and Arrowsmith (2008) documented high valley steepness indices (valley slope normalised for drainage area, a metric for channel erosion rates (DiBiase et al., 2010; Ouimet et al., 2009)) coincident with the zone of maximum uplift (Figure 4.2). I focus in to the scale of individual hillslopes to address two fundamental problems. Firstly, can hillslope morphology be used to predict the spatial distribution of uplift along the SAF recorded by Hilley and Arrowsmith (2008), with a view to predicting potential earthquake hazards in remote locations? Secondly, what is the nature of hillslope morphological adjustment in response to the known forcing by tectonic uplift?

I address these questions in the context of a model for sediment transport on hillslopes (Roering et al., 1999). This model assumes transport limited conditions on hillslopes, which considered appropriate for the weakly consolidated sediments of the Paso Robles Formation. Hillslope gradients are limited in rapidly eroding landscapes due to a transition from disturbance-driven creep-like transport processes to mass-wasting dominated flux with increased erosion rates (Binnie et al., 2007; Burbank et al., 1996; DiBiase et al., 2010; Ouimet et al., 2009). The model presented by Roering et al. (1999) has been demonstrated to be applicable in such cases (Gabet, 2000; Hurst et al., 2012; Pelletier and Cline, 2007; Roering, 2008; Roering et al., 2001b; Roering et al., 2007), predicting that on hillslopes denuding in concert with incision in an adjacent channel, the curvature directly at the divide/hilltop ($C_{HT}$) varies linearly with channel erosion rate ($E$).

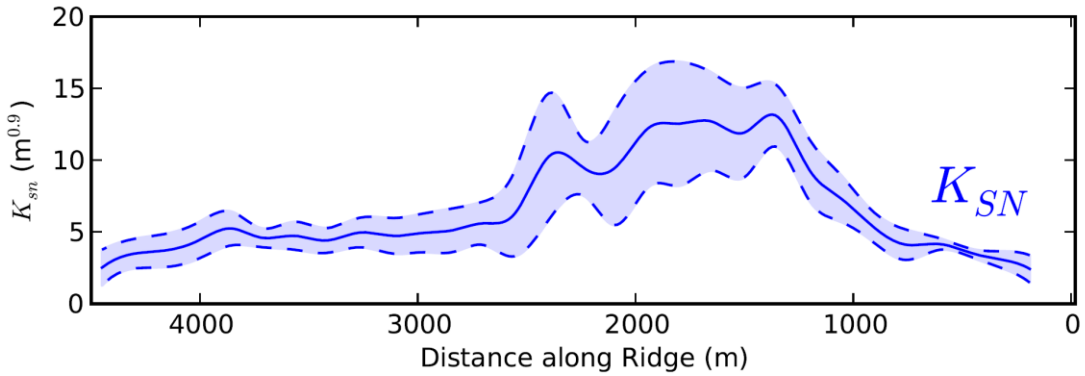


Figure 4.2: Distribution of channel steepness ($K_{SN}$) as a function of distance along the ridge (after Hilley and Arrowsmith, 2008). Shaded regions show standard deviation about binned averages, dashed lines are standard errors for the bin means.

Roering et al. (2007) derived analytical and non-dimensional solutions for hillslope form based on this non-linear, slope dependent sediment transport Equation, detailing a rigorous framework for analysing hillslope morphology. Their formulations allow exploration of links between erosion rates and topography based solely on topographic properties of hillslopes, particularly hilltop curvature ($C_{HT}$), mean hillslope gradient ($S$) and hillslope length ($L_H$). Hillslopes are characterized by a dimensionless relief, $R^*$, and an apparent erosion rate, $E^*$. The erosion rate is 'apparent' because $C_{HT}$ is used as a proxy: true and apparent erosion rates are only the same in steady state landscapes. According to Roering et al. (2007), steadily eroding landscapes should fall onto a constant curve of E* vs. R*. I recently developed algorithms to extract these metrics from such high-resolution topographic data (Hurst et al., 2012) and here extend them to a transient landscape with the aim to understand hillslope response to topographic growth and decay via tectonically generated uplift, and infer the correspondence between uplift and erosion rates.

## *4.2 Theory and Methods*

### 4.2.1 Theory on Hillslope Evolution and Predicted Morphology

The evolution of a one-dimensional hillslope following is modelled as (Roering et al., 1999):

$$\frac{\partial \zeta}{\partial t} = U - E = U - \frac{\partial q_s}{\partial x}, \text{ and} \qquad [4.1]$$

$$q_s = \frac{-DS}{1-(S/S_C)^2} \qquad [4.2]$$

where $\zeta$ is elevation [L], $t$ is time [T], $U$ is surface uplift rate [$LT^{-1}$], $E$ is erosion rate [$LT^{-1}$], $q_s$ is volumetric sediment flux [$L^2T^{-1}$], $x$ is distance along the hillslope, $D$ is a transport coefficient [$L^2\ T^{-1}$], $S$ is hillslope gradient and $S_C$ is a critical hillslope gradient toward which sediment flux becomes infinite. Roering et al. (2007) provided steady state solutions (i.e. when the condition $U=E$ is satisfied) for the above model which allow derivation of non-dimensional erosion rate $E^*$ and relief $R^*$ as functions of hilltop curvature $C_{HT}$, hillslope length $L_H$ and mean hillslope gradient $\overline{S}$:

$$E^* = \frac{E}{E_R} = \frac{\rho_r}{\rho_s} \cdot \frac{2\,E\,L_H}{D\,S_C} = \frac{2\,C_{HT}\,L_H}{S_C} \qquad [4.3]$$

$$R^* = \frac{\overline{S}}{S_C} = \frac{1}{E^*}\left\{\sqrt{1+(E^*)^2} - \ln\left[\frac{1}{2}\left(1+\sqrt{1+(E^*)^2}\right)\right] - 1\right\}. \qquad [4.4]$$

Where $E_R$ is a reference erosion rate and $\rho_r$ and $\rho_s$ are the densities of rock and dry soil respectively [$M\ L^{-3}$].

### 4.2.2 DEM Analysis

The topographic data was acquired by the National Centre for Airborne Laser Mapping. There were two principal concerns when preparing a DEM for this analysis. Firstly, the raw LiDAR point cloud contained returns misclassified as ground which have in fact come from small shrubs or bushes. These locations needed to be identified and preferentially smoothed. Secondly, hilltops on the Dragon's Back Pressure Ridge get extremely narrow (<2 m) where denudation is rapid, and so calculating reliable values for $C_{HT}$ is not straightforward.

#### 4.2.2.1 DEM Processing

I interpolated raw point cloud LiDAR returns (point density ~4 $m^{-2}$) to a 0.25 $m^2$ resolution grid using MCC-LiDAR (Evans and Hudak, 2007). This algorithm identifies locations in the point cloud where returns coincide spatially and removes the highest of these points. I do not use MCC-LiDAR to identify shrub vegetation since the algorithm is dependent on curvature, and hence has a tendency to misidentify sharp hilltops as vegetation. I justify interpolation to a 0.25 $m^2$ grid resolution by arguing that this allows the true location and elevations of point cloud data to be better spatially resolved in the gridded approximation of the surface, though likely results in needing to interpolate to many pixels with no nearby (<1 m) data in the point cloud. However this fine resolution allows us to calculate curvature over smaller windows, which is essential for resolving the curvature of narrow hilltops.

To remove low-lying vegetation, the gridded data were smoothed using a non-local means filtering algorithm (Buades et al., 2005). Filtering is based on the assumption of regularity, in other words that in the neighbourhood of the pixel of interest there are neighbourhoods that should look similar and therefore these non-local neighbourhoods can be used to predict the value at the original pixel. A non-local approach to DEM smoothing is particularly appealing towards the goal of removing vegetation which can be considered positive, high frequency noise since unlike many filtering techniques it does not assume that the noise is normally distributed.

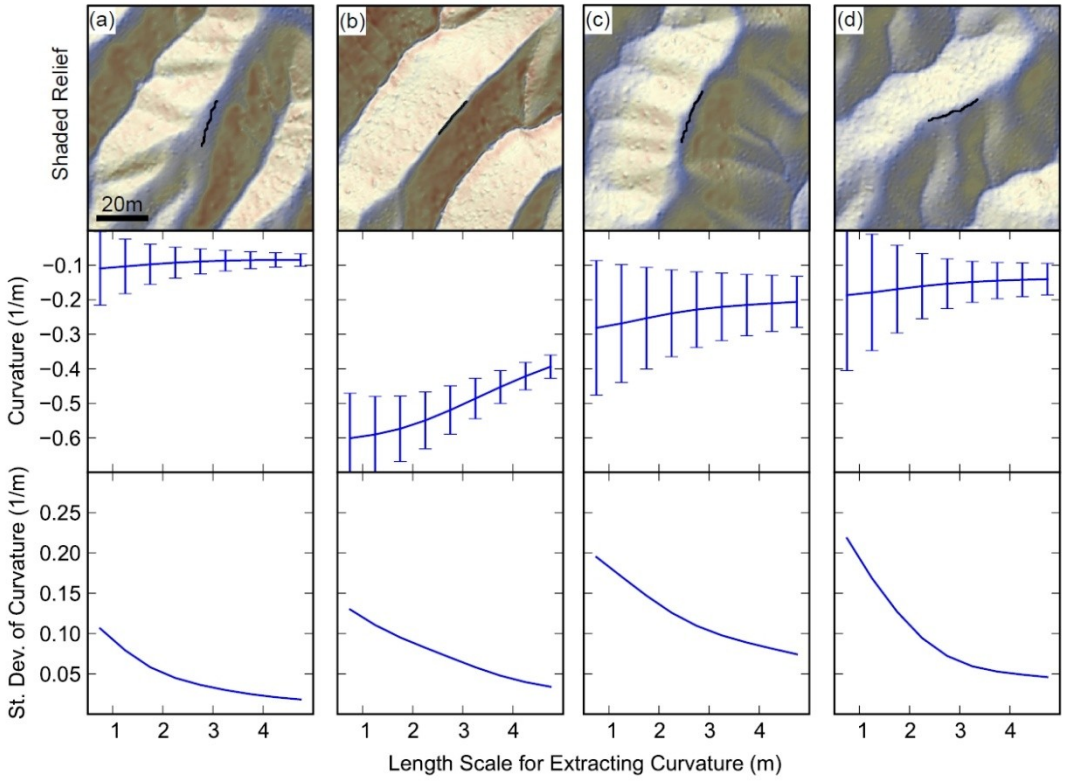


Figure 4.3: Variation in the hilltop curvature as a function of the length scale (or window size) over which curvature is extracted from the DEM. For each hilltop depicted in black in the shaded relief image, we extract the mean and standard deviation of curvature with a range of window sizes. Columns (a)-(d) are for hilltops distributed along the length of the DBPR interpreted as recording (a) transient response to uplift/erosion, (b) high erosion rate, steep planar hillslopes and narrow ridges, (c)-(d) relaxation of hillslope after uplift has ceased. For (a), (c) and (d) mean hilltop curvature is independent of window sizes above 2.5 m so this is the scale we use. On sharp hilltops with steep side slopes (b) negative hilltop curvature increases as the window size decreases suggesting we will underestimate $C_{HT}$ on such hilltops.

#### 4.2.3.1 Measuring Hilltop Curvature

Typically, topographic curvature is calculated over scales greater than the characteristic wavelength of high-frequency noise associated with surface roughness. At DBPR positive surface noise associated with low relief vegetation was smoothed. I varied the scale from 0.75 m to 5 m to test for scale effects. Figure 4.3 shows four hilltops distributed along the length of DBPR, and the associated variation in $C_{HT}$ and its standard deviation as the scale over which curvature was calculated varied. The selected hilltops are distributed along the length of DBPR, chosen to reflect inferred stages in landform development: (a) transient hillslope responding to uplift, characterised by low hilltop curvature but increasing slope; (b) hillslope in rapidly uplifting zone with steep planar hillslopes and sharp hilltop; (c) and (d) progressive relaxation following cessation of uplift, reduced slope gradients and lowering of $C_{HT}$. I observed that in all cases but (b), $C_{HT}$ varies little with length scales above ~2.5 m and there is a reduction in the standard deviation beyond this scale. This is the scale beyond which we see through high frequency noise in the landscape, therefore this was the length scale used in my analysis. The hilltop in (b) is extremely narrow and therefore with increasing length scale I are underestimating $C_{HT}$.

#### 4.2.3.2 Extracting Topographic Metrics

Following Hurst et al. (2012) I located hilltops as the adjoining margins of drainage basins extracted at a range of stream orders. In the DBPR I restricted analysis to interfluves, hilltops running roughly perpendicular to the SAF (Figure 4.1). Using a 0.25m digital elevation model, I calculated the aspect, gradient and curvature (Laplacian) of elevation from the coefficients of a 6-term quadratic surface fitted by least squares to all cells within a 2.5m window centred on the cell of interest. $C_{HT}$ was sampled directly at hilltops then a steepest descent trace was run from each hilltop pixel until a mask defining the channel network/valley fill was encountered. From this trace $L_H$ and $S$ were calculated.

### 4.2.4 Numerical Modelling of Hillslope Evolution

A one dimensional model of hillslope evolution in response to temporally variable uplift was implemented to make predictions for the temporal evolution of hillslope morphology. Equations 4.1 and 4.2 were solved forward through time for a portion of hillslope 60 m long (taken as the double of a mean $L_H$ from Figure 4.1b), whose boundaries were fixed at both ends to represent the location of bounding channels (therefore producing two 30 m long hillslopes). The parameter $D$ was taken from Arrowsmith et al. (1998) and $S_C$ was assumed to be 0.8. Setting $U=E$ at the boundaries, the hillslopes were subjected to a Gaussian uplift pulse (Figure 4.1b), and their morphological response recorded through time.

## *4.3 Results*

Figure 4.1b shows the distribution of $S$, $C_{HT}$ and $L_H$ along the DBPR with distance and time interchangeable (assuming a constant slip rate of 33 mm $a^{-1}$ on the SAF; Hilley and Arrowsmith 2008). As the initial surface is uplifted, topography develops and relief increases. From the onset of uplift, $S$, $C_{HT}$ and $L_H$ increase, presumably in response to increased erosion rates. By ~900 m (25 ka) $S$ values are high and increase very little from this point on, therefore I infer $S$ is limited by a process transition to landsliding. By 900 m, $L_H$ has also increased to a value that remains relatively constant during uplift and subsequent decay after uplift cessation. Uplift rates are high (> 1mm $a^{-1}$) from 900 m to 1800 m (25-55 ka) along the DBPR, yet $C_{HT}$ increases steadily, only attaining its maximum values ~20 ka after the uplift has declined. This is interpreted to reflect the erosional response to uplift and lag time in the system associated with the net time it takes for channels and subsequently hillslopes to increase their erosion rates in response to uplift.

The numerical model of hillslope evolution (Equations 4.1 and 4.2) predicted the path of a transient landscape in $E^*$ vs $R^*$ space in response to a simplified version of the uplift field experienced by the DBPR (see methods and supplementary materials). The simple model predicts a similar hysteretic adjustment in hillslope morphology.

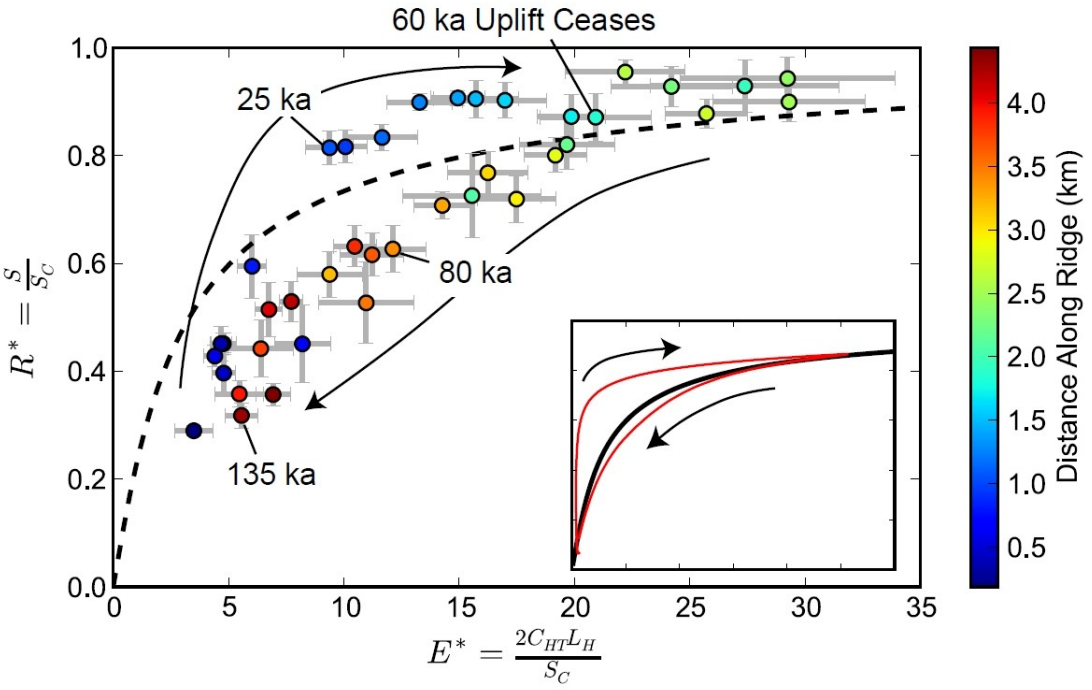


Figure 4.4: Variation in dimensionless erosion rate ($E^*$) and relief ($R^*$) with distance (colour bar) along the DBPR from SE to NW (assuming $S_C$ = 0.8). Dashed line indicates theoretical relationship for steady-state hillslopes. Grey error bars based on extremes in standard errors for measured $S$, $C_{HT}$ and $L_H$ illustrated in Figure 4.1. Substituting distance with time and assuming SAF slip rate of 33 mm $a^{-1}$ gives a time series of topographic development since the onset of uplift (Hilley and Arrowsmith, 2008) (i.e. 4500 m along ridge corresponds to c. 135 ka since a basin first experienced uplift). Inset plot shows the predictions of a 1D hillslope evolution model governed by Equation 4.1 ($L_H$ = 30m, see Figure 4.1b; $D$ = 0.008$m^2$ $a^{-1}$Arrowsmith et al. (1998); $S_C$ = 0.8), subject to a 60 ka uplift pulse with the form of a sine wave as shown by the black dashed line in Figure 4.1(b). The morphological evolution of hillslopes is distinct for adjustment during uplift verses relaxation after uplift has ceased. See Figure 4.5 to relate $E^*$ vs. $R^*$ to hillslope profiles.

## 4.4 Discussion

I previously hypothesised that a transient landscape would diverge from the steady E* vs. R* curve (Section 2.6; Hurst et al., 2012), doing so in a systematic way that would yield insight into the stage and trajectory of landscape evolution (Figure 4.4). Initially, increasing $S$, and $L_H$ and $C_{HT}$, elevate $R^*$ and $E^*$ respectively. $R^*$ doesn't increase significantly after 25 ka due to slope limitation by the inferred transition to landslide-dominated sediment flux. $E^*$ continues to increase driven by sharpening hilltops (increasingly negative $C_{HT}$) interpreted to be in response to rising erosion rates, even after uplift ceases at 60 ka. Note that it is likely that $C_{HT}$ is being underestimated on the sharpest ridges (since scale-invarient curvature cannot be observed; Figure 4.3) and therefore the magnitude of $E^*$ may too be underestimated for the narrowest hilltops. From 80 ka onwards both $E^*$ and $R^*$ decline gradually. The path of decline in $E^*$ verses $R^*$ space is distinct from the morphological response to landscape growth. Thus I find that if a landscape is adjusting to an increase in uplift by increasing erosion rates, hillslope morphology is distinct to a landscape relaxing due to a reduction/cessation of uplift/erosion.

I also find that the timescales of channel and hillslope adjustment to uplift are distinct. Previous work (Hilley and Arrowsmith, 2008) demonstrated that channel gradients adjust to both the onset and cessation of uplift at the DBPR in ~20 ka. Hillslopes appear to react to channel erosion rate rapidly and therefore $C_{HT}$ also lags behind uplift by ~20 ka. During landscape relaxation, $C_{HT}$ remains elevated for ~20ka before declining gently (Figure 4.1b). This suggests that whilst channels may have significantly reduced erosion rates, there may still be enhanced erosion and sediment transport on hillslopes, and that metrics for channel erosion rates may not necessarily reflect landscape-wide surface lowering in a relaxing landscape.

Finally I integrated the modelling results with field observations in a conceptual framework for the temporal evolution of DBPR (Figure 4.5). Accelerated

uplift tends to drive a wave of erosional adjustment which propagates into a landscape. Hilley and Arrowsmith (2008) showed that channel steepness adjusts rapidly to both increases and decreases in uplift. This means that on the scale of DBPR, channels are useful in indicating the current spatial distribution in uplift, but fail to record the history of adjustment. Because there is a delay in hillslope response, relief can grow without a commensurate change in apparent erosion rate, $E^*$, leading to data lying above the steady $E^*$ vs. $R^*$ curve (Figure 4.4). Following cessation of uplift, channels become gentler immediately whereas again hillslopes and hilltops are slower to respond, leading to points lying below the steady $E^*$ vs $R^*$ curve (Figure 4.4). This hysteresis in hillslope morphology has important implications for the interpretation of transient hillslopes; my findings may allow workers to tell a growing landscape from a decaying landscape based on topography alone.

## *4.5 Conclusions*

I show that the first-order attributes of the hillslope adjustments to changing tectonic rates are consistent with those expected when hillslopes denude according to a non-linear transport rule. I demonstrate that lags between changes in base-level lowering rate and hilltop curvature produce a hysteresis that can be used to distinguish landscapes that have recently experienced an increase in uplift rate from those that are adjusting to the cessation of uplift (Figure 4.4). These results suggest that hillslope forms provide a quantitative record of changes in base-level lowering rates, which may be used to infer tectonic histories when fluvial systems respond rapidly relative to hillslopes.

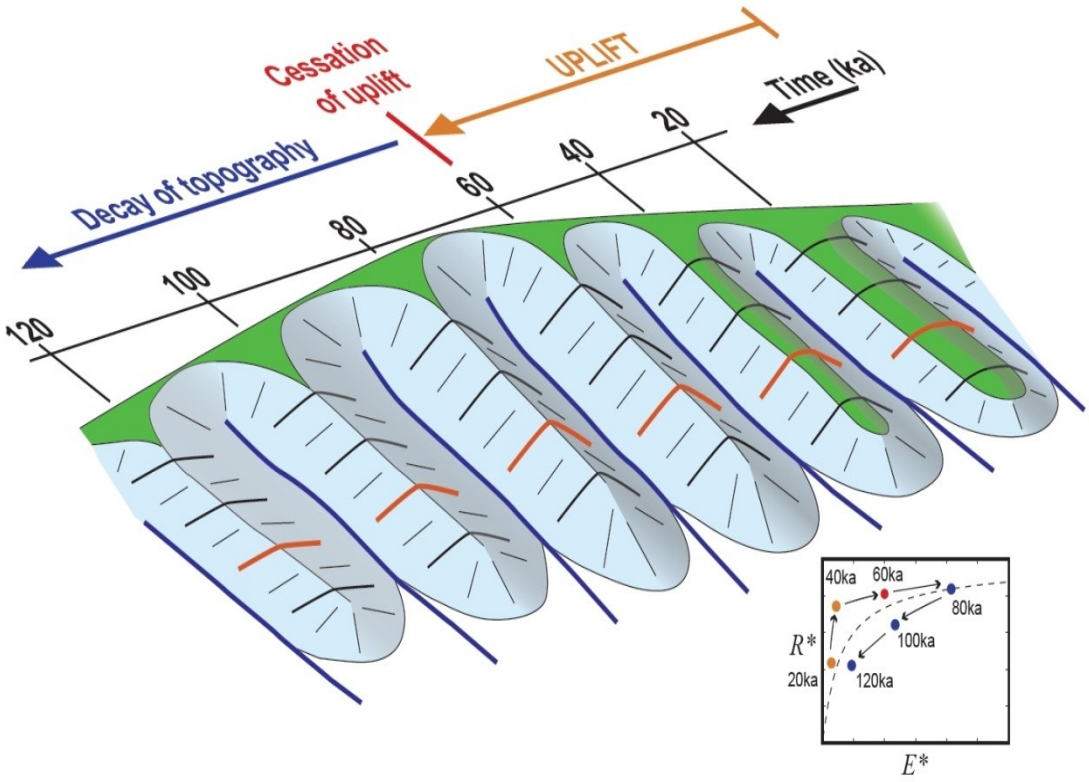


Figure 4.5: Schematic diagram illustrating the landscape response to onset and cessation of uplift and the expected distribution of $E^*$ vs. $R^*$ associated with this evolution (inset plot). Values for $E^*$ vs. $R^*$ reflect hillslope profiles highlighted in red on the schematic plot. Uplift triggers increased erosion rates in channels which dissect the original surface. This results in a wave of response propagating onto the hillslopes causing them to steepen (20-40 ka). Subsequently the hilltops begin to respond by becoming sharper (60-80 ka). Yet at 60 ka uplift ceases, channel slopes begin to decrease and the valleys begin accumulating sediment (Hilley and Arrowsmith, 2008). Hillslope gradients and hilltop curvature both reduce gradually in response to tailing off of channel erosion rates.

# 5 DISCUSSION

## *5.1 Overview and Synthesis*

This thesis has integrated high resolution topographic data with analytical and numerical model predictions to investigate the morphological response of hillslopes to transient boundary conditions driven by tectonic changes. To this end techniques were developed to exploit high resolution topographic datasets and interrogate modern hillslope morphology. Comparison of modern topography to model predictions is a vital approach to validating sediment transport models and constraining the style and timescale of response (Dietrich et al., 2003; Roering, 2008). This thesis endeavoured to demonstrate that therefore in turn it is possible to interpret boundary conditions (either rate of base-level fall or tectonic uplift rate) based on modern landscape morphology.

Combining existing and new CRN-derived basin-averaged erosion rates with parameters of topography such as mean hillslope gradient and hilltop curvature, chapter two validated the applicability of a nonlinear sediment transport model for hillslopes at the Feather River, California, which was supported by field observations. This allowed prediction of the distribution of erosion rates throughout the entire landscape using hilltop curvature as an erosion rate proxy. Further to this, the style of landscape response was demonstrably different depending on bedrock lithology in terms of the rate and style of hillslope adjustment to increased channel erosion rate (chapter three). Through detailed topographic analysis the details of these differences were revealed such that attempts to extract process rates from topography (i.e. erosion rates based on $C_{HT}$) could allow for this lithologic heterogeneity (by varying the sediment transport coefficient $D$). These two chapters

present and develop dialogue on the adjustment timescales for hillslopes responding to perturbation. Chapter two presents numerical evidence based on Roering et al. (2001a) that hillslope response times are relatively short in granitoid lithologies, yet in chapter three differences in hillslope morphology suggest that in metamorphosed volcanics the hillslope response time is longer despite knickpoints in the channel network having propagated further into the landscape.

In chapter four results are presented from a different field site where an unusual, but well constrained tectonic setting allows an ergodic substitution to be made (Hilley and Arrowsmith, 2008). By looking at changes in hillslope morphology along the length of the Dragon's Back Pressure Ridge landform, one is essentially looking back in time through a landscape subjected to and then deprived of tectonic uplift. I document the detailed morphological response to this setup which facilitates a time series of hillslope morphology to be reconstructed, and thus hillslope response time can be extracted directly from the topography. A hysteresis emerges whereby relief is distinct for growing landscapes compared to relaxing landscapes with the same apparent (i.e. non-dimensional) erosion rate, revealing the exciting possibility of deducing uplift history based on topography alone.

Whilst the bulk of this thesis is presented in three chapters written in stand-alone format for the purposes of publication, they form a combined contribution to better address outstanding questions in geomorphology.

## *5.2 Importance, Impact and Implications*

### 5.2.1 Hillslope Adjustment Timescales

In chapter two I use some numerical results from Roering et al. (2001a) to estimate the likely range of hillslope response times in the Feather River. These are likely tens of thousands to hundreds of thousands of years but vary with erosion rate.

At high erosion rates response times are short since hillslopes are already steep and the increase is accommodated through more frequent landsliding, transmitting the elevated erosion rate signal rapidly to the divide. At DBPR, the Roering et al. (2001a) approach to calculating hillslope adjustment timescale is inappropriate since the starting condition is a flat surface with zero erosion rather than an existing hillslope adjusted to some boundary condition. The hillslope is required to grow from flat, rather than having some existing form adjusted to another erosion rate. The formulation of (Roering et al., 2001a) was geared towards quantifying the response time to minor changes in erosion rate. Indeed using this calculation for a realistic range of hillslope parameters $D$, $S_C$ and $L_H$, predicts extremely short hillslope response times of 100-1000 years. Alternatively I adopted a highly simplified approach of calculating how long it would take to generate the relief required for an adjusted hillslope whose steady state was calculated analytically following Roering et al. (2007). Given the maximum uplift rate at DBPR, a hillslope length of $L_H$ = 30m and $S_C$ = 0.85, the time required to generate 24m of relief is ~19 ka (values taken from chapter four). This is similar to the response times suggested by (Hilley and Arrowsmith, 2008).

### 5.2.2 Hillslopes as an Erosion Rate Metric

Since topographic relief is limited by rock strength (Schmidt and Montgomery, 1995), and therefore not a reliable metric for erosion rate (Binnie et al., 2007; DiBiase et al., 2010; Montgomery, 2001; Montgomery and Brandon, 2002; Ouimet et al., 2009), research has focused on the predictive power of channel networks to infer erosion rates. Assuming channel form and evolution can be approximated by a model for bedrock channel evolution in which erosion rate is proportional to bed shear stress or stream power (Whipple and Tucker, 1999), the catchment-scale morphology of the channel network should reflect erosion rates. Channel slope should vary non-linearly with erosion rate, once normalised for drainage area and the concavity of the channel (Cyr et al., 2010; DiBiase et al., 2010;

Kirby et al., 2007; Kirby et al., 2003; Ouimet et al., 2009; Snyder et al., 2000). Ouimet et al. (2009) demonstrated a non-linear relationship between normalised steepness indices and erosion rates, exceeding those at which hillslopes become invariantly steep. Cyr et al. (2010) demonstrated that channel steepness may reflect erosion rates where hillslopes have become decoupled or lithologic contrasts prevent hillslope angle from being an appropriate topographic metric. For normalised steepness indices to reflect erosion rates, a basin-averaged approach must be taken in order to normalise for drainage area. Without a basin-averaged approach, steepness indices are not normalised for variation in the concavity of the channel and trends may be missed (Ponza et al., 2010). Whittaker et al. (2008) showed that the interpretation of the spatial distribution of normalised steepness indices in terms of distribution of surface uplift is not trivial in transient landscapes. The relationship between fluvial incision rates and metrics derived from the geometry of channel networks has been shown to be complicated by the existence of thresholds for fluvial erosion (Attal et al., 2011; DiBiase and Whipple, 2011; Lague et al., 2005; Snyder et al., 2003a; Snyder et al., 2003b), channel width adjustments in response to changes in boundary conditions (Attal et al., 2011; Finnegan et al., 2005; Whittaker et al., 2007b) and the role that sediment can play in modulating erosion rates (Cowie et al., 2008). The geomorphic characteristics of hillslopes have the potential to provide an independent test of the predictive power of channel steepness, whether the landscape is responding to a perturbation or not (Mudd and Furbish, 2007). The algorithms developed in this thesis to extract hillslope morphology will lend themselves well to this analysis since I can continue to trace down into the fluvial network in order to extract a channel steepness to which the hillslope is responding.

A recent study by DiBiase et al. (2012) has highlighted that a wealth of information can be extracted from hillslope morphology alone, provided that there is high resolution topographic data. Contrary to results from a 10 m resolution DEM (DiBiase et al., 2010), they found that catchment averaged slope measured from 1 m LiDAR increases with erosion rates in the San Gabriel Mountains, California, even

after the transition to landslide dominated sediment flux has been inferred, though mean hillslope gradient still becomes *less* sensitive to erosion rate. Additionally, DiBiase et al. (2012) introduced a technique to quantify the amount of bare rock exposed on a hillslope, calibrated against ultra high resolution panoramic photographs. Rock exposure increases linearly with erosion rates, and nonlinearly with mean hillslope gradient. An increase in rock exposure is likely reflecting the increased frequency of mass wasting events expected as erosion rates get higher. The increased exposure of bedrock outcrops on hillslopes documented by DiBiase et al. (2012) is pertinent to the ability to infer erosion rates from hilltop curvature. Increased rock exposure implies that the requirement of transport limited conditions may not be met. If hillslopes become gradient-limited due to a process transition to landslides then the hillslope is still behaving in a transport limited fashion over long timescales, otherwise the hillslope would have to get steeper through time. Therefore the erosion rate signal felt by hilltops will still be similar to that in the channel (though the mechanisms of sediment transport on the side slope will be somewhat more stochastic). Therefore in such settings, the techniques presented in chapter two only require that soil be readily transportable near to hilltops, where creep-like processes are inferred to dominate the sediment transport.

In chapters two and three I demonstrate that hillslope gradients in the Feather River may continue to increase slightly with rising hilltop curvature despite nonlinearity in the relationship (Figure 2.11). The Feather River spans a much narrower range of erosion rates than in the San Gabriel Mountains (up to a maximum 300mm $ka^{-1}$ inferred from $C_{HT}$ (Figure 2.12) and the spatial extent of higher erosion rates is limited to areas immediately proximal to the main river canyon. At the Dragon's Back Pressure Ridge uplift rates vary up to 2300 mm $ka^{-1}$ and hillslope gradients appear to be limited (Hilley and Arrowsmith, 2008) as corroborated in chapter four. This difference may however be linked to the nature of the underlying lithology. The Feather River sites are underlain by relatively hard Mesozoic granitoids and metamorphosed volcanics and there is patchy bedrock exposure in

steep portions of the landscape, similar to the predominantly granitic San Gabriel Mountains (DiBiase et al., 2012). However the DBPR site is underlain by weak, poorly consolidated sediments and the maximum attainable hillslope gradient may therefore be set by the angle of repose of those sediments. Rock strength and climate have been demonstrated to be important controls on the maximum hillslope gradient in threshold landscapes (Clarke and Burbank, 2011; Gabet et al., 2004; Korup and Weidinger, 2011) yet the work of DiBiase et al. (2012) reveals that hillslope morphology more sensitive to erosion and by inference, tectonic processes, than previously considered.

### 5.2.3 Ignorance of Chemical Weathering

The analyses presented in this thesis have focused on physical mechanisms of mass redistribution on hillslopes, assuming that mass loss by chemical denudation and transport as solutes is negligible compared to the physical displacement of rock and soil by surface transport processes. In the Feather River, Riebe et al. (2001b) measured chemical depletion by measuring the enrichment of the immobile element zirconium in soils. They demonstrated that chemical weathering rates typically comprised <20% of the total denudation rate derived from CRN analysis on those hillslopes. Further to this their data shows that chemical weathering rates scale with physical denudation rates, a result that is predicted by theoretical treatment of chemical weathering on hillslopes (Ferrier et al., 2012; Gabet and Mudd, 2009) and has been supported by other empirical studies (Anderson et al., 2002; Riebe et al., 2004; West et al., 2005). Increasing denudation delivers fresh mineral surfaces to the surface more rapidly, providing favoured sites for chemical alteration (Anderson et al., 2002).

Preliminary results looking at the influence of a transient erosion signal on the geochemistry of hillslope soils in Bald Rock Basin, a tributary to the Feather River (Yoo et al., 2011) suggest that chemical denudation rates may be higher than

previously documented by Riebe et al. (2001). This particularly influences my approximation of the sediment transport constant $D$ based on hilltop curvature by reducing the density of supplied material $\rho_r$ due to chemical alteration of saprolite. Additionally, the degree of saprolite weathering is also likely to vary with denudation rate (Dixon et al., 2009). On this basis it is plausible that $D$ may be influenced by erosion rate.

Field evidence suggests that tree turnover is the dominant mechanism of sediment transport. Whilst soil depths have been demonstrated to be relatively uniform across a gradient in erosion rate (Yoo et al., 2011) (see Appendix 1), variation in the textural properties and degree of chemical alteration in soil and saprolite likely result in differences in the mass of material moved during a tree throw event due to variation in soil density $\rho_s$. Whilst I do not have field data from which to directly quantify $D$ nor its spatial heterogeneity, I have demonstrated in chapter two that hilltop curvature varies systematically with erosion rates and that hillslope morphologies agree with theoretical sediment transport Equations which do not explicitly treat chemical processes of mass transport. Hence the introduction of this additional uncertainty influences more my ability to interpret absolute erosion rates based on hillslope morphology alone, but not predictions of the relative distribution of erosion rates across a landscape.

## *5.3 Research Opportunities and Future Work*

### 5.3.1 Application of Techniques in Other Landscapes

In this thesis I have put strong focus on the development of techniques to extract information about hillslope morphology from topographic data. The algorithms are freely available on request from the author. These tools can be applied to any topographic dataset regardless of quality or resolution, however users should

take care in interpreting the data generated since there may be resolution control on some hillslope properties.

$C_{HT}$ is particularly sensitive to varying data resolution. In chapter 2 and chapter 4 I demonstrated that $C_{HT}$ can be scale dependent, and that testing at various scales is required to determine the appropriate distance over which to measure $C_{HT}$. The reasons for this requirement are twofold, operating at different scales.

Firstly, high-resolution (i.e. LiDAR, 1 m post spacing) datasets tend to be noisy due to processes such as tree throw which roughen the surface at a local scale (e.g. Jyotsna and Haff, 1997). Therefore some method to smooth out this local variability and 'see through' to the first order morphology of the hillslope is needed. I advocate fitting polynomial surfaces to local windows of elevation, and calculating the curvature of the fitted surface as a preferred approach (see also (see also Roering et al., 2010). Varying the scale over which the surface is fitted, I then look for a scale range over which the curvature and variance of curvature are roughly constant, and chose the lowest scale in that range from which to calculate topographic parameters.

The second reason for testing the scale over which curvature is measured is that if either (i) hilltops become extremely narrow or (ii) the resolution of the dataset is coarse compared to the width of hilltops, then there will be a tendency to underestimate curvature. Note from Chapter 4 that for sharp, narrow hilltops it is not always possible to find scale invariant curvature and thus, ideally, a higher resolution of data would be required to better resolve the hilltop morphology (Figure 4.2). Consider also a coarse DEM at 30m resolution. In a high relief landscape the width of a hilltop may be only 10m, and will therefore only be represented by 1 pixel. However that pixel may not be centered at the true location of the topographic divide, underestimating the elevation of the ridge. As such curvature will be underestimated.

I have not come up with any explicit guidelines as to what resolution of data is required to perform the analysis presented here. Where airborne LiDAR datasets are available it should be possible to confidently quantify hilltop curvature, however with coarser resolution datasets it will depend on the width of hilltops. Nonetheless, techniques to trace from a hilltop to a nearby valley can be applied at any resolution (though potential error increases with increasing resolution) to quantify hillslope length, which may offer a method to independently test algorithms which measure drainage density.

### 5.3.2 Understanding Hillslope Response Timescales

At the DBPR I were able to estimate the response timescale of hillslopes to increased uplift based on real hillslope topography for the first time. Whilst this was based on a hitherto unique opportunity to substitute space for time in a real landscape, there are other field settings where there is potential to document hillslope response times. In transient landscapes characterised by fluvial knickpoints whose migration rate can be quantified (e.g. through CRN measurement) a space for time substitution might be made, as time since perturbation increases with distance downstream of the knickpoint. The ability to predict hillslope response times is critical to the use of hillslopes as indicators of landscape change, particularly hilltop curvature, since the hilltop will be the last part of a hillslope to 'feel' any changes that occur in an adjacent stream.

### 5.3.3 Tectonic Geomorphology

In chapter four I documented the morphological response of hillslopes to the onset and cessation of uplift along a portion of the dextral strike-slip San Andreas Fault. This work demonstrates that there is the potential for hillslopes to record not only the distribution of uplift along a fault but also whether the landscape is experiencing an increase or decrease in erosion rates, which may reflect the temporal

history of fault activity. The topographic analysis techniques developed in this thesis therefore great potential for interpreting fault activity in other tectonically active landscapes. For example Whittaker et al. (2008) presented detailed hydraulic and morphological data from rivers crossing active normal faults in the Italian Apennines. Catchment dynamics (e.g. sediment volume and grain-size distributions, channel and valley geometry) were distinct in basins crossing faults that are known to have experienced an increase in throw rates, from those which have not. (Attal et al., 2011) sought to explain these observations through numerical modeling of landscape evolution and were able to recreate the observed channel dynamics and long profile form.

Acquisition of high resolution topography would facilitate a similar approach to studying hillslopes, providing critical tests of surface process models by evaluating the spatial distribution of hillslope morphology, and allow evaluation of the potential for hillslopes to record the magnitude and timing of tectonic changes. For example, Densmore et al. (2005) demonstrated that topographic relief was limited in the footwall of active normal faults in the northeastern Basin and Range Province. Relief failed to correlate to known distributions of fault displacement. Densmore et al. (2007) found that slope-area scaling in catchments draining across such faults also becomes decoupled from throw rates ~10 km from fault tips. They concentrated their efforts to link fault activity to landscape evolution at the tips of these faults where the landscape is undergoing a transient adjustment to the onset of uplift through fault propagation. The increased availability of high resolution DEMs and techniques such as those developed in this thesis raises the possibility of revisiting such settings where we already have a good understanding of how the topography might be evolving to evaluate whether hillslope morphology (i.e. the spatial distribution of $C_{HT}$, $L_H$ and $S$) can reflect known distributions of fault throw, with a view to using the topography as a predictor of long term fault activity.

### 5.3.4 Organization in Landscapes

In chapter three I demonstrated that in a landscape responding to an increase in erosion rate, hillslope length ($L_H$) tends to decrease as the adjustment takes place. I hypothesized that this was related to an increase in the occurrence of debris flows which scour the floor of zero order basins. I have recently identified other landscapes undergoing accelerated erosion rates in which the change in landscape organization is striking. Preliminary data from a field site in the Idaho Batholith reveal that hillslope lengths decrease dramatically downstream of a knickpoint (Milodowski et al., in prep.). Landscape evolution models generally predict the opposite relationship, with drainage density decreasing with increasing erosion rates (e.g. Howard, 1997; Tucker and Bras, 1998). The models used in these studies do not incorporate the role of debris flows in valley evolution, nor do they consider variation in near surface hydrology. DiBiase et al., (2012) analyzed slope distributions in valley networks across a range of erosion rates and segregated the landscape into hillslopes, debris flow dominated-valleys, and fluvial-dominated valleys. They showed neatly that whilst there was no variation in drainage density with erosion rate, the downstream extent of debris flow-dominated valleys increased with erosion rates. DiBiase et al. (2012) focused on areas where the landscape could be assumed to be at steady state. Important questions emerge from the work of DiBiase et al. (2012), Howard (1997), Tucker and Bras (1998) and Milodowski et al. (in prep.): are the observe trends of hillslopes getting shorter with erosion rates in the Feather River a characteristic of transient landscapes only or are the theoretical reasons to expect such a relationship? For example if erosion rates increased, steeper hillslopes should lead to more overland flow, favouring higher drainage density. Can landscape evolution models replicate this change and if so how might including some debris flow erosion law (e.g. Stock and Dietrich, 2006) influence relationships between drainage density and erosion rate?

# 6 CONCLUSIONS

The primary conclusions of this thesis are:

1. Hilltop curvature measured from high resolution topography provides an indicator of erosion rate on hillslopes, on condition that a hillslope has adjusted fully to the incision rate in its bounding channel. This condition is likely to be met where the response timescale of the hillslope is short relative to the adjustment timescale of the fluvial network.

2. Description of non-dimensional hillslope properties may allow geomorphologists to test which model of hillslope sediment transport is most appropriate to conditions in a real landscape as well as to critically evaluate any assumptions that a landscape is at steady state.

3. Hillslope morphology, and the style and timescale of adjustment, are significantly influenced by the nature of underlying geology, even in a soil-mantled landscape where field evidence suggests the dominant driver of sediment transport in tree turnover. By documenting these differences I better understand the variability in sediment transport efficacy.

4. Hillslope lengths decrease with erosion rate. This suggests that valley forming processes become more efficient relative to hillslopes as the influence of debris flows allows valley heads to migrate further into the landscape. This is contrary to the findings of (DiBiase et al., 2012) who found that drainage density was independent of erosion rate in the San Gabriel

Mountains in Southern California. The different findings could potentially relate to environmental differences between the two studies sites, or differences in techniques used to extract topographic information from DEMs. A full treatment of drainage density, including comparison of measurement techniques, multiple field sites and numerical modelling studies is required to reconcile these differences.

5. Non-dimensional hillslope properties can also facilitate understanding whether hillslopes are still undergoing transient adjustment to a change in erosion or uplift rate. When hillslopes respond to an increase in erosion rate, their relief (or dimensionless relief) increases initially and their hilltop curvature (or dimensionless erosion rate) responds later, resulting in hillslopes that plot above an analytical relationship for steady-state morphology in a plot of dimensionless erosion rate vs. Dimensionless elief. Alternatively during landscape relaxation due to cessation of uplift or erosion, both relief and hilltop curvature reduce in concert such that hillslope morphology plots below the theoretical curve on a dimensionless erosion rate vs. Dimensionless relief plot. As such hillslope morphology may allow for identification of tectonically active sites in remote parts of the world with little historical seismic activity.

# 7 REFERENCES

Ahnert, F., 1970. Functional relationships between denudation, relief, and uplift in large mid-latitude drainage basins. American Journal of Science, 268(3), 243-263.

Ahnert, F., 1987. Approaches to dynamic equilibrium in theoretical simulations of slope development. Earth Surface Processes and Landforms, 12(1), 3-15, doi:10.1002/esp.3290120103.

Almond, P.C., Roering, J.J., Hughes, M.W., Lutter, F.S., C., L., 2008. Climatic and anthropogenic effects on soil transport rates and hillslope evolution Sediment dynamics in changing environments, Christchurch, New Zealand: International Association of Hydrological Science Publication, 325, 417-424.

Anderson, R.S., 1994. Evolution of the Santa Cruz Mountains, California, through tectonic growth and geomorphic decay. Journal of Geophysical Research - Earth Surface, 99(B10), 20161-20179, doi:10.1029/94jb00713.

Anderson, S.P., Dietrich, W.E., Brimhall, G.H., 2002. Weathering profiles, mass-balance analysis, and rates of solute loss: Linkages between weathering and erosion in a small, steep catchment. Geological Society of America Bulletin, 114(9), 1143-1158.

Andrews, D.J., Bucknam, R.C., 1987. Fitting degradation of shoreline scarps by a nonlinear diffusion-model. Journal of Geophysical Research-Solid Earth and Planets, 92(B12), 12857-12867.

Armitage, J.J., Duller, R.A., Whittaker, A.C., Allen, P.A., 2011. Transformation of tectonic and climatic signals from source to sedimentary archive. Nature Geoscience, 4(4), 231-235.

Arrowsmith, J.R., Rhodes, D.D., Pollard, D.D., 1998. Morphologic dating of scarps formed by repeated slip events along the San Andreas Fault, Carrizo Plain, California. Journal of Geophysical Research, 103(B5), 10141-10160, doi:10.1029/98jb00505.

Attal, M., Cowie, P.A., Whittaker, A.C., Hobley, D., Tucker, G.E., Roberts, G.P., 2011. Testing fluvial erosion models using the transient response of bedrock rivers to tectonic forcing in the Apennines, Italy. Journal of Geophysical Research - Earth Surface, 116(F2), F02005, doi:10.1029/2010jf001875.

Avouac, J.P., 1993. Analysis of scarp profiles - evaluation of errors in morphologic dating. Journal of Geophysical Research-Solid Earth, 98(B4), 6745-6754.

Avouac, J.P., Peltzer, G., 1993. Active tectonics in southern-Xinjiang, China - analysis of terrace riser and normal-fault scarp degradation along the Hotan-Gira fault system. Journal of Geophysical Research-Solid Earth, 98(B12), 21773-21807.

Avouac, J.P., Tapponnier, P., Bai, M., You, H., Wang, G., 1993. Active thrusting and folding along the northern Tien-Shan and late Cenozoic rotation of the Tarim relative to Dzungaria and Kazakhstan. Journal of Geophysical Research-Solid Earth, 98(B4), 6755-6804.

Balco, G., Stone, J.O., Lifton, N.A., Dunai, T.J., 2008a. A complete and easily accessible means of calculating surface exposure ages or erosion rates from 10Be and 26Al measurements. Quaternary Geochronology, 3(3), 174-195, doi:10.1016/j.quageo.2007.12.001.

Balco, G., Stone, J.O., Lifton, N.A., Dunai, T.J., 2008b. A complete and easily accessible means of calculating surface exposure ages or erosion rates from Be-10 and Al-26 measurements. Quaternary Geochronology, 3(3), 174-195, doi:10.1016/j.quageo.2007.12.001.

Begin, Z.B., 1992. Application of quantitative morphologic dating to paleo-seismicity of the northwestern Negev, Israel. Israeli Journal of Earth Sciences, 41, 95-103.

Bierman, P., Steig, E.J., 1996. Estimating rates of denudation using cosmogenic isotope abundances in sediment. Earth Surface Processes and Landforms, 21(2), 125-139.

Bierman, P.R., Caffee, M.W., Davis, P.T., Marsella, K., Pavich, M., Colgan, P., Mickelson, D., Larsen, J., 2002. Rates and timing of earth surface processes from in situ-produced cosmogenic Be-10. Beryllium: Mineralogy, Petrology, and Geochemistry, 50, 147-205.

Binnie, S.A., Phillips, W.M., Summerfield, M.A., Fifield, L.K., 2007. Tectonic uplift, threshold hillslopes, and denudation rates in a developing mountain range. Geology, 35(8), 743-746, doi:10.1130/g23641a.

Black, T.A., Montgomery, D.R., 1991. Sediment transport by burrowing mammals, Marin County, California. Earth Surface Processes and Landforms, 16(2), 163-172.

Bowman, D., Gerson, R., 1986. Morphology of the latest quaternary surface-faulting in the Gulf of Elat Region, eastern Sinai. Tectonophysics, 128(1), 97-119.

Bowman, D., Gross, T., 1989. Neotectonics in the northern Arava: Research Report to the Israel Department of Energy (in Hebrew).

Brown, E.T., Stallard, R.F., Larsen, M.C., Raisbeck, G.M., Yiou, F., 1995. Denudation rates determined from the accumulation of in situ-produced Be-10

in the Luquillo experimental forest, Puerto-Rico. Earth and Planetary Science Letters, 129(1-4), 193-202.

Buades, A., Coll, B., Morel, J.M., 2005. A non-local algorithm for image denoising, Computer Vision and Pattern Recognition, IEEE Computer Society Conference., pp. 60-65, doi:10.1109/cvpr.2005.38.

Burbank, D.W., Leland, J., Fielding, E., Anderson, R.S., Brozovic, N., Reid, M.R., Duncan, C., 1996. Bedrock incision, rock uplift and threshold hillslopes in the northwestern Himalayas. Nature, 379(6565), 505-510.

Burke, B.C., Heimsath, A.M., White, A.F., 2007. Coupling chemical weathering with soil production across soil-mantled landscapes. Earth Surface Processes and Landforms, 32(6), 853-873, doi:10.1002/esp.1443.

Busby, C.J., Putirka, K., 2009. Miocene evolution of the western edge of the Nevadaplano in the central and northern Sierra Nevada: palaeocanyons, magmatism, and structure. International Geology Review, 51(7-8), 670-701, doi:10.1080/00206810902978265.

Carretier, S., Ritz, J.F., Jackson, J., Bayasgalan, A., 2002. Morphological dating of cumulative reverse fault scarps: examples from the Gurvan Bogd fault system, Mongolia. Geophysical Journal International, 148(2), 256-277, doi:10.1046/j.1365-246X.2002.01599.x.

Cecil, M.R., Ducea, M.N., Reiners, P.W., Chase, C.G., 2006. Cenozoic exhumation of the northern Sierra Nevada, California, from (U-Th)/He thermochronology. Geological Society of America Bulletin, 118(11-12), 1481-1488, doi:10.1130/b25876.1.

Clapp, E.M., Bierman, P.R., Caffee, M., 2002. Using Be-10 and Al-26 to determine sediment generation rates and identify sediment source areas in an arid region drainage basin. Geomorphology, 45(1-2), 89-104.

Clapp, E.M., Bierman, P.R., Nichols, K.K., Pavich, M., Caffee, M., 2001. Rates of sediment supply to arroyos from upland erosion determined using in situ produced cosmogenic Be-10 and Al-26. Quaternary Research, 55(2), 235-245.

Clark, D.H., 1995. Extent, timing, and climatic significance of latest Pleistocene and Holocene glaciation in the Sierra Nevada, California. Doctor of Philosophy Ph.D. Thesis, University of Washington, 193 pp.

Clark, M., K., Maheo, G., Saleeby, J., Farley, K., A., 2005. The non-equilibrium landscape of the southern Sierra Nevada, California. GSA Today, 15(9), 4-10.

Clark, M.L., Roberts, D.A., Ewel, J.J., Clark, D.B., 2011. Estimation of tropical rain forest aboveground biomass with small-footprint lidar and hyperspectral sensors. Remote Sensing of Environment, 115(11), 2931-2942.

Clarke, B.A., Burbank, D.W., 2010. Bedrock fracturing, threshold hillslopes, and limits to the magnitude of bedrock landslides. Earth and Planetary Science Letters, 297(3-4), 577-586.

Clarke, B.A., Burbank, D.W., 2011. Quantifying bedrock-fracture patterns within the shallow subsurface: Implications for rock mass strength, bedrock landslides, and erodibility. Journal of Geophysical Research - Earth Surface, 116(F4), F04009, doi:10.1029/2011jf001987.

Codilean, A.T., 2006. Calculation of the cosmogenic nuclide production topographic shielding scaling factor for large areas using DEMs. Earth Surface Processes and Landforms, 31(6), 785-794, doi:10.1002/esp.1336.

Codilean, A.T., Bishop, P., Stuart, F.M., Hoey, T.B., Fabel, D., Freeman, S.P.H.T., 2008. Single-grain cosmogenic 21Ne concentrations in fluvial sediments reveal spatially variable erosion rates. Geology, 36(2), 159-162, doi:10.1130/g24360a.1.

Colman, S.M., Watson, K., 1983. Ages estimated from a diffusion Equation model for scarp degradation. Science, 221(4607), 263-265.

Constantine, J.A., Schelhaas, M.-J., Gabet, E., Mudd, S.M., 2012. Limits of windthrow-driven hillslope sediment flux due to varying storm frequency and intensity. Geomorphology, 175–176(0), 66-73, doi:10.1016/j.geomorph.2012.06.022.

Cowie, P.A., Whittaker, A.C., Attal, M.l., Roberts, G., Tucker, G.E., Ganas, A., 2008. New constraints on sediment-flux dependent river incision: Implications for extracting tectonic signals from river profiles. Geology, 36(7), 535-538, doi:10.1130/g24681a.1.

Crosby, B.T., Whipple, K.X., Gasparini, N.M., Wobus, C.W., 2007. Formation of fluvial hanging valleys: Theory and simulation. Journal of Geophysical Research-Earth Surface, 112(F3), doi:10.1029/2006jf000566.

Culling, W.E.H., 1960. Analytical theory of erosion. Journal of Geology, 68(3), 336-344.

Culling, W.E.H., 1963. Soil creep and the development of hillside slopes. The Journal of Geology, 71(2), 127-161.

Cyr, A.J., Granger, D.E., Olivetti, V., Molin, P., 2010. Quantifying rock uplift rates using channel steepness and cosmogenic nuclide-determined erosion rates: Examples from northern and southern Italy. Lithosphere, 2(3), 188-198, doi:10.1130/l96.1.

Daly, C., G. Taylor, and W. Gibson 1997. The PRISM approach to mapping precipitation and temperature. 10th Conference on Applied Climatology, Reno, NV., American Meteorological Society, 10-12.

Davis, W.M., 1892. The convex profile of badland divides. Science, 20, 245.

Day, H.W., Bickford, M.E., 2004. Tectonic setting of the Jurassic Smartville and Slate Creek complexes, northern Sierra Nevada, California. Geological Society of America Bulletin, 116(11-12), 1515-1528, doi:10.1130/b25416.1.

Densmore, A.L., Dawers, N.H., Gupta, S., Guidon, R., 2005. What sets topographic relief in extensional footwalls? Geology, 33(6), 453-456, doi:10.1130/g21440.1.

Densmore, A.L., Ellis, M.A., Anderson, R.S., 1998. Landsliding and the evolution of normal-fault-bounded mountains. Journal of Geophysical Research, 103(B7), 15203-15219, doi:10.1029/98jb00510.

Densmore, A.L., Gupta, S., Allen, P.A., Dawers, N.H., 2007. Transient landscapes at fault tips. Journal of Geophysical Research-Earth Surface, 112(F3), F03S08, doi:10.1029/2006jf000560.

Desilets, D., Zreda, M., Prabu, T., 2006. Extended scaling factors for in situ cosmogenic nuclides: New measurements at low latitude. Earth and Planetary Science Letters, 246(3), 265-276.

DiBiase, R.A., Heimsath, A.M., Whipple, K.X., 2012. Hillslope response to tectonic forcing in threshold landscapes. Earth Surface Processes and Landforms, 37(8), 855-865, doi:10.1002/esp.3205.

DiBiase, R.A., Whipple, K.X., 2011. The influence of erosion thresholds and runoff variability on the relationships among topography, climate, and erosion rate. Journal of Geophysical Research-Earth Surface, 116(F4), F04036, doi:10.1029/2011jf002095.

DiBiase, R.A., Whipple, K.X., Heimsath, A.M., Ouimet, W.B., 2010. Landscape form and millennial erosion rates in the San Gabriel Mountains, CA. Earth and Planetary Science Letters, 289(1-2), 134-144, doi:10.1016/j.epsl.2009.10.036.

Dietrich, W., E., Bellugi, D., G., Sklar, L., S., Stock, J., D., Heimsath, A., M., Roering, J., J., 2003. Geomorphic transport laws for predicting landscape form and dynamics, Prediction in Geomorphology, Geophysical Monograph 135, . Geophysical Monograph Series. American Geophysical Union, Washington, DC, pp. 1-30, doi:10.1029/gm135.

Dietrich, W.E., Perron, J.T., 2006. The search for a topographic signature of life. Nature, 439(7075), 411-418.

Dixon, J.L., Heimsath, A.M., Amundson, R., 2009. The critical role of climate and saprolite weathering in landscape evolution. Earth Surface Processes and Landforms, 34(11), 1507-1521, doi:10.1002/esp.1836.

Donoghue, D.N.M., Watt, P.J., 2006. Using LiDAR to compare forest height estimates from IKONOS and Landsat ETM+ data in Sitka spruce plantation forests. International Journal of Remote Sensing, 27(11), 2161-2175, doi:10.1080/01431160500396493.

Duller, R.A., Whittaker, A.C., Fedele, J.J., Whitchurch, A.L., Springett, J., Smithells, R., Fordyce, S., Allen, P.A., 2010. From grain size to tectonics. Journal of Geophysical Research-Earth Surface, 115(F3), F03022, doi:10.1029/2009jf001495.

Dunai, T.J., 2000. Scaling factors for production rates of in situ produced cosmogenic nuclides: a critical reevaluation. Earth and Planetary Science Letters, 176(1), 157-169.

Dunai, T.J., 2010. Cosmogenic nuclides : principles, concepts and applications in the earth surface sciences. Cambridge University Press, Cambridge, UK ; New York.

Dunai, T.J., LÃ³pez, G.A.G.l., Juez-LarrÃ©, J., 2005. Oligoceneâ€“Miocene age of aridity in the Atacama Desert revealed by exposure dating of erosion-sensitive landforms. Geology, 33(4), 321-324, doi:10.1130/g21184.1.

Dunne, J., Elmore, D., Muzikar, P., 1999. Scaling factors for the rates of production of cosmogenic nuclides for geometric shielding and attenuation at depth on sloped surfaces. Geomorphology, 27(1-2), 3-11, doi:10.1016/s0169-555x(98)00086-5.

Dunne, T., Malmon, D.V., Mudd, S.M., 2010. A rain splash transport Equation assimilating field and laboratory measurements. Journal of Geophysical Research-Earth Surface, 115, doi:10.1029/2009jf001302.

Enzel, Y., Amit, R., Porat, N., Zilberman, E., Harrison, B.J., 1996. Estimating the ages of fault scarps in the Arava, Israel. Tectonophysics, 253(3-4), 305-317.

Evans, I.S., 1980. An integrated system of terrain analysis and slope mapping. Zeitschrift fur Geomorphologie, 36, 274-295.

Evans, J.S., Hudak, A.T., 2007. A Multiscale Curvature Algorithm for Classifying Discrete Return LiDAR in Forested Environments. Geoscience and Remote Sensing, IEEE Transactions, 45(4), 1029-1038, doi:10.1109/tgrs.2006.890412.

Fernandes, N.F., Dietrich, W.E., 1997. Hillslope evolution by diffusive processes: The timescale for equilibrium adjustments. Water Resources Research, 33(6), 1307-1318.

Ferrier, K.L., Kirchner, J.W., Finkel, R.C., 2012. Weak influences of climate and mineral supply rates on chemical erosion rates: Measurements along two altitudinal transects in the Idaho Batholith. Journal of Geophysical Research-Earth Surface, 117(F2), F02026, doi:10.1029/2011jf002231.

Figueroa, A.M., Knott, J.R., 2010. Tectonic geomorphology of the southern Sierra Nevada Mountains (California): Evidence for uplift and basin formation. Geomorphology, 123(1), 34-45.

Finnegan, N.J., Roe, G., Montgomery, D.R., Hallet, B., 2005. Controls on the channel width of rivers: Implications for modeling fluvial incision of bedrock. Geology, 33(3), 229-232, doi:10.1130/g21171.1.

Foufoula-Georgiou, E., Ganti, V., Dietrich, W.E., 2010. A nonlocal theory of sediment transport on hillslopes. Journal of Geophysical Research-Earth Surface, 115, F00A16, doi:10.1029/2009jf001280.

Furbish, D.J., Fagherazzi, S., 2001. Stability of creeping soil and implications for hillslope evolution. Water Resources Research, 37(10), 2607-2618.

Furbish, D.J., Haff, P.K., Dietrich, W.E., Heimsath, A.M., 2009. Statistical description of slope-dependent soil transport and the diffusion-like coefficient. Journal of Geophysical Research-Earth Surface, 114, doi:10.1029/2009jf001267.

Furbish, D.J., Hamner, K.K., Schmeeckle, M., Borosund, M.N., Mudd, S.M., 2007. Rain splash of dry sand revealed by high-speed imaging and sticky paper splash targets. Journal of Geophysical Research-Earth Surface, 112(F1), doi:10.1029/2006jf000498.

Gabet, E.J., 2000. Gopher bioturbation: Field evidence for non-linear hillslope diffusion. Earth Surface Processes and Landforms, 25(13), 1419-1428.

Gabet, E.J., 2003. Sediment transport by dry ravel. Journal of Geophysical Research-Solid Earth, 108(B1), doi:10.1029/2001jb001686.

Gabet, E.J., Mudd, S.M., 2009. A theoretical model coupling chemical weathering rates with denudation rates. Geology, 37(2), 151-154, doi:10.1130/g25270a.1.

Gabet, E.J., Mudd, S.M., 2010. Bedrock erosion by root fracture and tree throw: A coupled biogeomorphic model to explore the humped soil production function and the persistence of hillslope soils. Journal of Geophysical Research-Earth Surface, 115, doi:10.1029/2009jf001526.

Gabet, E.J., Pratt-Sitaula, B.A., Burbank, D.W., 2004. Climatic controls on hillslope angle and relief in the Himalayas. Geology, 32(7), 629-632, doi:10.1130/g20641.1.

Gabet, E.J., Reichman, O.J., Seabloom, E.W., 2003. The effects of bioturbation on soil processes and sediment transport. Annual Review of Earth and Planetary Sciences, 31, 249-273, doi:10.1146/annurev.earth.31.100901.141314.

Gallen, S.F., Wegmann, K.W., Frankel, K.L., Hughes, S., Lewis, R.Q., Lyons, N., Paris, P., Ross, K., Bauer, J.B., Witt, A.C., 2011. Hillslope response to knickpoint migration in the Southern Appalachians: implications for the evolution of post-orogenic landscapes. Earth Surface Processes and Landforms, 36(9), 1254-1267, doi:10.1002/esp.2150.

Gangodagamage, C., Belmont, P., Foufoula-Georgiou, E., 2011. Revisiting scaling laws in river basins: New considerations across hillslope and fluvial regimes. Water Resources Research, 47(7), W07508, doi:10.1029/2010wr009252.

Gilbert, G., K., 1877. Report on the Geology of the Henry Mountains. Goverment Printing Office, Washington.

Gilbert, G.K., 1909. The convexity of hilltops. Journal of Geology, 17(4), 344-350.

Gilbert, G.K., Dutton, C.E., Geographical, Region, G.S.o.t.R.M., 1877. Report on the geology of the Henry Mountains. G.P.O., Washington D.C.

Gosse, J.C., Phillips, F.M., 2001. Terrestrial in situ cosmogenic nuclides: theory and application. Quaternary Science Reviews, 20(14), 1475-1560, doi:10.1016/s0277-3791(00)00171-2.

Granger, D.E., 2006. A review of burial dating methods using 26Al and 10Be. Geological Society of America Special Papers, 415, 1-16, doi:10.1130/2006.2415(01).

Granger, D.E., Kirchner, J.W., Finkel, R., 1996. Spatially averaged long-term erosion rates measured from in situ-produced cosmogenic nuclides in alluvial sediment. Journal of Geology, 104(3), 249-257.

Granger, D.E., Riebe, C.S., Kirchner, J.W., Finkel, R.C., 2001. Modulation of erosion on steep granitic slopes by boulder armoring, as revealed by cosmogenic Al-26 and Be-10. Earth and Planetary Science Letters, 186(2), 269-281.

Hall, S.A., Burke, I.C., Box, D.O., Kaufmann, M.R., Stoker, J.M., 2005. Estimating stand structure using discrete-return lidar: an example from low density, fire prone ponderosa pine forests. Forest Ecology and Management, 208(1-3), 189-209.

Hanks, T.C., 2000. The age of scarplike landforms from diffusion-Equation analysis. In: J.S. Noller, Sowers, J. M., Lettis, W. R. (Ed.), Quaternary geochronology: Methods and applications. American Geophysical Union, Washington, D.C., pp. 313-338.

Hanks, T.C., Andrews, D.J., 1989. Effect of far-field slope on morphologic dating of scarplike landforms. Journal of Geophysical Research-Solid Earth and Planets, 94(B1), 565-573.

Hanks, T.C., Bucknam, R.C., Lajoie, K.R., Wallace, R.E., 1984. Modification of wave-cut and faulting controlled landforms. Journal of Geophysical Research, 89(B7), 5771-5790.

Hanks, T.C., Wallace, R.E., 1985. Morphological analysis of the Lake Lahontan shoreline and Beachfront fault scarps, Pershing County, Nevada. Bulletin of the Seismological Society of America, 75(3), 835-846.

Heimsath, A.M., Chappell, J., Dietrich, W.E., Nishiizumi, K., Finkel, R.C., 2000. Soil production on a retreating escarpment in southeastern Australia. Geology, 28(9), 787-790.

Heimsath, A.M., DiBiase, R.A., Whipple, K.X., 2012. Soil production limits and the transition to bedrock-dominated landscapes. Nature Geoscience, doi:10.1038/ngeo1380

Heimsath, A.M., Dietrich, W.E., Nishiizumi, K., Finkel, R.C., 1997. The soil production function and landscape equilibrium. Nature, 388(6640), 358-361.

Heimsath, A.M., Dietrich, W.E., Nishiizumi, K., Finkel, R.C., 1999. Cosmogenic nuclides, topography, and the spatial variation of soil depth. Geomorphology, 27(1-2), 151-172.

Heimsath, A.M., Dietrich, W.E., Nishiizumi, K., Finkel, R.C., 2001. Stochastic processes of soil production and transport: Erosion rates, topographic variation and cosmogenic nuclides in the Oregon Coast Range. Earth Surface Processes and Landforms, 26(5), 531-552.

Heimsath, A.M., Furbish, D.J., Dietrich, W.E., 2005. The illusion of diffusion: Field evidence for depth-dependent sediment transport. Geology, 33(12), 949-952.

Heisinger, B., Lal, D., Jull, A., Kubik, P., Ivy-Ochs, S., Knie, K., Nolte, E., 2002a. Production of selected cosmogenic radionuclides by muons: 2. Capture of negative muons. Earth and Planetary Science Letters, 200(3), 357-369.

Heisinger, B., Lal, D., Jull, A.J.T., Kubik, P., Ivy-Ochs, S., Neumaier, S., Knie, K., Lazarev, V., Nolte, E., 2002b. Production of selected cosmogenic radionuclides by muons 1. Fast muons. Earth and Planetary Science Letters, 200(3-4), 345-355.

Hijmans, R.J., Cameron, S.E., Parra, J.L., Jones, P.G., Jarvis, A., 2005. Very high resolution interpolated climate surfaces for global land areas. International Journal of Climatology, 25(15), 1965-1978, doi:10.1002/joc.1276.

Hilley, G.E., Arrowsmith, J.R., 2008. Geomorphic response to uplift along the Dragon's Back pressure ridge, Carrizo Plain, California. Geology, 36(5), 367-370, doi:10.1130/g24517a.1.

Hobley, D.E.J., Sinclair, H.D., Cowie, P.A., 2010. Processes, rates, and time scales of fluvial response in an ancient postglacial landscape of the northwest Indian Himalaya. Geological Society of America Bulletin, 122(9-10), 1569-1584, doi:10.1130/b30048.1.

Holmgren, J., Nilsson, M., Olsson, H., 2003. Simulating the effects of lidar scanning angle for estimation of mean tree height and canopy closure. Canadian Journal of Remote Sensing, 29(5), 623-632.

House, M.A., Wernicke, B.P., Farley, K.A., 1998. Dating topography of the Sierra Nevada, California, using apatite (U-Th)/He ages. Nature, 396(6706), 66-69.

House, M.A., Wernicke, B.P., Farley, K.A., 2001. Paleo-geomorphology of the Sierra Nevada, California, from (U-Th)/He ages in apatite. American Journal of Science, 301(2), 77-102.

Howard, A.D., 1988. Equilibrium models in geomorphology. In: M.G. Anderson (Ed.), Modelling Geomorphological Systems. John Wiley, New York, pp. 49-72.

Howard, A.D., 1994. A detachment-limited model of drainage basin evolution. Water Resources Research, 30(7), 2261-2285.

Howard, A.D., 1997. Badland morphology and evolution: Interpretation using a simulation model. Earth Surface Processes and Landforms, 22(3), 211-227.

Hughes, M.W., Almond, P.C., Roering, J.J., 2009. Increased sediment transport via bioturbation at the last glacial-interglacial transition. Geology, 37(10), 919-922, doi:10.1130/g30159a.1.

Hurst, M.D., Mudd, S.M., Walcott, R., Attal, M., Yoo, K., 2012. Using hilltop curvature to derive the spatial distribution of erosion rates. Journal of Geophysical Research-Earth Surface, 117(F2), F02017, doi:10.1029/2011jf002057.

Hurst, M.D., Mudd, S.M., Yoo, K., Attal, M., Walcott, R., 2013. Influence of lithology on hillslope morphology and response to tectonic forcing in the northern Sierra Nevada of California. Journal of Geophysical Research: Earth Surface, n/a-n/a, doi:10.1002/jgrf.20049.

Ivy-Ochs, S., SchlÃ¼chter, C., Kubik, P.W., Dittrich-Hannen, B., Beer, J.r., 1995. Minimum 10Be exposure ages of early Pliocene for the Table Mountain plateau and the Sirius Group at Mount Fleming, Dry Valleys, Antarctica. Geology, 23(11), 1007-1010, doi:10.1130/0091-7613(1995)023<1007:mbeaoe>2.3.co;2.

Jones, C.H., Farmer, G.L., Unruh, J., 2004. Tectonics of Pliocene removal of lithosphere of the Sierra Nevada, California. Geological Society of America Bulletin, 116(11-12), 1408-1422, doi:10.1130/b25397.1.

Jungers, M.C., Bierman, P.R., Matmon, A., Nichols, K., Larsen, J., Finkel, R., 2009. Tracing hillslope sediment production and transport with in situ and meteoric 10Be. Journal of Geophysical Research-Earth Surface, 114(F4), F04020, doi:10.1029/2008jf001086.

Jyotsna, R., Haff, P.K., 1997. Microtopography as an indicator of modern hillslope diffusivity in arid terrain. Geology, 25(8), 695-698, doi:10.1130/0091-7613(1997)025<0695:maaiom>2.3.co;2.

Kirby, E., Johnson, C., Furlong, K., Heimsath, A., 2007. Transient channel incision along Bolinas Ridge, California: Evidence for differential rock uplift adjacent

to the San Andreas fault. Journal of Geophysical Research-Earth Surface, 112(F3), doi:10.1029/2006jf000559.

Kirby, E., Ouimet, W., 2011. Tectonic geomorphology along the eastern margin of Tibet: insights into the pattern and processes of active deformation adjacent to the Sichuan Basin. In: R.R.L. Gloaguen (Ed.), Growth and Collapse of the Tibetan Plateau. Geological Society Special Publication, pp. 165-188, doi:10.1144/sp353.9.

Kirby, E., Whipple, K.X., Tang, W.Q., Chen, Z.L., 2003. Distribution of active rock uplift along the eastern margin of the Tibetan Plateau: Inferences from bedrock channel longitudinal profiles. Journal of Geophysical Research-Solid Earth, 108(B4), doi:10.1029/2001jb000861.

Kirchner, J.W., Riebe, C.S., Ferrier, K.L., Finkel, R.C., 2006. Cosmogenic nuclide methods for measuring long-term rates of physical erosion and chemical weathering. Journal of Geochemical Exploration, 88(1â€“3), 296-299.

Komar, P.D., Inman, D.L., 1970. Longshore sand transport on beaches. Journal of Geophysical Research, 75(30), 5914-5927.

Korup, O., 2008. Rock type leaves topographic signature in landslide-dominated mountain ranges. Geophysical Research Letters, 35(11), L11402, doi:10.1029/2008gl034157.

Korup, O., Schlunegger, F., 2007. Bedrock landsliding, river incision, and transience of geomorphic hillslope-channel coupling: Evidence from inner gorges in the Swiss Alps. Journal of Geophysical Research-Earth Surface, 112, doi:10.1029/2006jf000710.

Korup, O., Schlunegger, F., 2009. Rock-type control on erosion-induced uplift, eastern Swiss Alps. Earth and Planetary Science Letters, 278(3-4), 278-285.

Korup, O., Weidinger, J.T., 2011. Rock type, precipitation, and the steepness of Himalayan threshold hillslopes. In: R. Gloaguen, Ratschbacher L. (Ed.), Growth and Collapse of the Tibetan Plateau. Special Publications. Geological Society, London, pp. 235-249, doi:10.1144/sp353.12.

Lague, D., Hovius, N., Davy, P., 2005. Discharge, discharge variability, and the bedrock channel profile. Journal of Geophysical Research: Earth Surface, 110(F4), F04006, doi:10.1029/2004jf000259.

Lal, D., 1991. Cosmic-ray labeling of erosion surfaces - in-situ nuclide production rates and erosion models. Earth and Planetary Science Letters, 104(2-4), 424-439.

Larsen, I.J., Montgomery, D.R., 2012. Landslide erosion coupled to tectonics and river incision. Nature Geoscience, 5(7), 468-473, doi:doi:10.1038/ngeo1479.

Lashermes, B., Foufoula-Georgiou, E., Dietrich, W.E., 2007. Channel network extraction from high resolution topography using wavelets. Geophysical Research Letters, 34, doi:10.1029/2007gl031140.

Lea, N.L., 1992. An aspect driven kinematic routing algorithm. In: A.J. Parsons, A.D. Abrahams (Eds.), Overland flow: Hydraulics and erosion mechanics. Chapman & Hall, New York, pp. 147-175.

Lefsky, M.A., Cohen, W.B., Acker, S.A., Parker, G.G., Spies, T.A., Harding, D., 1999. Lidar remote sensing of the canopy structure and biophysical properties of douglas-fir western hemlock forests. Remote Sensing of Environment, 70(3), 339-361.

Lifton, N.A., Bieber, J.W., Clem, J.M., Duldig, M.L., Evenson, P., Humble, J.E., Pyle, R., 2005. Addressing solar modulation and long-term uncertainties in scaling secondary cosmic rays for in situ cosmogenic nuclide applications. Earth and Planetary Science Letters, 239, 140-161, doi:10.1016/j.epsl.2005.07.001.

Marshall, J.A., Sklar, L.S., 2012. Mining soil databases for landscape-scale patterns in the abundance and size distribution of hillslope rock fragments. Earth Surface Processes and Landforms, 37(3), 287-300, doi:10.1002/esp.2241.

Martin, Y., Church, M., 1997. Diffusion in landscape development models: On the nature of basic transport relations. Earth Surface Processes and Landforms, 22(3), 273-279.

Masarik, J., Reedy, R.C., 1995. Terrestrial cosmogenic-nuclide production systematics calculated from numerical simulations. Earth and Planetary Science Letters, 136(3-4), 381-395.

Matsushi, Y., Matsuzaki, H., 2010. Denudation rates and threshold slope in a granitic watershed, central Japan. Nuclear Instruments and Methods in Physics Research B, 268, 1201-1204.

Mattson, A., Bruhn, R.L., 2001. Fault slip rates and initiation age based on diffusion Equation modeling: Wasatch Fault Zone and eastern Great Basin. Journal of Geophysical Research, 106(B7), 13739-13750, doi:10.1029/2001jb900003.

McKean, J.A., Dietrich, W.E., Finkel, R.C., Southon, J.R., Caffee, M.W., 1993. Quantification of soil production and downslope creep rates from cosmogenic Be-10 accumulations on a hillslope profile. Geology, 21(4), 343-346.

Molnar, P., Anderson, R.S., Anderson, S.P., 2007. Tectonics, fracturing of rock, and erosion. Journal of Geophysical Research-Earth Surface, 112(F3), F03014, doi:10.1029/2005jf000433.

Molnar, P., England, P., 1990. Late Cenozoic upift of mountain-ranges and global climate change - chicken or egg? Nature, 346, 29-34, doi:10.1038/346029a0.

Monaghan, M.C., McKean, J., Dietrich, W., Klein, J., 1992. BE-10 chronometry of bedrock-to-soil conversion rates. Earth and Planetary Science Letters, 111(2-4), 483-492.

Montgomery, D.R., 2001. Slope distributions, threshold hillslopes, and steady-state topography. American Journal of Science, 301(4-5), 432-454.

Montgomery, D.R., Brandon, M.T., 2002. Topographic controls on erosion rates in tectonically active mountain ranges. Earth and Planetary Science Letters, 201(3-4), 481-489.

Montgomery, D.R., Dietrich, W.E., 1988. Where do channels begin? Nature, 336(6196), 232-234.

Montgomery, D.R., Foufoula-Georgiou, E., 1993. Channel network source representation using digital elevation models. Water Resources Research, 29(12), 3925-3934.

Moore, I.D., Grayson, R.B., Ladson, A.R., 1991. Digital terrain modeling - a review of hydrological, geomorpological, and biological applications. Hydrological Processes, 5(1), 3-30.

Moosdorf, N., Hartmann, J., Dürr, H.H., 2010. Lithological composition of the North American continent and implications of lithological map resolution for dissolved silica flux modeling. Geochem. Geophys. Geosyst., 11(11), Q11003, doi:10.1029/2010gc003259.

Mudd, S.M., Furbish, D.J., 2004. Influence of chemical denudation on hillslope morphology. Journal of Geophysical Research-Earth Surface, 109(F2), doi:10.1029/2003jf000087.

Mudd, S.M., Furbish, D.J., 2005. Lateral migration of hillcrests in response to channel incision in soil-mantled landscapes. Journal of Geophysical Research-Earth Surface, 110(F4), doi:10.1029/2005jf000313.

Mudd, S.M., Furbish, D.J., 2007. Responses of soil-mantled hillslopes to transient channel incision rates. Journal of Geophysical Research-Earth Surface, 112(F3), doi:10.1029/2006jf000516.

Mudd, S.M., Yoo, K., 2010. Reservoir theory for studying the geochemical evolution of soils. Journal of Geophysical Research-Earth Surface, 115(F3), F03030, doi:10.1029/2009jf001591.

Naesset, E., 1997. Determination of mean tree height of forest stands using airborne laser scanner data. ISPRS Journal of Photogrammetry and Remote Sensing, 52(2), 49-56.

Nash, D.B., 1980a. Forms of bluffs degraded for different lengths of time in Emmet County, Michigan, U.S.A. Earth Surface Processes, 5, 331-341.

Nash, D.B., 1980b. Morphologic dating of degraded normal-fault scarps. Journal of Geology, 88(3), 353-360.

Nash, D.B., 1984. Morphologic dating of fluvial terrace scarps and fault scarps near west Yellowstone, Montana. Geological Society of America Bulletin, 95(12), 1413-1424.

Niemi, N.A., Oskin, M., Burbank, D.W., Heimsath, A.M., Gabet, E.J., 2005. Effects of bedrock landslides on cosmogenically determined erosion rates. Earth and Planetary Science Letters, 237(3-4), 480-498, doi:10.1016/j.epsl.2005.07.009.

Nilsson, M., 1996. Estimation of tree heights and stand volume using an airborne lidar system. Remote Sensing of Environment, 56(1), 1-7.

Nishiizumi, K., Imamura, M., Caffee, M.W., Southon, J.R., Finkel, R.C., McAninch, J., 2007. Absolute calibration of< sup> 10</sup> Be AMS standards. Nuclear Instruments and Methods in Physics Research Section B: Beam Interactions with Materials and Atoms, 258(2), 403-413.

Nishiizumi, K., Lal, D., Klein, J., Middleton, R., Arnold, J.R., 1986a. Production of BE-10 amd AL-26 by cosmic-rays in terrestrial quartz insitu and implications for erosion rates. Nature, 319(6049), 134-136.

Nishiizumi, K., Lal, D., Klein, J., Middleton, R., Arnold, J.R., 1986b. PRODUCTION OF BE-10 AND AL-26 BY COSMIC-RAYS IN TERRESTRIAL QUARTZ INSITU AND IMPLICATIONS FOR EROSION RATES. Nature, 319(6049), 134-136.

Nivière, B., Marquis, G., 2000. Evolution of terrace risers along the upper Rhine graben inferred from morphologic dating methods: evidence of climatic and tectonic forcing. Geophysical Journal International, 141(3), 577-594, doi:10.1046/j.1365-246x.2000.00123.x.

Norton, K.P., von Blanckenburg, F., Schlunegger, F., Schwab, M., Kubik, P.W., 2008. Cosmogenic nuclide-based investigation of spatial erosion and hillslope channel coupling in the transient foreland of the Swiss Alps. Geomorphology, 95(3-4), 474-486.

O'Callaghan, J.F., Mark, D.M., 1984. The extraction of drainage networks from digital elevation data. Computer Vision, Graphics, and Image Processing, 28(3), 323-344.

Oguchi, T., 1997. Drainage density and relative relief in humid steep mountains with frequent slope failure. Earth Surface Processes and Landforms, 22(2), 107-120, doi:10.1002/(sici)1096-9837(199702)22:2<107::aid-esp680>3.0.co;2-u.

Ouimet, W.B., Whipple, K.X., Granger, D.E., 2009. Beyond threshold hillslopes: Channel adjustment to base-level fall in tectonically active mountain ranges. Geology, 37(7), 579-582, doi:10.1130/g30013a.1.

Owen, J.J., Amundson, R., Dietrich, W.E., Nishiizumi, K., Sutter, B., Chong, G., 2011. The sensitivity of hillslope bedrock erosion to precipitation. Earth Surface Processes and Landforms, 36(1), 117-135, doi:10.1002/esp.2083.

Palumbo, L., Hetzel, R., Tao, M., Li, X., 2010. Topographic and lithologic control on catchment-wide denudation rates derived from cosmogenic Be-10 in two mountain ranges at the margin of NE Tibet. Geomorphology, 117(1-2), 130-142, doi:10.1016/j.geomorph.2009.11.019.

Passalacqua, P., Do Trung, T., Foufoula-Georgiou, E., Sapiro, G., Dietrich, W.E., 2010a. A geometric framework for channel network extraction from lidar: Nonlinear diffusion and geodesic paths. Journal of Geophysical Research-Earth Surface, 115(F1), F01002, doi:10.1029/2009jf001254.

Passalacqua, P., Tarolli, P., Foufoula-Georgiou, E., 2010b. Testing space-scale methodologies for automatic geomorphic feature extraction from lidar in a complex mountainous landscape. Water Resources Research, 46(11), W11535, doi:10.1029/2009wr008812.

Pelletier, J.D., Cline, M.L., 2007. Nonlinear slope-dependent sediment transport in cinder cone evolution. Geology, 35(12), 1067-1070, doi:10.1130/g23992a.1.

Pelletier, J.D., DeLong, S.B., Al-Suwaidi, A.H., Cline, M., Lewis, Y., Psillas, J.L., Yanites, B., 2006. Evolution of the Bonneville shoreline scarp in west-central Utah: Comparison of scarp-analysis methods and implications for the diffusion model of hillslope evolution. Geomorphology, 74(1â€“4), 257-270.

Pelletier, J.D., McGuire, L.A., Ash, J.L., Engelder, T.M., Hill, L.E., Leroy, K.W., Orem, C.A., Rosenthal, W.S., Trees, M.A., Rasmussen, C., Chorover, J., 2011. Calibration and testing of upland hillslope evolution models in a dated landscape: Banco Bonito, New Mexico. Journal of Geophysical Research-Earth Surface, 116(F4), F04004, doi:10.1029/2011jf001976.

Perron, J.T., Dietrich, W.E., Kirchner, J.W., 2008. Controls on the spacing of first-order valleys. Journal of Geophysical Research-Earth Surface, 113(F4), doi:10.1029/2007jf000977.

Perron, J.T., Kirchner, J.W., Dietrich, W.E., 2009. Formation of evenly spaced ridges and valleys. Nature, 460(7254), 502-505.

Petit, C., Gunnell, Y., Gonga-Saholiariliva, N., Meyer, B., Séguinot, J., 2009. Faceted spurs at normal fault scarps: Insights from numerical modeling. Journal of Geophysical Research-Earth Surface, 114(B5), B05403, doi:10.1029/2008jb005955.

Phillips, F.M., Leavy, B.D., Jannik, N.O., Elmore, D., Kubik, P.W., 1986. THE ACCUMULATION OF COSMOGENIC CL-36 IN ROCKS - A METHOD FOR SURFACE EXPOSURE DATING. Science, 231(4733), 41-43.

Pierce, K.L., Colman, S.M., 1986. Effect of height and orientation (microclimate) on geomorphic degradation rates and processes, late-glacial terrace scarps in central Idaho. GSA Bulletin, 97, 869-885.

Poesen, J., Lavee, H., 1994. Rock fragments in top soils: significance and processes. Catena, 23(1-2), 1-28.

Ponza, A., Pazzaglia, F.J., Picotti, V., 2010. Thrust-fold activity at the mountain front of the Northern Apennines (Italy) from quantitative landscape analysis. Geomorphology, 123(3-4), 211-231, doi:10.1016/j.geomorph.2010.06.008.

Porder, S., Vitousek, P.M., Chadwick, O.A., Chamberlain, C.P., Hilley, G.E., 2007. Uplift, erosion, and phosphorus limitation in terrestrial ecosystems. Ecosystems, 10(1), 158-170, doi:10.1007/s10021-006-9011-x.

Processes, 2010. Landscapes on the Edge: New Horizons for Research on Earth's Surface. Committee on Challenges and Opportunities in Earth Surface, The National Academies Press.

Reneau, S.L., 1988. Depositional and erosional history of hollows: Application to landslide location and frequency, long-term erosion rates, and the effects of climatic change. Ph.D., University of California, Berkeley, 328 pp.

Reneau, S.L., Dietrich, W.E., Rubin, M., Donahue, D.J., Jull, A.J.T., 1989. Analysis of hillslope erosion rates using dated colluvial deposits. Journal of Geology, 97(1), 45-63.

Riebe, C.S., Kirchner, J.W., Finkel, R.C., 2004. Erosional and climatic effects on long-term chemical weathering rates in granitic landscapes spanning diverse climate regimes. Earth and Planetary Science Letters, 224(3-4), 547-562.

Riebe, C.S., Kirchner, J.W., Granger, D.E., Finkel, R.C., 2000. Erosional equilibrium and disequilibrium in the Sierra Nevada, inferred from cosmogenic Al-26 and Be-10 in alluvial sediment. Geology, 28(9), 803-806.

Riebe, C.S., Kirchner, J.W., Granger, D.E., Finkel, R.C., 2001a. Minimal climatic control on erosion rates in the Sierra Nevada, California. Geology, 29(5), 447-450.

Riebe, C.S., Kirchner, J.W., Granger, D.E., Finkel, R.C., 2001b. Strong tectonic and weak climatic control of long-term chemical weathering rates. Geology, 29(6), 511-514.

Riggins, S.G., Anderson, R.S., Anderson, S.P., Tye, A.M., 2011a. Solving a conundrum of a steady-state hilltop with variable soil depths and production rates, Bodmin Moor, UK. Geomorphology, 128(1-2), 73-84, doi:10.1016/j.geomorph.2010.12.023.

Riggins, S.G., Anderson, R.S., Anderson, S.P., Tye, A.M., 2011b. Solving a conundrum of a steady-state hilltop with variable soil depths and production rates, Bodmin Moor, UK. Geomorphology, In Press.

Riihimaki, C.A., Reiners, P.W., 2012. Empirical evidence of climate's role in Rocky Mountain landscape evolution. Journal of Geophysical Research-Earth Surface, 117(F2), F02007, doi:10.1029/2011jf002137.

Roering, J.J., 2004. Soil creep and convex-upward velocity profiles: Theoretical and experimental investigation of disturbance-driven sediment transport on hillslopes. Earth Surface Processes and Landforms, 29(13), 1597-1612, doi:10.1002/esp.1112.

Roering, J.J., 2008. How well can hillslope evolution models "explain" topography? Simulating soil transport and production with high-resolution topographic data. Geological Society of America Bulletin, 120(9-10), 1248-1262, doi:10.1130/b26283.1.

Roering, J.J., Almond, P., Tonkin, P., McKean, J., 2002. Soil transport driven by biological processes over millennial time scales. Geology, 30(12), 1115-1118.

Roering, J.J., Almond, P., Tonkin, P., McKean, J., 2004. Constraining climatic controls on hillslope dynamics using a coupled model for the transport of soil and tracers: Application to loess-mantled hillslopes, South Island, New Zealand. Journal of Geophysical Research-Earth Surface, 109(F1), doi:10.1029/2003jf000034.

Roering, J.J., Gerber, M., 2005. Fire and the evolution of steep, soil-mantled landscapes. Geology, 33(5), 349-352, doi:10.1130/g21260.1.

Roering, J.J., Kirchner, J.W., Dietrich, W.E., 1999. Evidence for nonlinear, diffusive sediment transport on hillslopes and implications for landscape morphology. Water Resources Research, 35(3), 853-870.

Roering, J.J., Kirchner, J.W., Dietrich, W.E., 2001a. Hillslope evolution by nonlinear, slope-dependent transport: Steady state morphology and equilibrium adjustment timescales. Journal of Geophysical Research-Solid Earth, 106(B11), 16499-16513, doi:10.1029/2001JB000323.

Roering, J.J., Kirchner, J.W., Sklar, L.S., Dietrich, W.E., 2001b. Hillslope evolution by nonlinear creep and landsliding: An experimental study. Geology, 29(2), 143-146.

Roering, J.J., Marshall, J., Booth, A.M., Mort, M., Jin, Q.S., 2010. Evidence for biotic controls on topography and soil production. Earth and Planetary Science Letters, 298(1-2), 183-190, doi:10.1016/j.epsl.2010.07.040.

Roering, J.J., Perron, J.T., Kirchner, J.W., 2007. Functional relationships between denudation and hillslope fonn and relief. Earth and Planetary Science Letters, 264(1-2), 245-258, doi:10.1016/j.epsl.2007.09.035.

Rosenbloom, N.A., Anderson, R.S., 1994. Hillslope and channel evolution in a marine terraced landscape, Santa-Cruz, California. Journal of Geophysical Research-Solid Earth, 99(B7), 14013-14029.

Saatchi, S.S., Harris, N.L., Brown, S., Lefsky, M., Mitchard, E.T.A., Salas, W., Zutta, B.R., Buermann, W., Lewis, S.L., Hagen, S., Petrova, S., White, L., Silman, M., Morel, A., 2011. Benchmark map of forest carbon stocks in tropical regions across three continents. Proceedings of the National Academy of Sciences, 108(24), 9899-9904, doi:10.1073/pnas.1019576108.

Saleeby, J., Foster, Z., 2004. Topographic response to mantle lithosphere removal in the southern Sierra Nevada region, California. Geology, 32(3), 245-248, doi:10.1130/g19958.1.

Saleeby, J., Saleeby, Z., Nadin, E., Maheo, G., 2009. Step-over in the structure controlling the regional west tilt of the Sierra Nevada microplate: eastern escarpment system to Kern Canyon system. International Geology Review, 51(7-8), 634-669, doi:10.1080/00206810902867773.

Schaetzl, R.J., Follmer, L.R., 1990. Longevity of treethrow microtopography: implications for mass wasting. Geomorphology, 3(2), 113-123, doi:10.1016/0169-555X(90)90040-W.

Schmidt, J., Evans, I.S., Brinkmann, J., 2003. Comparison of polynomial models for land surface curvature calculation. International Journal of Geographical Information Science, 17(8), 797-814, doi:10.1080/1365881031000159605 8.

Schmidt, K.M., Montgomery, D.R., 1995. Limits to relief. Science, 270(5236), 617-620.

Simpson, J.A., 1983. Elemental and isotopic composition of the galactic cosmic-rays. Annual Review of Nuclear and Particle Science, 33, 323-381.

Sklar, L., Dietrich, W.E., 1998. River longitudinal profiles and bedrock incision models: stream power and the influence of sediment supply. In: E.E. Wohl, K.J. Tinkler (Eds.), River over rock: fluvial processes in bedrock channels. Geophysical Monograph Series. American Geophysical Union, Washington D. C., pp. 237-260, doi:10.1029/GM107p0237.

Sklar, L.S., Dietrich, W.E., 2004. A mechanistic model for river incision into bedrock by saltating bed load. Water Resources Research, 40(6), doi:10.1029/2003wr002496.

Slatton, K.C., Carter, W.E., Shrestha, R.L., Dietrich, W., 2007. Airborne Laser Swath Mapping: Achieving the resolution and accuracy required for geosurficial research. Geophysical Research Letters, 34(23), L23S10, doi:10.1029/2007gl031939.

Small, E.E., Anderson, R.S., 1995. Geomorphically driven late Cenozoic uplift in the Sierra Nevada, California. Science, 270(5234), 277-280.

Small, E.E., Anderson, R.S., Hancock, G.S., 1999. Estimates of the rate of regolith production using Be-10 and Al-26 from an alpine hillslope. Geomorphology, 27(1-2), 131-150.

Small, E.E., Anderson, R.S., Repka, J.L., Finkel, R., 1997. Erosion rates of alpine bedrock summit surfaces deduced from in situ Be-10 and Al-26. Earth and Planetary Science Letters, 150(3-4), 413-425.

Snyder, N.P., Whipple, K.X., Tucker, G.E., Merritts, D.J., 2000. Landscape response to tectonic forcing: Digital elevation model analysis of stream profiles in the Mendocino triple junction region, northern California. Geological Society of America Bulletin, 112(8), 1250-1263.

Snyder, N.P., Whipple, K.X., Tucker, G.E., Merritts, D.J., 2003a. Channel response to tectonic forcing: field analysis of stream morphology and hydrology in the Mendocino triple junction region, northern California. Geomorphology, 53(1-2), 97-127.

Snyder, N.P., Whipple, K.X., Tucker, G.E., Merritts, D.J., 2003b. Importance of a stochastic distribution of floods and erosion thresholds in the bedrock river incision problem. Journal of Geophysical Research-Solid Earth, 108(B2), doi:10.1029/2001jb001655.

Spelz, R.M., Fletcher, J.M., Owen, L.A., Caffee, M.W., 2008. Quaternary alluvial-fan development, climate and morphologic dating of fault scarps in Laguna Salada, Baja California, Mexico. Geomorphology, 102(3-4), 578-594.

Stock, G.M., Anderson, R.S., Finkel, R.C., 2004. Pace of landscape evolution in the Sierra Nevada, California, revealed by cosmogenic dating of cave sediments. Geology, 32(3), 193-196, doi:10.1130/g20197.1.

Stock, G.M., Anderson, R.S., Finkel, R.C., 2005a. Rates of erosion and topographic evolution of the Sierra Nevada, California, inferred from cosmogenic Al-26 and Be-10 concentrations. Earth Surface Processes and Landforms, 30(8), 985-1006, doi:10.1002/esp.1258.

Stock, J.D., Dietrich, W.E., 2006. Erosion of steepland valleys by debris flows. Geological Society of America Bulletin, 118(9-10), 1125-1148, doi:10.1130/b25902.1.

Stock, J.D., Montgomery, D.R., Collins, B.D., Dietrich, W.E., Sklar, L., 2005b. Field measurements of incision rates following bedrock exposure: Implications for process controls on the long profiles of valleys cut by rivers and debris flows. Geological Society of America Bulletin, 117(1-2), 174-194, doi:10.1130/b25560.1.

Stone, J.O., 2000. Air pressure and cosmogenic isotope production. Journal of Geophysical Research-Solid Earth, 105(B10), 23753-23759.

Strahler, A.N., 1950. Equilibrium theory of erosional slopes approached by frequency distribution analysis; Part II. American Journal of Science, 248(11), 800-814, doi:10.2475/ajs.248.11.800.

Strahler, A.N., 1952. Hypsometric (Area-Altitude) analysis of erosional topography. Geological Society of America Bulletin, 63(11), 1117-1142.

Tapponnier, P., Meyer, B., Avouac, J.P., Peltzer, G., Gaudemer, Y., Guo, S.M., Xiang, H.F., Yin, K.L., Chen, Z.T., Cai, S.H., Dai, H.G., 1990. Active thrusting and folding in the Qilian-Shan and decoupling between upper crust and mantle in northeastern Tibet. Earth and Planetary Science Letters, 97(3-4), 382-&.

Tucker, G.E., Bradley, D.N., 2010. Trouble with diffusion: Reassessing hillslope erosion laws with a particle-based model. Journal of Geophysical Research-Earth Surface, 115, doi:10.1029/2009jf001264.

Tucker, G.E., Bras, R.L., 1998. Hillslope processes, drainage density, and landscape morphology. Water Resources Research, 34(10), 2751-2764.

Tucker, G.E., Hancock, G.R., 2010. Modelling landscape evolution. Earth Surface Processes and Landforms, 35(1), 28-50, doi:10.1002/esp.1952.

Tucker, G.E., McCoy, S.W., Whittaker, A.C., Roberts, G.P., Lancaster, S.T., Phillips, R., 2011. Geomorphic significance of postglacial bedrock scarps on normal-fault footwalls. Journal of Geophysical Research-Earth Surface, 116(F1), F01022, doi:10.1029/2010jf001861.

Unruh, J.R., 1991. The uplift of the Sierra Nevada and implications for the late Cenozoic epeirogeny in the western cordillera. Geological Society of America Bulletin, 103(11), 1395-1404.

US Army Corps of Engineers, 1984. Shore Protection Manual. US Government Printing Office, Washington, DC.

.

Wahrhaftig, C., Birman, J.H., 1965. The Quaternary of the Pacific mountain system. In: H.E. Wright, Jr., D.G. Frey (Eds.), The Quaternary of the United States. Princeton University Press, New Jersey, pp. 299-340.

Wakabayashi, J., Sawyer, T.L., 2001. Stream incision, tectonics, uplift, and evolution of topography of the Sierra Nevada, California. Journal of Geology, 109(5), 539-562.

Walther, S.C., Roering, J.J., Almond, P.C., Hughes, M.W., 2009. Long-term biogenic soil mixing and transport in a hilly, loess-mantled landscape: Blue Mountains of southeastern Washington. Catena, 79(2), 170-178.

Warbington, R., Beardsley, D., 2002. Estimates of Old Growth Forests on the 18 National Forests of the Pacific Southwest Region. USDA Forest Service, US Department of Agriculture, Forest Service, Pacific Southwest Region.

West, A.J., Galy, A., Bickle, M., 2005. Tectonic and climatic controls on silicate weathering. Earth and Planetary Science Letters, 235(1-2), 211-228.

Whipple, K.X., 2001. Fluvial landscape response time: How plausible is steady-state denudation? American Journal of Science, 301(4-5), 313-325.

Whipple, K.X., 2004. Bedrock rivers and the geomorphology of active orogens. Annual Review of Earth and Planetary Sciences, 32, 151-185, doi:10.1146/annurev.earth.32.101802.120356.

Whipple, K.X., Tucker, G.E., 1999. Dynamics of the stream-power river incision model: Implications for height limits of mountain ranges, landscape response timescales, and research needs. Journal of Geophysical Research-Solid Earth, 104(B8), 17661-17674.

Whittaker, A.C., 2012. How do landscapes record tectonics and climate? Lithosphere, 4(2), 160-164, doi:10.1130/rf.l003.1.

Whittaker, A.C., Attal, M., Allen, P.A., 2010. Characterising the origin, nature and fate of sediment exported from catchments perturbed by active tectonics. Basin Research, 22(6), 809-828, doi:10.1111/j.1365-2117.2009.00447.x.

Whittaker, A.C., Attal, M.l., Cowie, P.A., Tucker, G.E., Roberts, G., 2008. Decoding temporal and spatial patterns of fault uplift using transient river long profiles. Geomorphology, 100(3-4), 506-526.

Whittaker, A.C., Cowie, P.A., Attal, M., Tucker, G.E., Roberts, G.P., 2007a. Contrasting transient and steady-state rivers crossing active normal faults: new field observations from the Central Apennines, Italy. Basin Research, 19(4), 529-556, doi:10.1111/j.1365-2117.2007.00337.x.

Whittaker, A.C., Cowie, P.A., Attal, M.l., Tucker, G.E., Roberts, G.P., 2007b. Bedrock channel adjustment to tectonic forcing: Implications for predicting river incision rates. Geology, 35(2), 103-106, doi:10.1130/g23106a.1.

Wilkinson, M.T., Chappell, J., Humphreys, G.S., Fifield, K., Smith, B., Hesse, P., 2005a. Soil production in heath and forest, Blue Mountains, Australia: Influence of lithology and palaeoclimate. Earth Surface Processes and Landforms, 30(13), 1683-1685, doi:10.1002/esp.1311.

Wilkinson, M.T., Chappell, J., Humphreys, G.S., Fifield, K., Smith, B., Hesse, P., 2005b. Soil production in heath and forest, Blue Mountains, Australia: Influence of lithology and palaeoclimate (vol 30, pg 923, 2005). Earth Surface Processes and Landforms, 30(13), 1683-1685, doi:10.1002/esp.1311.

Willett, S.D., Brandon, M.T., 2002. On steady states in mountain belts. Geology, 30(2), 175-178.

Wobus, C., Whipple, K.X., Kirby, E., Snyder, N., Johnson, J., Spyropolou, K., Crosby, B., Sheehan, D., 2006a. Tectonics from topography: Procedures, promise, and pitfalls, Geological Society of America Special Papers, pp. 55-74, doi:10.1130/2006.2398(04)

Wobus, C.W., Crosby, B.T., Whipple, K.X., 2006b. Hanging valleys in fluvial systems: Controls on occurrence and implications for landscape evolution. Journal of Geophysical Research-Earth Surface, 111(F2), doi:10.1029/2005jf000406.

Yoo, K., Amundson, R., Heimsath, A.M., Dietrich, W.E., 2005. Process-based model linking pocket gopher (Thomomys bottae) activity to sediment transport and soil thickness. Geology, 33(11), 917-920, doi:10.1130/g21831.1.

Yoo, K., Mudd, S.M., 2008a. Discrepancy between mineral residence time and soil age: Implications for the interpretation of chemical weathering rates. Geology, 36(1), 35-38, doi:10.1130/g24285a.1.

Yoo, K., Mudd, S.M., 2008b. Toward process-based modeling of geochemical soil formation across diverse landforms: A new mathematical framework. Geoderma, 146(1-2), 248-260, doi:10.1016/j.geoderma.2008.05.029.

Yoo, K., Weinman, B., Mudd, S.M., Hurst, M., Attal, M., Maher, K., 2011. Evolution of hillslope soils: The geomorphic theater and the geochemical play. Applied Geochemistry, 26, S149-S153, doi:10.1016/j.apgeochem.2011.03.054.

Zevenbergen, L.W., Thorne, C.R., 1987. Quantitative analysis of land surface topography. Earth Surface Processes and Landforms, 12(1), 47-56.

# 8 APPENDIX 1 – SOIL THICKNESS DATA

Central to the analysis, interpretations and conclusions presented in chapters 2 and 3 is the assumption that a nonlinear sediment transport model (i.e. Equation 1.4) provides an appropriate approximation of hillslope sediment flux throughout the Feather River landscape. Critically, this model assumes that hillslopes are in a transport-limited state, that is to say that their morphology is governed by the efficacy of sediment transport, with sediment being readily available for transport, rather than being limited by the production of transportable material from underlying bedrock (i.e. a weathering-limited condition). Therefore a requisite condition for the applicability of Equation 1.4 is that the Feather River landscape is soil-mantled and that the soils present are thick enough that they can be modelled as transport-limited components of the landscape. In this appendix I present all available data pertinent to testing the requirement for soil-mantled, transport limited hillslopes.

Field measurements of soil depth were made along three transects in Bald Rock Basin (Figure A1). This basin is a small tributary ($< 1$ km$^2$) draining directly into the Feather River. The main tributary channel contains a knickpoint in its longitudinal profile interpreted to represent the transmission of a signal of accelerated erosion rates in the main channel (see Figure 2.7). The three transects were located on hillslopes that met the channel above, adjacent to, and below the knickpoint, and are therefore expected to be experiencing differing erosion rates. Soil depth was measured using three different techniques: (i) excavating soil pits to examine a soil profile and locate the soil-saprolite boundary; (ii) augering through the soil and inspecting the texture of excavated material to identify the soil-saprolite transition; and (iii) using a tile probe to penetrate the soil to a refusal depth and measuring this depth. Digging soil pits is considered the most reliable method to quantify a soil depth since it best facilitates accurate identification of the soil-saprolite boundary. Identification of this boundary was based on colour (influenced

by soil moisture content) and presence/absence of rock texture in the profile. These criteria are the same as those used to identify the boundary from augered material however the precision with which the depth to the boundary could be resolved was limited by the questionable preservation of rock texture in augered saprolite (particularly when highly weathered) and the depth of penetration between sample inspection (typically c. 10 cm). Finally use of a probe facilitated a large dataset to be amassed relatively quickly but suffered a number of limitations. Firstly where saprolite was weak the probe penetrates beyond the soil-saprolite boundary, frequently bottoming out (i.e. the probe reaches its full length deep into the surface), this occurred most in portions of the landscape interpreted to be slowly eroding where the saprolite therefore has had longer in the near surface to weather. Alternatively where rock fragments were present in the soil, the probe would refuse to penetrate further despite the soil potentially being thicker. Rock fragments tend to be larger and more abundant in rapidly eroding portions of a landscape (Marshall and Sklar, 2011). Hence there is the likelihood that probe data will overestimate soil depths in slowly eroding portions of a landscape and underestimate soil depth in rapidly eroding areas.

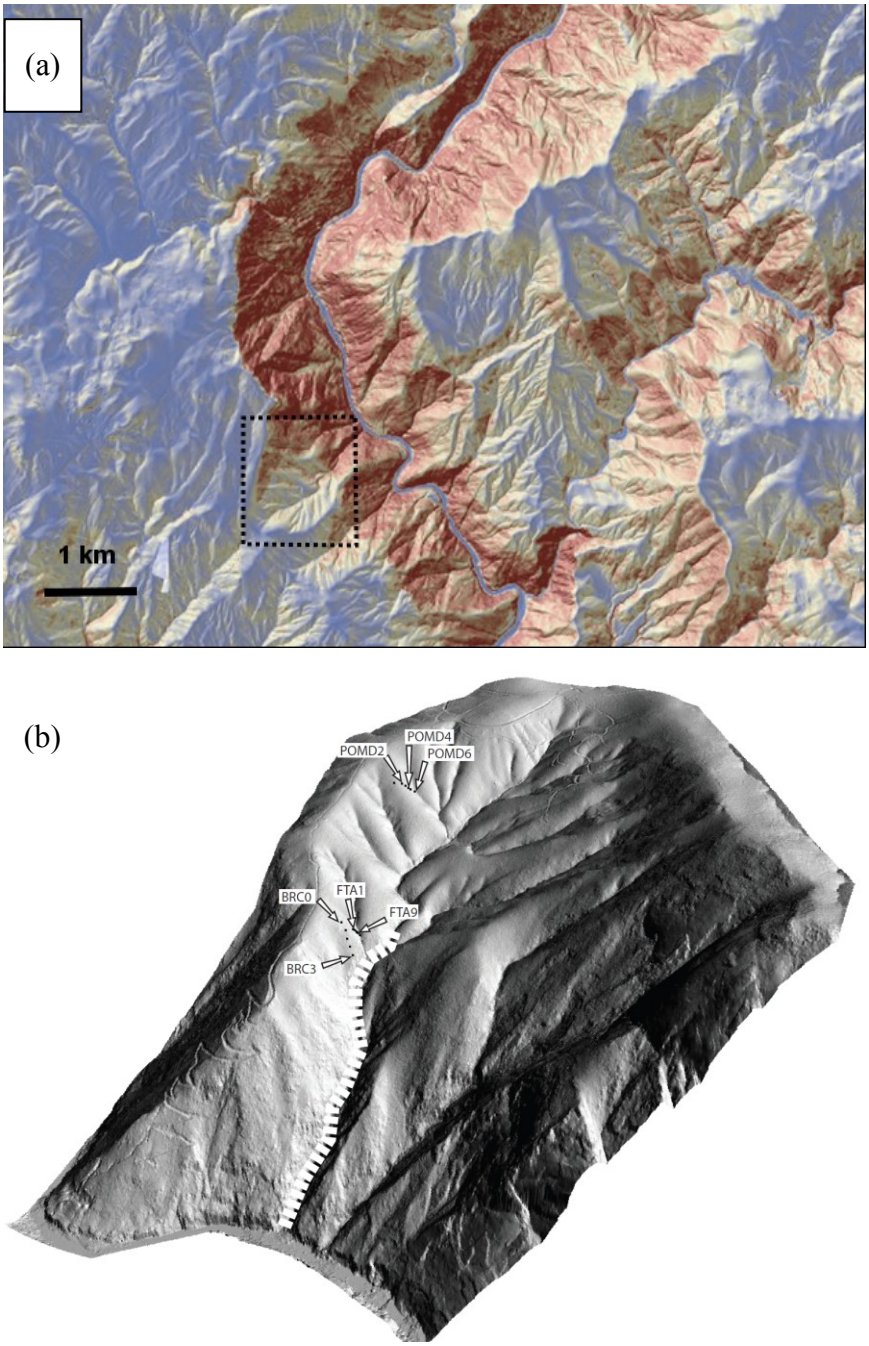


Figure A1: (a) Shaded relief and slope map of Feather River Canyon picked out by steep slopes (shaded red) compared to gentle slopes of an elevated relict surface (shaded blue). Dashed black box shows the location of Bald Rock Basin shown from an oblique perspective facing west in (b). Soil depth measurements were taken along three transects in Bald Rock Basin shown in (b). Dashed white line shows the extent of the steepened reach in the river profile, downstream of a prominent knickpoint.

The distribution of soil depths measured by the three methods is shown in Figure A3. Soil thickness measured by excavating soil pits (Figure A3a) typically vary between 30 and 60cm. Soil thicknesses vary little from the POMD transect to FTA however soil depths at BRC located downstream of the knickpoint appear to be slightly thinner. Soil thicknesses measured by augering suggest that the variability of soil thickness may increase from POMD to FTA to BRC with the interquartile range increasing as depicted by the box plots (Figre A3b). Augering would suggest that soil depths tend to be greatest along the BRC transect. Finally, probing data (Figure A3c) suggests the thickest soils are in POMD with a median value of ~115 cm, significantly higher than thicknesses at POMD measured by the other two techniques. Soil thicknesses dervived from probing at FTA and BRC are much lower than at POMD but both still demonstrate a significant soil cover.

The data suggested that despite an inferred large gradient in erosion rates, the three transects all maintain a thick soil cover, and the variability of soil depth would suggest that soil thickness is set by the mechanisms that act to disturb the soil, rather than being weathering limited (Yoo et al., 2011). This implied that soil thickness seems to be set primarily by the depth of root action in this forested landscape, and it's spatial variability (which I have not measured). Therefore I interpreted that the hillslopes are in a transport limited state and that Equation 1.5 may offer a reasonable approximation of the sediment transport dynamics in the Feather River region, which was subsequently tested and supported in Chapter 2.

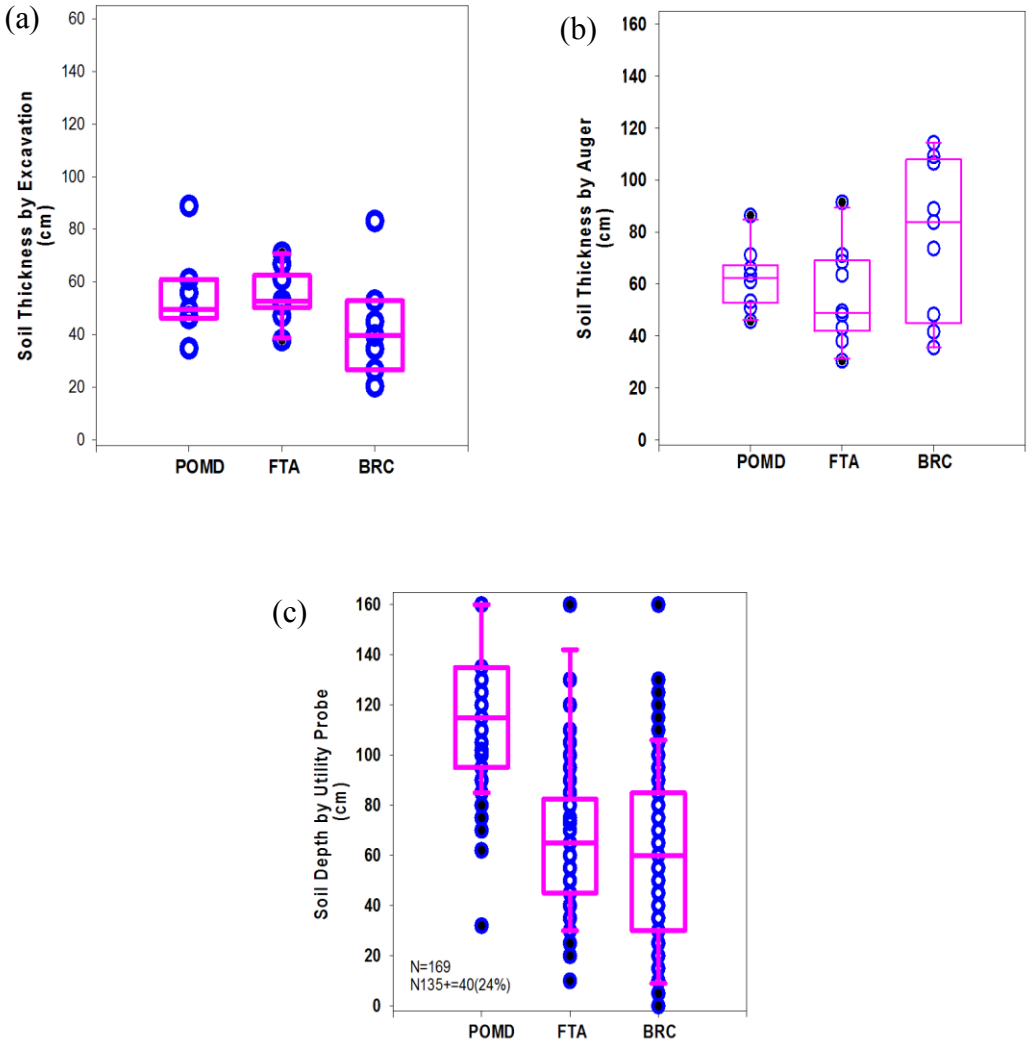


Figure A3: Distribution of soil thicknesses at three transects highlighted in Figure A2. Soil depth was measured by (a) excavating soil pits and identifying the soil/saprolite boundary; (b) augering and identifying the change in material texture from soil to saprolite; and (c) probing to a refusal depth. Blue circles are the raw data and pink box plots show the median and upper and lower quartiles, whilst the whiskers show the 5$^{th}$ and 95$^{th}$ percentiles.